Available online at www.sciencedirect.com
SCIENCE DIRECT®
Coordination Chemistry Reviews 238–239 (2003) 83–126
COORDINATION CHEMISTRY REVIEWS
www.elsevier.com/locate/ccr

Double perturbation theory: a powerful tool in computational coordination chemistry

Jochen Autschbach *, Tom Ziegler

Department of Chemistry, University of Calgary, Calgary, Alberta, Canada T2N 1N4

Received 10 April 2002; accepted 27 September 2002

Contents

* Corresponding author. Present address: Lehrstuhl fuer Theoretische Chemie, Universitaet Erlangen-Nuernberg, Egerlandstr. 3, D-91058 Erlangen, Germany. Tel.: +49-9131-85-25021; fax: +49-9131-85-27736.
E-mail addresses: jochen.autschbach@chemie.uni-erlangen.de (J. Autschbach), ziegler@chem.ucalgary.ca (T. Ziegler).

0010-8545/03/$ - see front matter
doi:10.1016/S0010-8545(02)00287-4

Abstract

Quantum mechanical double perturbation theory offers a route to access a large variety of important chemical and physical molecular properties. The properties that are considered here can be defined as the second derivative of the total energy of a molecule with respect to perturbation parameters arising from, e.g. frequency-dependent or -independent external electric and magnetic fields, nuclear and electronic magnetic moments, relativistic corrections, nuclear displacements, etc. The accessible properties cover, among others, the important fields of electronic and vibrational spectra, nuclear magnetic resonance (NMR), electron paramagnetic resonance (EPR) and optical activity. We will outline the methodology that gives access to these properties, and discuss a number of them in detail together with applications to transition metal compounds. All these properties are treated within the same theoretical framework in order to illustrate the similarities between them.

Keywords: Double perturbation theory; Computational coordination chemistry; Second-order energy derivatives; Molecular properties

1. Introduction

A first principles based theoretical description of the properties of transition metal complexes is still a challenge, even 70 years after the formulation of quantum mechanics and the enormous progress in methodology-, hardware-, and software-development during the last decades. Many researchers have in the past focused on the problem of electron correlation and the proper incorporation of its influence in the determination of ground state energies and molecular structures. From this, a wealth of chemical information can be extracted, such as reaction mechanism and pathways and related thermodynamical and kinetic data [1].

The availability of accurate energies together with the corresponding wavefunctions or Kohn–Sham density functional orbitals at the same time offers the route to many interesting and important molecular properties that can formally be defined as second derivatives of the ground state energy. Even though it is in principle straightforward to derive explicit expressions for such properties in a formal theoretical framework, the implementation of their computation within one of the common approximate quantum chemical methods can in practice be cumbersome and time consuming. Furthermore, transition metal complexes often represent systems that are too large to be treated with highly accurate correlated ab-initio methods. Therefore, many qualitative and semi-quantitative studies of molecular properties have in the past been carried out based on qualitative molecular orbital models, semi-empirical wavefunctions, or Hartree–Fock theory. Nowadays, density functional theory [2] (DFT) offers a computationally feasible alternative to Hartree–Fock computations that affords a much higher accuracy of the results at comparable cost. At the same time, DFT retains the much desired orbital description of the molecules. Therefore, DFT is often the method of choice for the theoretical study of transition metal coordination compounds and data from a number of recent studies is available. Alternatively, semi-empirical methods are still widely used for such systems and provide a large body of numerical data and interpretations. Highly accurate correlated ab-initio results for most second-order properties of transition metal compounds are rather rare and valuable for comparison with experimental data as well as benchmark results for computational methods.

It is our purpose here to give a concise overview over some of the molecular properties that are defined as second derivatives of the molecular energy with respect to 'small perturbations' and discuss specific examples involving applications to transition metal coordination compounds. All the properties are treated within the same theoretical framework, which is formulated in very basic quantum chemical terms. We want to illustrate the similarities between all these properties from very different fields of science and technology, which sometimes have been dealt with theoretically by seemingly unrelated formalisms. For this purpose, we will outline in Section 2 the general theoretical framework as well as describe some of the common approximate methods. In Section 3 examples for such second-order properties are discussed together with applications to transition metal complexes. Emphasis will be put on DFT results. Some concluding remarks are presented in Section 4. Among the properties that are described in this paper are electronic excitations and vibrational spectra, nuclear magnetic resonance (NMR) observables (nuclear shielding and spin–spin coupling), optical activity (optical rotations and circular dichroism), electron paramagnetic resonance (EPR), and relativistic heavy-atom effects on the chemical bond. Some related third-order properties are mentioned in this context as well. It should be noted at this point that throughout the article 'relativistic effects' will be treated equivalent to other properties. It is true that these effects are not physically observable quantities. However, much has been learned about the differences in the observable properties between light and heavy elements from studying relativistic effects on the electronic structure of atoms and molecules computationally. Though not directly observable, these effects are to a large extent responsible for the observable trends in the lower part of the periodic table.

2. Theoretical framework

In this section we outline how second derivatives of the energy of a molecule can be formulated and calculated. We start with the general time-dependent description, switch from there to the frequency domain, and obtain the frequency-independent static formulae as special cases in the zero frequency limit. We will restrict ourselves to the Born–Oppenheimer approximation, i.e. the nuclei are kept fixed and only the electronic degrees of freedom are included in the quantum mechanical formalism. Also, for simplicity we assume a non-degenerate ground state of the system under investigation. Electromagnetic fields will be treated semi-classically. The theory will be outlined in a pragmatic way in order to sketch the underlying principles without presenting too many practical or technical details. For this reason we have also omitted the use of second quantization notation throughout. The theoretical section is intended to be self-contained, therefore some well-known textbook knowledge will be repeated for that purpose. We assume that the reader is familiar with the concept of quantum mechanical wavefunction, expectation values, and the bra-ket notation.

Dimensionless atomic units with the electronic charge $e=1$, electronic mass $m_e=1$, Planck's constant $h=2\pi$, $4\pi\varepsilon_0=1$ and the speed of light $c\approx 137.036$ are used throughout the theoretical section. Consequently, factors of e, m_e, $\hbar=h/(2\pi)=1$ and $4\pi\varepsilon_0$ are omitted in the equations. In these atomic units the fine structure constant α equals $1/c$.

2.1. The sum-over-states formula

Let us consider a perturbation of a property B of a molecule. The stationary expectation value of B is given by

$$B_0=\langle\Psi_0|\hat{B}|\Psi_0\rangle \tag{1}$$

$\hat{B}$ is the quantum mechanical operator for the observable B, and '0' denotes the ground state as the reference state for which the property is to be evaluated. For simplicity of notation, we will use the same symbol for the physical property and its expectation value instead of writing $\langle B\rangle$ for the latter. The time-independent wavefunction $\Psi_0=\Psi_0(\boldsymbol{\tau})$ is assumed to be known, and is an exact solution of the time-independent many electron Schrödinger equation (SE, or a relativistically modified version of it)

$$\hat{H}\Psi_0=\Psi_0 E_0 \tag{2}$$

$\boldsymbol{\tau}=\boldsymbol{x}_1\boldsymbol{x}_2\ldots\boldsymbol{x}_N$ represent the space and spin degrees of freedom of all N electrons. The Hamiltonian $\hat{H}=\hat{H}(\boldsymbol{\tau})$ is supposed to be time-independent, in which case the solution $\Psi_0(t)$ of the time-dependent SE,

$$\hat{H}\Psi_0(t)=i\dot{\Psi}_0(t) \tag{3}$$

($\dot{\Psi}(t)$ is the time derivative of $\Psi(t)$) is simply given by

$$\Psi_0(t)=\Psi_0\,\mathrm{e}^{-iE_0t} \tag{4}$$

Note that we do not use different symbols for the time-dependent and the time-independent wavefunctions, but rather distinguish them by explicitly noting the time-dependence for the former as $\Psi_0(t)=\Psi_0(\boldsymbol{\tau};t)$. Unless explicitly noted, the symbol Ψ refers to time-independent wavefunctions. Further, notation of the dependence on $\boldsymbol{\tau}$ will be omitted except in cases where it is needed in order to avoid confusion.

In this work, we consider physical properties B that are defined as derivatives of the energy E with respect to an external perturbation λ_1 such as an electric or magnetic field, nuclear displacements, etc., i.e. as the derivative of

$$E_0=\langle\Psi_0|\hat{H}|\Psi_0\rangle \tag{5}$$

Using a common notation for the perturbation (note that we will use the notation $E^{(2)}$, etc. for higher derivatives accordingly), B_0 is given by

$$B_0=E_0^{(1)}=\left.\frac{\partial E_0}{\partial\lambda_1}\right|_{\lambda_1=0}=\langle\Psi_0|\hat{H}^{(1)}|\Psi_0\rangle \tag{6}$$

In the last equation, the fact that Ψ_0 is a solution of the time-independent SE has been used in order to eliminate terms that contain derivatives of the wavefunction (Hellmann–Feynman theorem [3]). It is seen that Eq. (1) represents the usual first-order perturbed energy expression, with $\hat{B}$ being the perturbed Hamiltonian to first-order, i.e. $\hat{B}=\hat{H}^{(1)}$ using the same notation as in Eq. (6). Examples for such properties are the electric or magnetic dipole moment of a molecule, the energy gradient with respect to nuclear displacements, or the relativistic energy correction to first-order. Employing the 'perturbation series expansion' convention of Ref. [4] that is widely used in quantum chemistry [5], E, B, Ψ, $\hat{H}$, and other quantities are expressed as perturbation series of the form,

$$E=E^{(0)}+E^{(1)}\lambda_1+E^{(2)}\lambda_1^2+\ldots \tag{7a}$$

$$B=B^{(0)}+B^{(1)}\lambda_1+B^{(2)}\lambda_1^2+\ldots \tag{7b}$$

etc. Note that $B^{(1)}=2E^{(2)}$, $B^{(2)}=3E^{(3)}$, etc., i.e. a nth-order perturbation of B with respect to the same perturbation λ_1 represents (up to a possible prefactor[1]) a $n+1$th-order perturbation of the energy. Generalizations to more than one perturbation such as

[1] The prefactor stems from the convention of writing the perturbation series in the form (7) and not in the alternative form of a Taylor series.

$$E = E^{(0,0)} + E^{(1,0)}\lambda_1 + E^{(0,1)}\lambda_2 + E^{(1,1)}\lambda_1\lambda_2 + E^{(2,0)}\lambda_1^2 + \ldots \tag{8}$$

and so on can be made. The perturbation of B by a different λ_2 represents a double first-order perturbation $E^{(1,1)}$ of the energy in the form

$$B^{(0,1)} = \left.\frac{\partial B}{\partial \lambda_2}\right|_{\lambda_2=0} = E^{(1,1)} = \left.\frac{\partial^2 E}{\partial\lambda_1\partial\lambda_2}\right|_{\lambda_1=0,\lambda_2=0}$$

$$= \langle \Psi_0^{(0,0)}|\hat{H}^{(1,0)}|\Psi_0^{(0,1)}\rangle + \langle \Psi_0^{(0,1)}|\hat{H}^{(1,0)}|\Psi_0^{(0,0)}\rangle + \langle \Psi_0^{(0,0)}|\hat{H}^{(1,1)}|\Psi_0^{(0,0)}\rangle$$

$$= \langle \Psi_0^{(0,0)}|\hat{B}^{(0,0)}|\Psi_0^{(0,1)}\rangle + \langle \Psi_0^{(0,1)}|\hat{B}^{(0,0)}|\Psi_0^{(0,0)}\rangle + \langle \Psi_0^{(0,0)}|\hat{B}^{(0,1)}|\Psi_0^{(0,0)}\rangle \tag{9}$$

with the zeroth-order term now being $B^{(0,0)} = E^{(1,0)}$, etc.

It is the quantity $B^{(0,1)}$ or $B^{(1)}$ with which the present work is dealing. Many well known physical properties of molecules, some of which are of particular importance in various spectroscopic methods, are directly or indirectly related to such second-order energy derivatives. In many cases, the second perturbation is time dependent, and the perturbation of B is experimentally observed as a function of the frequency ω of a perturbing field. Since the familiar time-independent expressions for $E^{(1,1)}$ or $E^{(2)}$ are simply given by the $\omega \to 0$ limit of the respective frequency-dependent expressions, we will consider such static properties as special cases at the end of this section.

For some important properties, the last term in Eq. (9) that refers to $\hat{H}^{(1,1)} = \hat{B}^{(0,1)}$ is either non-existent or small. As an exception, e.g. in NMR calculations it represents the diamagnetic term. Generally, this term is easy to compute since it only involves an expectation value with the (known) reference state wavefunction. Therefore, we will omit a discussion of it for the rest of this section and concentrate on the remaining terms. In the applications section we will point out whether a term with $\hat{H}^{(1,1)}$ is present in the computations or not.

In order to evaluate the perturbation of B_0 in Eq. (9), to lowest order the first-order wavefunction $\Psi_0^{(1)}(t)$ or $\Psi_0^{(1,0)}(t)$ or $\Psi_0^{(0,1)}(t)$, respectively, referring to one of the perturbations is needed. Let us suppose that the perturbation is time-dependent and can be represented by the operator

$$\hat{H}^{(1)}(\boldsymbol{\tau}; t) = \hat{A}(\boldsymbol{\tau})F(t) \tag{10}$$

i.e. the operator is separable into a spatial part and a function of time. From a purely theoretical point of view, the most straightforward way in which to obtain an explicit expression for the perturbed wavefunction is to use the complete set of unperturbed eigenfunctions $\Psi_j^{(0)}(t)$ of $\hat{H}^{(0)}$ as a basis set for $\Psi_0^{(1)}(t)$:

$$\Psi_0^{(1)}(t) = \sum_{j\neq 0} \Psi_j^{(0)}(t)C_j(t) \tag{11}$$

The coefficients $C_j(t)$ are yet unknown. The time dependent SE obtained from Eq. (3) to first-order in one of the perturbation parameters reads

$$\hat{H}^{(1)}\Psi_0^{(0)}(t) + \hat{H}^{(0)}\Psi_0^{(1)}(t) = i\dot{\Psi}_0^{(1)}(t) \tag{12}$$

Please note that we will omit the superscript (0) in the following for simplicity of notation, i.e. E_j, Ψ_j and Ψ_0 refer to the unperturbed system. Substituting Eq. (11) in Eq. (12) yields with Eq. (3), after multiplying from the left with $\Psi_j(t)$ and integrating over space, a differential equation for the coefficients C_j:

$$\dot{C}_j(t) = -i\langle \Psi_j(t)|\hat{H}^{(1)}(t)|\Psi_0(t)\rangle = -i\langle \Psi_j|\hat{A}|\Psi_0\rangle F(t)\, e^{i(E_j-E_0)t} \tag{13}$$

We consider a perturbation that has been switched on in the past (at $t \to -\infty$) and equate the coefficients at time t as

$$C_j(t) = -i\int_{-\infty}^{t} dt'\langle \Psi_j|\hat{A}|\Psi_0\rangle F(t')\, e^{i(E_j-E_0)t'} \tag{14}$$

From substitution of Eq. (14) into Eq. (11), the time-dependent first-order perturbation of B is obtained from Eq. (9) as

$$B_0^{(1)}(t) = \int_{-\infty}^{\infty} dt'\ \Theta(t-t')F(t) \cdot \int d\tau d\tau' \,[\hat{B}(\tau)\hat{A}(\tau')\chi_0(\tau,\tilde{\tau},\tau',\tilde{\tau}';\ t-t')]_{\substack{\tilde{\tau}=\tau \\ \tilde{\tau}'=\tau'}} \tag{15}$$

with the many electron response function for the reference state '0'

$$\chi_0(\tau,\tilde{\tau},\tau',\tilde{\tau}';t-t') = -i\sum_{j\neq 0}[\Psi_0^*(\tilde{\tau})\Psi_j(\tau)\Psi_j^*(\tilde{\tau}')\Psi_0(\tau')\, e^{-i(E_j-E_0)(t-t')} - \Psi_j^*(\tilde{\tau})\Psi_0(\tau)\Psi_0^*(\tilde{\tau}')\Psi_j(\tau')\, e^{i(E_j-E_0)(t-t')}] \tag{16}$$

The operators $\hat{A}$ and $\hat{B}$ in Eq. (15) are understood to act only on Ψ, not on Ψ^*, therefore, we have used the notation with $\tilde{\tau}$ and $\tilde{\tau}'$. Θ is the Heavyside step function, $\Theta(t) = 0$ for $t < 0$ and $\Theta(t) = 1$ for $t > 0$, and has been introduced in order to allow an extension of the integration range in Eq. (15) to $+\infty$. The presence of the Θ function is also intimately related to the η-limiting process in Eq. (17) below [6].

The knowledge of the response function $\chi_0(\tau,\tilde{\tau},\tau',\tilde{\tau}';\ t-t')$ allows the computation of the first-order perturbation of any property B of a molecule with respect to a perturbation of the form (10). In most cases it is convenient to study the frequency dependence of $B^{(1)}$ instead of its time dependence. For this purpose, the Fourier components of $\chi_0(\tau,\tilde{\tau},\tau',\tilde{\tau}';\ t-t')$ are of interest. After introducing a convergence factor of

$\exp(-\eta(t-t'))$, application of the Fourier Convolution Theorem [7] yields from Eq. (15)

$$\chi_0(\tau,\tilde{\tau},\tau',\tilde{\tau}';\ \omega)=\lim_{\eta\to 0}\sum_{j\neq 0}\left[\frac{\Psi_0^*(\tilde{\tau})\Psi_j(\tau)\Psi_j^*(\tilde{\tau}')\Psi_0(\tau')}{\omega+i\eta-(E_j-E_0)}-\frac{\Psi_j^*(\tilde{\tau})\Psi_0(\tau)\Psi_0^*(\tilde{\tau}')\Psi_j(\tau')}{\omega+i\eta+(E_j-E_0)}\right] \tag{17}$$

With this, the frequency dependent perturbation of B_0 for frequency ω is obtained as

$$B_0^{(1)}(\omega)=\int \mathrm{d}\tau\mathrm{d}\tau'[\hat{B}(\tau)\hat{A}(\tau')\chi_0(\tau,\tilde{\tau},\tau',\tilde{\tau}';\ \omega)]_{\substack{\tilde{\tau}=\tau\\ \tilde{\tau}'=\tau'}} \tag{18}$$

This result is usually written explicitly in the form of a sum-over-states (SOS) formula:

$$B_0^{(1)}(\omega)=\lim_{\eta\to 0}\sum_{j\neq 0}\left[\frac{\langle\Psi_0|\hat{B}|\Psi_j\rangle\langle\Psi_j|\hat{A}|\Psi_0\rangle}{\omega+i\eta-(E_j-E_0)}-\frac{\langle\Psi_j|\hat{B}|\Psi_0\rangle\langle\Psi_0|\hat{A}|\Psi_j\rangle}{\omega+i\eta+(E_j-E_0)}\right] \tag{19}$$

The convergence factor η can be neglected except for situations where ω is very close to one of the E_j-E_0 values such that the first-order response of B_0 becomes singular without η. We will therefore set $\eta=0$ from now on. The zero frequency limit of the last equation then yields the well known time-independent SOS second-order energy perturbation expression

$$B_0^{(1)}(0)=\sum_{j\neq 0}\frac{2\mathrm{Re}\langle\Psi_0|\hat{B}|\Psi_j\rangle\langle\Psi_j|\hat{A}|\Psi_0\rangle}{E_0-E_j} \tag{20}$$

An important detail to note here is that the final expression for the time-independent double first-order perturbation $E^{(1,1)}$ of the energy is independent of the order in which the derivatives have been taken (interchange theorem [5]). One can alternatively consider a perturbation $A^{(1)}$ of the property A with $\hat{H}^{(1)}(\tau)=\hat{B}(\tau)$ and obtain the same final result for $B^{(1)}$ and $A^{(1)}$, respectively. Eq. (20) is usually directly derived from the time-independent SE through an expansion of the time-independent first-order perturbed wavefunction in the basis of the complete set of time-independent eigenfunctions of $\hat{H}$. The perturbed wavefunction is in this case directly obtained as

$$\Psi_0^{(1)}=\sum_{j\neq 0}\frac{\langle\Psi_j|\hat{A}|\Psi_0\rangle}{E_0-E_j}\Psi_j \tag{21}$$

Since the energy E_j in the time-independent SE originates from the time-dependent term $\exp(-iE_jt)$ of the time-dependent wavefunction $\Psi_j(t)$, the energy denominators of Eqs. (19) and (20) are really of the same origin, independent of how the expression has been derived.

Though the SOS expression for $B_0^{(1)}(\omega)$ that we have obtained in this section is formally exact, its practical use is somewhat limited since it requires the explicit knowledge of the complete set of exact many electron wavefunctions and energies. In most practical cases, however, only an approximate ground state wavefunction (usually within some basis set expansion) is known, and it is desirable to obtain a result for $B_0^{(1)}(\omega)$ that does not require the explicit knowledge of all (or any) of the excited states wavefunctions. Furthermore, in many cases of interest the perturbation operators $\hat{A}$ and $\hat{B}$ are one-electron operators which will simplify the final equations substantially. In the next section, we will discuss how $B_0^{(1)}(\omega)$ can be obtained within the orbital model for such perturbations, and we will briefly mention some methods that have been developed to overcome the limitations of approximate schemes.

We have to stress here that the finite basis set approximation usually adopted in practical computations causes some limitations to the applicability of Eq. (19) or approximations to it that are discussed in the next section. Namely, in an incomplete basis Eq. (6) only holds in case that the basis functions are independent of the perturbation. Otherwise, the simple (Hellmann–Feynman) term on the right hand side of Eq. (6), that finally leads to Eq. (19), is not the only contribution to $B^{(0)}$. This is the case, for example, when standard nucleus-centered Gauss- or Slater-type basis sets are employed and derivatives of the energy with respect to nuclear displacements are involved [8–11]. Another example is the use of magnetic field dependent basis functions (GIAOs [12,13] or IGLOs [14]) in NMR computations in order to enforce gauge-independent results, since the basis then also depends on the perturbation (external magnetic field). In these cases additional terms due to the incompleteness of the basis set arise that are negligible for sufficiently large and well chosen basis sets. Also, for non variational energy expressions (MP2 or coupled cluster), the right hand side of Eq. (6) is not exactly valid [9]. A detailed physical interpretation of the results obtained from computations of molecular properties should be based on results that do not contain excessively large correction terms due to basis set incompleteness, therefore we will not discuss these terms here despite their importance in practical computations. However, it will be pointed out in Section 3 whether such corrections terms are necessary for the property under discussion in case standard atom-centered quantum chemical basis sets or field-dependent basis functions are employed.

2.2. One-particle perturbations operators

In many cases such as perturbations by electric and magnetic multipole fields, the perturbation operators $\hat{A}$ and $\hat{B}$ are one-particle operators, as mentioned above:

$$\hat{A}(\tau)=\sum_{k=1}^{N}\hat{a}(\boldsymbol{x}_k),\quad \hat{B}(\tau)=\sum_{k=1}^{N}\hat{b}(\boldsymbol{x}_k) \tag{22}$$

k counts here the electrons. In order to evaluate $B_0^{(1)}(\omega)$ with respect to the perturbation A, we can assume the existence a perturbed one particle density matrix $\Gamma_{\hat{a}0}^{(1)}(\boldsymbol{x},\tilde{\boldsymbol{x}};\omega)$ from which $B_0^{(1)}(\omega)$ can be evaluated by

$$B_0^{(1)}(\omega)=\int \mathrm{d}\boldsymbol{x}\cdot[\hat{b}(\boldsymbol{x})\Gamma_{\hat{a}0}^{(1)}(\boldsymbol{x},\tilde{\boldsymbol{x}};\omega)]_{\tilde{\boldsymbol{x}}=\boldsymbol{x}} \tag{23}$$

Likewise, we can use Eq. (22) in Eq. (18) and integrate over all variables but $\boldsymbol{x}_k$ in each term to obtain, after renaming each $\boldsymbol{x}_k$ to $\boldsymbol{x}_1$ and $\boldsymbol{x}'_k$ to $\boldsymbol{x}'_1$,

$$\begin{aligned}B_0^{(1)}(\omega)&=\int \mathrm{d}\boldsymbol{x}_1\mathrm{d}\boldsymbol{x}'_1\\&\quad\cdot\left[\hat{b}(\boldsymbol{x}_1)\hat{a}(\boldsymbol{x}'_1)\cdot N\int \mathrm{d}\boldsymbol{x}_2\ldots\mathrm{d}\boldsymbol{x}_N\mathrm{d}\boldsymbol{x}'_2\ldots\mathrm{d}\boldsymbol{x}'_N\right.\\&\quad\left.\cdot\chi_0(\tau,\tilde{\tau},\tau',\tilde{\tau}';\omega)\right]_{\substack{\tilde{\tau}=\tau\\ \tilde{\tau}'=\tau'}}\\&=\int \mathrm{d}\boldsymbol{x}\mathrm{d}\boldsymbol{x}'\cdot[\hat{b}(\boldsymbol{x})\hat{a}(\boldsymbol{x}')\chi_0(\boldsymbol{x},\tilde{\boldsymbol{x}},\boldsymbol{x}',\tilde{\boldsymbol{x}}';\omega)]_{\substack{\tilde{\boldsymbol{x}}=\boldsymbol{x}\\ \tilde{\boldsymbol{x}}'=\boldsymbol{x}'}}\end{aligned} \tag{24}$$

This discloses the relation between the first-order perturbation of the one-particle density matrix and the integral over all but one variable of the response function in Eq. (18). The perturbed density matrix is obtained by acting with the perturbation operator $\hat{a}(\boldsymbol{x}')$ on $\chi_0(\boldsymbol{x},\tilde{\boldsymbol{x}},\boldsymbol{x}',\tilde{\boldsymbol{x}}';\omega)$ and integrating over $\boldsymbol{x}'$ after setting $\tilde{\boldsymbol{x}}'=\boldsymbol{x}'$. A frequently disucssed restriction within the Kohn–Shan DFT approcah is the following: Within the Kohn–Sham DFT approximation, one usually has easy access only to the density matrix of the noninteracting reference system which differs from the density matrix of the interacting electronic system that is needed in Eq. (23). However, for many common perturbations the final result is in principle exact. This is obviously the case when $\hat{b}$ is a simple multiplicative operator, but also generally true if the result of $\hat{b}$ acting on the perturbed one-particle density matrix can be expressed by some function of spatial and spin coordinates multiplied with the perturbed density, spin density or , depending on the formalism, the current density [15]. Because of the restriction 'in principle' in the previous sentence, Kohn–Sham DFT methods are discussed together with other approximate methods in this section since the exact density functional is not known and all applications are based on approximate functionals.

2.3. Approximate methods

2.3.1. The RPA equation: Hartree–Fock, Kohn–Sham DFT, and semiempirical approaches

The *orbital model* is of utmost importance in theoretical chemistry. One reason is that it usually serves as a starting approximation for explicitly correlated computations, but it has also provided a wealth of interpretations that are not easy to extract from a more complex picture. Furthermore, the orbital model has proven to offer a practical way by which to overcome difficulties with kinetic energy functionals in DFT, and has therefore much contributed to the current popularity of Kohn–Sham DFT [2]. We will not elaborate on details of DFT and Hartree–Fock theory here but only recall that both methods and related semi-empirical schemes rely on a set of orthonormal[2] one-electron wavefunctions $\varphi_k(x)$ a.k.a. (spin)-orbitals or molecular (spin)-orbitals (MOs).

Each orbital is a solution of a time-independent one-particle equation

$$\hat{h}\varphi_k=\varphi_k\cdot\varepsilon_k \tag{25}$$

with its time-dependent counterpart

$$\hat{h}\varphi_k(t)=i\dot{\varphi}_k(t)\,;\quad \varphi_k(t)=\varphi_k\cdot\mathrm{e}^{-i\varepsilon_k t} \tag{26}$$

in complete analogy to Eqs. (2) and (3). We will not specify the explicit form of $\hat{h}(\boldsymbol{x})$ here since it depends on the actual method being used. In all cases we will assume that the Pauli principle is properly accounted for in order to ensure that the electrons are indistinguishable. In practical computations, the orbitals are usually expanded in a finite set of basis functions (such as atom centered Gauss- or Slater-type functions). Therefore, together with the N 'occupied' orbitals there is a finite number of 'unoccupied' or 'virtual' orbitals available. The set of orbitals serves as a convenient orthonormal one-particle basis set in the following.

In the independent particle model (IPM), the electrons are supposed to move completely independently from each other such that the total energy E_j of a many-electron state Ψ_j equals $\Sigma_k^{\mathrm{occ}}\varepsilon_k$, with the ε_k being the energies of the 'occupied' orbitals from which Ψ_j and/or the electron density is constructed. This is different from the situation where all orbitals are coupled by an effective potential as in the Hartree–Fock or DFT approaches. In both these methods, the effective one-electron operator $\hat{h}$ contains a Coulomb interaction term of the form

$$V^{\mathrm{C}}(\boldsymbol{x})=\int \mathrm{d}\boldsymbol{x}'\cdot\frac{\sum_k^{\mathrm{occ}}\varphi_k^*(\boldsymbol{x}')\varphi_k(\boldsymbol{x}')}{|\boldsymbol{x}-\boldsymbol{x}'|} \tag{27}$$

[2] This is not a necessary condition but greatly simplifies the final equations without loss of generality.

and also a so-called exchange V^{X} (Hartree–Fock) or exchange-correlation V^{XC} (DFT) term. The presence of these operators in $\hat{h}(\boldsymbol{x})$ generally causes $\Sigma_k^{occ}\varepsilon_k \neq E_j$. More important here, though, it is quite obvious that a perturbation due to $\hat{a}$ that causes a change in the orbitals to first-order also causes a first-order potential $V_{\hat{a}}^{(1)C} + V_{\hat{a}}^{(1)X \text{ or } XC}$ that needs to be treated properly in order to obtain a correct result for $B^{(1)}(\omega)$ within the chosen approach.

For a system of N truly independent particles, each orbital can be treated completely individually and the perturbation of B_0 is simply given by the sum over all individual contributions to $B_0^{(1)}$ from the occupied single particle wavefunctions φ_k with energies ε_k. Accordingly, in the IPM Eq. (18) reads by replacing $\hat{A}$ and $\hat{B}$ by $\hat{a}$ and $\hat{b}$, each Ψ_k with φ_k, each E_k with ε_k, and by summing over all N occupied orbitals:

$$B_0^{(1)\mathrm{IPM}}(\omega) = \int \mathrm{d}\boldsymbol{x}\mathrm{d}\boldsymbol{x}' \cdot [\hat{b}(\boldsymbol{x})\hat{a}(\boldsymbol{x}')\chi_0^{\mathrm{IPM}}(\boldsymbol{x},\tilde{\boldsymbol{x}},\boldsymbol{x}',\tilde{\boldsymbol{x}}';\omega)]_{\substack{\tilde{\boldsymbol{x}}=\boldsymbol{x}\\ \tilde{\boldsymbol{x}}'=\boldsymbol{x}'}} \tag{28}$$

with

$$\chi_0^{\mathrm{IPM}}(\boldsymbol{x},\tilde{\boldsymbol{x}},\boldsymbol{x}',\tilde{\boldsymbol{x}}';\omega) = \lim_{\eta\to 0}\sum_k^{occ}\sum_{a\neq k}\left[\frac{\varphi_k^*(\tilde{\boldsymbol{x}})\varphi_a(\boldsymbol{x})\varphi_a^*(\tilde{\boldsymbol{x}}')\varphi_k(\boldsymbol{x}')}{\omega + i\eta - (\varepsilon_a - \varepsilon_k)} - \frac{\varphi_a^*(\tilde{\boldsymbol{x}})\varphi_k(\boldsymbol{x})\varphi_k^*(\tilde{\boldsymbol{x}}')\varphi_a(\boldsymbol{x}')}{\omega + i\eta + (\varepsilon_a - \varepsilon_k)}\right] \tag{29}$$

Employing occupation numbers n_k for each orbital φ_k, the IPM response function can be written in a more compact form in which it is usually found in textbooks and research articles:

$$\chi_0^{\mathrm{IPM}}(\boldsymbol{x},\tilde{\boldsymbol{x}},\boldsymbol{x}',\tilde{\boldsymbol{x}}';\omega) = \sum_k\sum_a (n_k - n_a)\frac{\varphi_k^*(\tilde{\boldsymbol{x}})\varphi_a(\boldsymbol{x})\varphi_a^*(\tilde{\boldsymbol{x}}')\varphi_k(\boldsymbol{x}')}{\omega + i\eta - (\varepsilon_a - \varepsilon_k)} \tag{30}$$

We have explicitly noted the limiting process for η once more, but will again set $\eta = 0$ from now on for simplicity. For a system of independent electrons, the perturbation of B_0 is simply related to the IPM response function that can be readily evaluated from the set of occupied and unoccupied orbitals. Somewhat more lengthy expressions would be obtained in case $\hat{A}$ and/or $\hat{B}$ were two-electron operators, but nevertheless explicit formulae could be obtained in a straightforward way from Eq. (18) or Eq. (19) and evaluated once the set of occupied and virtual orbitals within a given basis set is known.

As already mentioned, however, in the IPM the effect of a perturbation of the effective potential in the one-particle SE that yields the orbitals is neglected. Consideration of this first-order effective potential is usually referred to as a 'coupled' perturbation approach, whereas straightforward application of the IPM results in an 'uncoupled' procedure. We will outline here how the respective coupled solution is obtained in the time-dependent DFT [15–23] and the Hartree–Fock [6,24–27] perturbation approaches. It has been shown that the concept of the IPM response function is very useful in the context of evaluation of the first-order perturbed effective potential. The perturbation operator $\hat{a}$ is now referred to as the *external perturbation*, whereas the *effective perturbation* $\hat{V}_{\hat{a}}^{(1)}$ is the combination of $\hat{a}$ with the first-order change of the effective (Hartree–Fock or Kohn–Sham) Coulomb (C) and exchange (X) or exchange-correlation (XC) potential, which in turn will be computable once the perturbed density matrix is available:

$$\hat{V}_{\hat{a}}^{(1)} = \hat{a} + \hat{V}^{(1)C} + \hat{V}^{(1)X \text{ or } XC} \tag{31}$$

Using the IPM response function in Eq. (28) in conjunction with this effective perturbation instead of $\hat{a}$ alone yields the correct result $B^{(1)}(\omega)$. This is due to the fact that all coupling effects between the electrons due to the perturbation are included in $\hat{V}_{\hat{a}}^{(1)}$ and the electrons can therefore otherwise be treated as if they were independent in order to set up the response function. This procedure does not require the knowledge of the true response function, i.e.

$$B_0^{(1)}(\omega) = \int \mathrm{d}\boldsymbol{x}\mathrm{d}\boldsymbol{x}' \cdot [\hat{b}(\boldsymbol{x})\hat{V}_{\hat{a}}^{(1)}(\boldsymbol{x}')\chi_0^{\mathrm{IPM}}(\boldsymbol{x},\tilde{\boldsymbol{x}},\boldsymbol{x}',\tilde{\boldsymbol{x}}';\omega)]_{\substack{\tilde{\boldsymbol{x}}=\boldsymbol{x}\\ \tilde{\boldsymbol{x}}'=\boldsymbol{x}'}}$$

$$= \int \mathrm{d}\boldsymbol{x}\mathrm{d}\boldsymbol{x}' \cdot [\hat{b}(\boldsymbol{x})\hat{a}(\boldsymbol{x}')\chi_0(\boldsymbol{x},\tilde{\boldsymbol{x}},\boldsymbol{x}',\tilde{\boldsymbol{x}}';\omega)]_{\substack{\tilde{\boldsymbol{x}}=\boldsymbol{x}\\ \tilde{\boldsymbol{x}}'=\boldsymbol{x}'}} \tag{32}$$

By comparison with Eq. (23) it can be seen that this procedure yields the correct perturbed density matrix $\Gamma_{\hat{a}0}^{(1)}(\omega)$, which will consequently be the quantity to consider from now on. We start by writing the perturbed density matrix in the basis of occupied and virtual orbitals as

$$\Gamma_{\hat{a}0}^{(1)}(\boldsymbol{x},\tilde{\boldsymbol{x}};\omega) = \sum_{k,a} P_{ka}^{(1)}(\omega)\varphi_a^*(\tilde{\boldsymbol{x}})\varphi_k(\boldsymbol{x}) \tag{33}$$

in order to convert the problem of finding an unknown function into the determination of the numerical coefficients $P_{ka}^{(1)}(\omega)$. Once the coefficients $P_{ka}^{(1)}$ are known, the quantity $B^{(1)}(\omega)$ can be computed. Using the effective perturbation Eq. (31) in Eq. (32) yields by comparison with Eq. (23) for the density matrix

$$\Gamma_{\hat{a}0}^{(1)}(\boldsymbol{x},\tilde{\boldsymbol{x}};\omega) = \sum_{k,a}\frac{n_k - n_a}{\omega - (\varepsilon_a - \varepsilon_k)} V_{ak}^{(1)}\varphi_k^*(\tilde{\boldsymbol{x}})\varphi_a(\boldsymbol{x}) \tag{34}$$

Here,

$$V^{(1)}_{ak} = \langle \varphi_a | \hat{V}^{(1)}_{\hat{a}} | \varphi_k \rangle \tag{35}$$

are the matrix elements of the effective perturbation. From a comparison of Eq. (34) with Eq. (33) one obtains

$$P^{(1)}_{ak}(\omega) = \frac{n_k - n_a}{\omega - (\varepsilon_a - \varepsilon_k)} \; V^{(1)}_{ak} \tag{36}$$

Note that the time-dependent density matrix $P^{(1)}_{ak}(t)$ due to a Hermitian time-dependent perturbation is Hermitian. Accordingly, the Fourier transform of this quantity affords the property $P^{(1)}_{ak}(\omega) = P^{(1)}_{ak}{}^*(-\omega)$. We have to stress here that $V^{(1)}_{ak}$ depends on $P^{(1)}_{ak}(\omega)$, therefore, Eq. (36) is only a defining equation, but does in practice not offer a direct solution to the problem. (See below, however, for remarks on attempts to achieve direct 'self-consistent' solutions.)

The matrix elements of the first-order Coulomb and the X or XC potential are now in turn written in terms of the density matrix elements $P^{(1)}_{ak}(\omega)$ and the so-called coupling matrix K as

$$V^{(1)\mathrm{C}}_{ak} + V^{(1)\mathrm{XC}}_{ak} = \sum_{b,j} K_{ak,bj} P^{(1)}_{bj}(\omega)$$
$$= \sum_{b,j} (K^{\mathrm{C}}_{ak,bj} + K^{\mathrm{X,\,XC}}_{ak,bj}) P^{(1)}_{bj}(\omega) \tag{37}$$

The Coulob and XC part of K are given by

$$K^{\mathrm{C}}_{ak,bj} = \int \mathrm{d}\boldsymbol{x}\mathrm{d}\boldsymbol{x}' \cdot \varphi^*_a(\boldsymbol{x})\varphi_k(\boldsymbol{x}) \frac{1}{|r - r'|} \varphi_b(\boldsymbol{x}')\varphi^*_j(\boldsymbol{x}') \tag{38a}$$

$$K^{\mathrm{XC}}_{ak,bj} = \int \mathrm{d}\boldsymbol{x}\mathrm{d}\boldsymbol{x}' \cdot \varphi^*_a(\boldsymbol{x})\varphi_k(\boldsymbol{x}) f_{\mathrm{XC}}(\boldsymbol{x}, \boldsymbol{x}', \omega)\varphi_b(\boldsymbol{x}')\varphi^*_j(\boldsymbol{x}') \tag{38b}$$

with the XC-kernel $f_{\mathrm{XC}}(\boldsymbol{x}, \boldsymbol{x}', \omega)$ being the $t \to \omega$ Fourier transform of

$$f_{\mathrm{XC}}(\boldsymbol{x}, \boldsymbol{x}', t - t') = \frac{\delta V_{\mathrm{XC}}(\boldsymbol{x}, t)}{\delta \rho(\boldsymbol{x}', t')} \tag{39}$$

V_{XC} is here the DFT exchange-correlation potential. In DFT applications often, a frequency independent approximation for f_{XC} is used. Very common in molecular computations is here the 'adiabatic local density approximation' (ALDA). In the Hartree–Fock approach, the exchange part of the coupling matrix is instead given by

$$K^{\mathrm{X}}_{ak,bj} = -\int \mathrm{d}\boldsymbol{x}\mathrm{d}\boldsymbol{x}' \cdot \varphi^*_a(\boldsymbol{x})\varphi_b(\boldsymbol{x}) \frac{1}{|r - r'|} \varphi_k(\boldsymbol{x}')\varphi^*_j(\boldsymbol{x}') \tag{40}$$

Upon substitution of Eq. (37) into Eq. (36) one obtains the following linear equation system:

$$\sum_{b,j} \left[\delta_{ab}\delta_{ij} \frac{\omega - (\varepsilon_b - \varepsilon_j)}{n_j - n_b} - K_{ak,bj} \right] P^{(1)}_{bj}(\omega) = a_{ak}, \quad j \neq b \tag{41}$$

The a_{ak} are the matrix elements of the external perturbation operator $\hat{a}$. Once the coupling matrix is known, the solution of the equation system (41) yields directly the unknown coefficients $P^{(1)}_{ak}(\omega)$.

By writing all matrix elements in a vector–matrix notation, the equation system (41) can be written in a very compact form. The vector–matrix notation is based on a composite index (ak) (or (bj)), respectively, that counts all orbital pairs with $n_a < n_k$ but not vice versa, i.e. the occupied-virtual orbital pairs. The usage of this composite index requires that both $P^{(1)}_{ak} = X_{(ak)}$ and $P^{(1)}_{ka} = Y_{(ak)}$ are specified in the equation system. Likewise, the matrix elements of the external perturbation will be denoted with $a_{ak} = Q_{(ak)}$ and $a_{ka} = R_{(ak)}$. Eq. (41) reads in this notation

$$\left[\begin{pmatrix} \mathsf{A} & \mathsf{B} \\ \mathsf{B}^* & \mathsf{A}^* \end{pmatrix} - \omega \begin{pmatrix} \mathsf{C} & 0 \\ 0 & -\mathsf{C} \end{pmatrix} \right] \begin{pmatrix} \boldsymbol{X} \\ \boldsymbol{Y} \end{pmatrix} = \begin{pmatrix} \boldsymbol{Q} \\ \boldsymbol{R} \end{pmatrix} \tag{42}$$

with

$$A_{(ak),(bj)} = \delta_{ab}\delta_{kj} \frac{\varepsilon_b - \varepsilon_j}{n_b - n_j} - K_{ak,bj} \tag{43a}$$

$$B_{(ak),(bj)} = -K_{ak,jb} \tag{43b}$$

$$C_{(ak),(bj)} = \delta_{ab}\delta_{kj} \frac{1}{n_b - n_j} \Rightarrow \mathsf{C} = -1 \tag{43c}$$

Note that vectors based on the composite index (ak) or (bj) are denoted by bold roman italic symbols $\boldsymbol{A}, \boldsymbol{B}, \ldots \boldsymbol{X}, \boldsymbol{Y}, \boldsymbol{Z}$, while matrices are denoted by sans serif symbols $\mathsf{A}, \mathsf{B}, \ldots \mathsf{X}, \mathsf{Y}, \mathsf{Z}$. The matrix C is just the negative unit matrix but has been included explicitly here for compatibility with previously published work on time-dependent DFT response theory [17].

In the time-dependent DFT case, the coupling matrix is evaluated based on an approximate form for Eq. (38b). In the time-dependent Hartree–Fock response theory, a formally equivalent equation system is obtained, but the Hartree–Fock part (40) of the coupling matrix has to be used instead. Using the common 'physicist's notation' for the two-electron matrix elements, the matrices A and B read explicitly in this case:

$$A_{(ak),(bj)} = \delta_{ab}\delta_{kj} \frac{\varepsilon_b - \varepsilon_j}{n_b - n_j} - \langle aj \| kb \rangle \tag{44a}$$

$$B_{(ak),(bj)} = -\langle ab \| kj \rangle \tag{44b}$$

In semi-empirical methods, the computation of certain expensive two-electron integrals is neglected, but otherwise these approaches are technically equivalent to the Hartree–Fock method (i.e. semi-empirical wavefunctions are approximations to the Hartree–Fock ones). Therefore, the methodology of double perturba-

tion theory can be based on Eq. (42) as well. However, we will not elaborate on details.

The time-dependent Hartree–Fock perturbation method is also frequently referred to as the 'random phase approximation' (RPA) [6,24,27]. It is the time-dependent version [28] of the coupled perturbed Hartree–Fock (CPHF) method, to which the RPA reduces in the zero-frequency limit. In the DFT case, the familiar coupled perturbed Kohn–Sham (CPKS) equations are obtained. Because of the presence of the two-electron integrals $\langle ab||kj\rangle$ in Eq. (44b), which are formally related to matrix elements of $1/r_{12}$ between the ground state wavefunction and doubly excited determinants, the RPA method is sometimes described as containing some correlation that goes beyond the flexibility of a basis of singly substituted determinants. Other authors argue that the same results as for RPA can formally be obtained within a finite-field perturbation based on the standard Hartree–Fock scheme, therefore the RPA solution does not really incorporate correlation [29]. We will use the term 'RPA equation' in the following when collectively referring to time-dependent Hartree–Fock or DFT methods, since the underlying equation has the same structure in both cases.

As in Section 2.1, the time-independent perturbation results for static external perturbations are obtained from Eq. (42) for the limit $\omega \to 0$. However, the explicit computation and the storage of the matrices K, A, or B is in practice not possible for all but the smallest molecules and basis sets. The reason is that the number of matrix elements is $(\mathrm{occ}\cdot\mathrm{virt})^2$, where occ is the number of occupied and virt the number of virtual orbitals. Therefore, in existing computer code, Eq. (42) is usually solved iteratively in such a way that the matrices are never stored. Nevertheless, we will refer to Eq. (42) when quoting results obtained from time-dependent or time-independent double perturbation theory based on the Hartree–Fock or semi-empirical methods or DFT. It is also possible to carry out a straightforward self-consistent solution of Eq. (36) with $V^{(1)}_{ak} = a_{ak}$ as a starting approximation. From the so obtained initial approximation for $P^{(1)}_{ak}(\omega)$, the first-order Coulomb- and X or XC potential can then be computed explicitly and be used to obtain a first approximation of $V^{(1)}_{ak}$. The procedure is repeated until self-consistency is reached, and the solution is the same as the one directly obtained from Eq. (42) [30–32]. Various, but in principle very related [33], methods are available in order to accelerate the usually very slow convergence of such a procedure [9,34,35]. They are based on the conjugate gradient technique [36] and have been used in the context of the iterative solution of Eq. (36) [37], finding a subset of eigenvectors of very large matrices [38–40], and to accelerate the convergence of the SCF cycle in Hartree–Fock and density functional calculations [41,42].

In order to simplify the following discussion we will assume real orbitals from now on. It is clear from inspection of Eq. (19) that $B^{(1)}(\omega)$ must exhibit poles at the excitation energies of the system under investigation. This offers an elegant way of computing a large number of (in principle all) excitation energies, without solving the SE for a number or all of the excited states, by finding a way of identifying the poles of $B^{(1)}(\omega)$ from Eq. (42). This is facilitated by finding the formal solution of Eq. (42) and identifying the frequencies for which this solution exhibits singularities. For either real or imaginary perturbation operators, only the symmetric part $(\boldsymbol{X}+\boldsymbol{Y})$ or the antisymmetric part $(\boldsymbol{X}-\boldsymbol{Y})$ of the perturbed density matrix, respectively, need to be known, not each element individually. Most perturbation operators that we discuss later fall into this category. With real orbitals, $\mathsf{A}=\mathsf{A}^*$, $\mathsf{B}=\mathsf{B}^*$ in Eq. (42), the two equations obtained explicitly from the 2×2 matrix yield upon addition and subtraction, e.g. for $(\boldsymbol{X}+\boldsymbol{Y})$

$$[(\mathsf{A}+\mathsf{B})+\omega^2\mathsf{S}](\boldsymbol{X}+\boldsymbol{Y}) = (\boldsymbol{Q}+\boldsymbol{R}) \tag{45}$$

with

$$\mathsf{S} = -\mathsf{C}(\mathsf{A}-\mathsf{B})^{-1}\mathsf{C} \tag{46}$$

This implies that

$$(\boldsymbol{X}+\boldsymbol{Y}) = [(\mathsf{A}+\mathsf{B})+\omega^2\mathsf{S}]^{-1}(\boldsymbol{Q}+\boldsymbol{R}) \tag{47}$$

is the formal solution of Eq. (45). This involves the non-Hermitian eigenvalue problem $[\mathsf{S}^{-1}(\mathsf{A}+\mathsf{B})+\omega_{0j}^2]\boldsymbol{F}_{0j}=0$ in order to invert the matrix in Eq. (47). For various reasons [17,43], it is more convenient to transform Eq. (45) such that a Hermitian matrix is to be inverted in order to obtain the formal solution for $(\boldsymbol{X}+\boldsymbol{Y})$. After insertion of $1=\mathsf{S}^{-1/2}\mathsf{S}^{1/2}$ between $[(\mathsf{A}+\mathsf{B})+\omega^2\mathsf{S}]$ and $(\boldsymbol{X}+\boldsymbol{Y})$ in Eq. (45), and multiplication with $\mathsf{S}^{-1/2}$ from the left one obtains

$$(\boldsymbol{X}+\boldsymbol{Y}) = \mathsf{S}^{-1/2}[\omega^2-\Omega]^{-1}\mathsf{S}^{-1/2}(\boldsymbol{Q}+\boldsymbol{R}) \tag{48}$$

with

$$\Omega = -\mathsf{S}^{-1/2}(\mathsf{A}+\mathsf{B})\mathsf{S}^{-1/2} \tag{49}$$

From this, it can be seen that the squares of the excitation energies, $\omega_{0j}^2=(E_0-E_j)^2$, can be obtained from solving the Hermitian pseudo-eigenvalue problem

$$\Omega\boldsymbol{F}_{0j} = \boldsymbol{F}_{0j}\cdot\omega_{0j}^2 \tag{50}$$

since for these particular values of ω the matrix $[\omega^2-\Omega]^{-1}$ exhibits singularities. The transition moments for the excitations can at the same time be obtained from the eigenvectors $\boldsymbol{F}_{0j}$ by comparison of the SOS expression of the perturbed electric or magnetic dipole moment with the result obtained from Eq. (48):

$$\boldsymbol{D}_{0j} = \omega_{0j}^{-1/2}\boldsymbol{D}\mathsf{S}^{-1/2}\boldsymbol{F}_{0j} \tag{51a}$$

$$\boldsymbol{M}_{0j} = \omega_{0j}^{1/2}\mathsf{C}^{-1/2}\boldsymbol{M}\mathsf{S}^{1/2}\boldsymbol{F}_{0j} \tag{51b}$$

with $\boldsymbol{D}$ and $\boldsymbol{M}$ being the (ak) matrix elements of the one-electron electric and magnetic dipole operator, respectively. In Section 3 we will discuss applications of the solution of Eq. (50) as well since the resulting spectra (UV–vis and CD) are, as can be seen from the preceding discussion, implicitly based on a second-order perturbation treatment of the molecular energy.

Certain approximations to Eq. (42) and thus the eigenvalue problem (50) can be made. First of all, neglecting all contributions of K in Eq. (42) directly recovers the 'uncoupled' IPM result of Eq. (28), which is related to Eq. (36) through the approximation $V_{ak} \approx a_{ak}$. Including only elements of K in A in which the spatial parts of φ_a and φ_b on the one hand, and of φ_k and φ_j on the other hand, are identical and neglecting all elements of B results for the Hartree–Fock case in a SOS approach in which all the excited states are approximated by singly substituted Slater determinants ('single transition approximation'). Note that only the triplet excited states are properly described by single Slater determinants. However, both singlet and triplet excitation energies are obtained from Eq. (50), the former in the single transition approximation of the Hartree–Fock approach being identical to the energy difference between the singlet-spin linear combination of two singly substituted determinants and the ground state wavefunction. Including the full matrix A but neglecting B (Tamm–Dancoff approximation, TDA) corresponds to a SOS approach in which the excited states wavefunctions are not just individual singly substituted determinants but energy minimizing linear combinations of them (CI singles = CIS [44]). This allows for a much better approximate treatment of the excited states as compared to the single transition approximation but is—at least formally—less accurate than the RPA. However, the TDA is a way around certain problems related to the unphysical dependence of the lowest triplet state in diatomics on the internuclear distance. This is also true for a related approximation in the time-dependent DFT case. See, e.g. Ref. [45] for details and further references.

2.3.2. Truncated CI

A number of results for second-order properties have been published based explicitly on the SOS formula (19). A rather simple approach is here to perform a configuration interaction (CI) computation that is limited to only including singly substituted determinants in the CI expansion (CI-singles = CIS [44]). Since this procedure is relatively inexpensive as compared to more elaborate CI expansions, a large number of excited states wavefunctions and energies can sometimes be computed explicitly. Based on this, the SOS formula for second-order properties can be directly applied once the matrix elements for the perturbation operators between the ground-state and the excited states wavefunctions have been evaluated. This approach has recently been used, e.g. for the computation of nonlinear optical phenomena [46,47].

The IPM response function (29) can be obtained from Eq. (17) assuming a system of noninteracting electrons and a SOS procedure in which the excited states wavefunctions are described by singly substituted determinants. From this it can be rationalized that the RPA equation, which is also derived using the IPM response function, yields similar results as the CIS-SOS procedure because a similar flexibility (the basis of all singly substituted determinants) is available in order to describe the perturbed wavefunction. However, the RPA equations involve, as discussed previously, also matrix elements with doubly excited determinants due to the response of the effective potential which are not included in the CIS-SOS scheme. The latter is equivalent, as already mentioned, to the RPA in which B has been neglected (i.e. the TDA).

In case excitation energies are of interest, CI methods are frequently employed. The CIS method is computationally cheap, but does often not yield reliable results because of the severe approximations that are made. Time dependent DFT performs significantly better, in particular for low-lying excitation energies [19,20]. More accurate results are obtained from higher quality CI methods, among them the rather popular multi reference doubles-CI (MRDCI). For further details and alternative accurate ab-initio methods (for instance CASPT2) for the calculation of excitation energies we refer to Ref. [48] and literature cited therein. For general applications in transition metal chemistry, these methods are often too costly and therefore not in widespread use, but can provide very accurate benchmark results for smaller complexes.

2.3.3. Finite field methods

Instead of pursuing an analytic solution approach in order to calculate $B^{(1)}$, it is also possible to carry out the differentiation in Eq. (9) numerically, i.e. the perturbation is calculated from the finite difference

$$B^{(1)} \approx \frac{B[\hat{H}^{(0)} + \lambda\hat{A}] - B[\hat{H}^{(0)}]}{\lambda} \tag{52}$$

for small λ. B is here written as a functional of the Hamiltonian. A common application is the case of a static electric field. The advantage of this method is that it can be applied to most cases for which expectation values of $B^{(0)}$ can be calculated, without much effort regarding the methodology- and program development. However, there are various disadvantages of this method as well. Often the balance between a numerically stable procedure (requires a not too small λ) and the

requirement for a small λ value (the exact derivative is obtained for the limit $\lambda \to 0$) is not easy to achieve. Variational instability of the perturbation operator can also cause severe problems. Without allowing for complex orbitals (due to an imaginary perturbation operator), it is also not straightforwardly applicable to magnetic field perturbations. Therefore, we will not further elaborate on details on these types of numerical derivative methods and focus on the analytic methodology instead.

2.3.4. More generalized methods

The 'bottom-up' way we followed in Section 2.3.1 in order to derive explicit equations by which the second-order energy perturbation can be calculated is often too cumbersome within a more sophisticated correlated ab-initio procedure. Equations of similar structure as Eq. (42) have been derived for the multi configuration self-consistent field (MCSCF) method, and explicit expressions for frequency dependent polarizabilities have been reported based on, e.g. MP2 energies. Equations-of-motion (EOM), propagator, and Green's function methods have been developed as very general powerful tools in order to derive explicit expressions for perturbed properties within ab-initio methods. In contrast to the derivations presented in Section 2.3.1 these methods are rather 'top-down' approaches in the sense that first general expressions for the perturbed quantity are derived, from which working equations within a specific approximate computational scheme are then obtained by specifying the type of ground state wavefunctions and the function or operator space in which the perturbation is represented. It is beyond the scope of this article to outline details of these methods. However, we should mention that the RPA Eq. (42) is recovered from these methods once a single-determinant reference function and the restriction to single substitutions are specified within these schemes. For a more detailed description see, e.g. Refs. [6,27,43,49].

2.4. Hamiltonian terms due to electromagnetic fields and relativity

A comment about the units being employed is appropriate here: As long as only electric fields are present, the choice of units is rather unambiguous. However, when substituting atomic units (see the beginning of Section 2) in equations related to magnetic properties, different prefactors containing the speed of light c are obtained depending on whether the equations have originally been formulated in the SI or in the Gaussian (c.g.s) system of units. The latter is still very popular in research dealing with magnetic properties. We follow the choice of McWeeny's textbook [6] here, based on equations in SI units that are converted to atomic units based on the conversion factors mentioned earlier. Factors of $\mu_0/(4\pi)$ appear here as $1/c^2$ in atomic units.

So far we have not specified an explicit form for the Hamiltonian or whether a two- or four-component relativistic formalism or a nonrelativistic one is used. Once the choice for a certain type of Hamiltonian has been made, the perturbation operators due to the presence of electromagnetic fields and other perturbations need to be derived based on this Hamiltonian. There are a number of different ways to incorporate relativistic effects into molecular quantum mechanics. For details see, for example, Refs. [50–52]. Since so-called fully relativistic four-component computations on transition metal clusters are still far from being routinely applied, or even feasible, we will in the following present only two methods in some detail that are first-order perturbative treatments of relativistic effects. Among these two methods, the two-component Pauli operator is perhaps familiar to many readers. Lately, also variationally stable two-component approaches such as the Douglas–Kroll–Hess method [51] and so-called regular approximations [53–55] have been successfully used in computations of properties of transition metal compounds. We refer to Section 3 for examples. It is important to note that the particular form of the perturbation terms due to electromagnetic fields in the relativistic case depend on the particular Hamiltonian that has been chosen to approximate the relativistic kinematic of the electrons. It is beyond the scope of this article to discuss the various possibilities even only for the currently more common relativistic methods. However, the nonrelativistic limit ($c \to \infty$)—shared by all relativistic methods—is presented in detail. Relativistic corrections to the resulting nonrelativistic terms due to external and nuclear electromagnetic fields given later in this section refer only to the more familar Pauli Hamiltonian for two reasons: first they have been quoted and analyzed (with varying degrees of detail) in many publications dealing with properties of transition metal complexes, and second to provide an example in order to outline in which way electromagetic field perturbations enter a relativistic Hamiltonian.

The usual way in which to derive the perturbation operators in Eq. (9) related to electromagnetic fields is to make the minimal substitution $\hat{\boldsymbol{p}} \to \hat{\boldsymbol{\pi}} = \hat{\boldsymbol{p}} + \boldsymbol{A}$ for the momentum operator for each electron, and addition of the external electric potential, $-\phi$, to the Hamiltonian. Here, $\boldsymbol{A}$ is the vector potential associated with the electromagnetic fields by

$$\boldsymbol{E} = -\boldsymbol{\nabla}\phi - \partial\boldsymbol{A}/\partial t \tag{53a}$$

$$\boldsymbol{B} = \boldsymbol{\nabla} \times \boldsymbol{A} \tag{53b}$$

For a time-independent homogeneous external magnetic field, the vector potential might be written as $\boldsymbol{A}^{\text{ext}} = (1/2)\boldsymbol{B}^{\text{ext}} \times \boldsymbol{r}$. For the properties being discussed in this article, the fields can arise from external time-

dependent or time-independent electric and magnetic fields and from the magnetic fields associated with the spin magnetic moments of the nuclei and the electrons. A multitude of terms arise upon consideration of all these effects in a four-component relativistic many-electron Hamiltonian after transformation to two-component form [6,50,56] even in the nonrelativistic limit. We will not consider all of these terms but list expressions for some important one-electron operators and a few two-electron terms.

Our starting point will be the nonrelativistic many-electron Hamiltonian of a molecule in the absence of electromagnetic fields. We write the additional terms in the Hamiltonian arising from the presence of electromagnetic fields as well as relativistic corrections as

$$\hat{H}' = \hat{H}^{\mathrm{elec}} + \hat{H}^{\mathrm{mag}} + \hat{H}^{\mathrm{rel}'} + \hat{H}^{\mathrm{rel}''}$$

$$= \sum_{k=1}^{N} [\hat{h}^{\mathrm{elec}}(\boldsymbol{x}_k) + \hat{h}^{\mathrm{mag}}(\boldsymbol{x}_k) + \hat{h}^{\mathrm{rel}'}(\boldsymbol{x}_k) + \hat{h}^{\mathrm{rel}''}(\boldsymbol{x}_k)]$$

$$+ 2\text{-electron terms} \tag{54}$$

where $\hat{H}^{\mathrm{elec}}$ contains the additional terms from external electric fields, $\hat{H}^{\mathrm{mag}}$ the ones from magnetic fields, $\hat{H}^{\mathrm{rel}'}$ relativistic corrections, and $\hat{H}^{\mathrm{rel}''}$ external field corrections to $\hat{H}^{\mathrm{rel}'}$. The $\hat{h}$ are the corresponding one-electron operators. From these additional operators one can then get expressions for $\hat{B} = \hat{H}^{(1,0)}$, $\hat{A} = \hat{H}^{(0,1)}$ and $\hat{B}^{(0,1)} = \hat{H}^{(1,1)}$ to use in Eq. (9) and related approximate schemes.

We start with the nonrelativistic operators due to electromagnetic fields. The Hamiltonian term due to an external electric dipole field $\boldsymbol{E}$ is described by the one-electron operator

$$\hat{h}^{\mathrm{elec}} = -\boldsymbol{E} \cdot \hat{\boldsymbol{d}} \tag{55}$$

with $\hat{\boldsymbol{d}} = -\boldsymbol{r}$ being the electric dipole moment operator for an electron. In case of a perturbing magnetic field $\boldsymbol{B}$ with its related vectorpotential $\boldsymbol{A}$, the nonrelativistic terms $\hat{h}^{\mathrm{mag}}$ in Eq. (54) are obtained as

$$\hat{h}^{\mathrm{mag}} = \frac{1}{2}(\boldsymbol{A}\hat{\boldsymbol{p}} + \hat{\boldsymbol{p}}\boldsymbol{A} + 2i\hat{\boldsymbol{S}}[\hat{\boldsymbol{p}} \times \boldsymbol{A} + \boldsymbol{A} \times \hat{\boldsymbol{p}}] + \boldsymbol{A}^2) \tag{56}$$

$\hat{\boldsymbol{S}} = (1/2)\boldsymbol{\sigma}_{\mathrm{s}}$ is here the spin operator, with $\boldsymbol{\sigma}_{\mathrm{s}}$ being the three-vector of the 2×2 Pauli spin matrices. The subscript s is used in order to distinguish $\boldsymbol{\sigma}_{\mathrm{s}}$ from the symbol $\boldsymbol{\sigma}$ for the chemical shielding tensor. The vector potential $\boldsymbol{A} = \boldsymbol{A}^{\mathrm{ext}} + \boldsymbol{A}^{\mathrm{nuc}}$ may arise from two different sources: one from an external magnetic field $\boldsymbol{B}^{\mathrm{ext}}$, the other one from the magnetic field $\boldsymbol{B}^{\mathrm{nuc}}$ due to the nuclear magnetic moments $\boldsymbol{\mu}_A$. $\boldsymbol{A}^{\mathrm{nuc}}$ is, for point-like nuclei, given by

$$\boldsymbol{A}^{\mathrm{nuc}} = \frac{1}{c^2} \sum_{A}^{\mathrm{Nuclei}} \frac{\boldsymbol{\mu}_A \times \boldsymbol{r}_A}{r_A^3} \tag{57}$$

Here, $\boldsymbol{r}_A$ denotes the distance vector between the electron and a nucleus A, and r_A its length. We do not yet explicitly specify $\boldsymbol{B}^{\mathrm{ext}}$ or $\boldsymbol{A}^{\mathrm{ext}}$, but substitute $\boldsymbol{B}^{\mathrm{nuc}} = \boldsymbol{\nabla} \times \boldsymbol{A}^{\mathrm{nuc}}$ by the use of Eq. (57) in Eq. (56). One obtains from Eq. (56)

$$\hat{h}^{\mathrm{mag}} = \boldsymbol{A}^{\mathrm{ext}^2} + \hat{h}^{\mathrm{OZ}} + \hat{h}^{\mathrm{SZ}} + \hat{h}^{\mathrm{OP}} + \hat{h}^{\mathrm{DS}} + \hat{h}^{\mathrm{FC}} + \hat{h}^{\mathrm{SD}} + \hat{h}^{\mathrm{OD}} \tag{58}$$

with

$$\hat{h}^{\mathrm{OZ}} = -\hat{\boldsymbol{\mu}}_{\mathrm{e}} \cdot \boldsymbol{B}^{\mathrm{ext}} \tag{59a}$$

$$\hat{h}^{\mathrm{SZ}} = \hat{\boldsymbol{S}} \cdot \boldsymbol{B}^{\mathrm{ext}} = -\hat{\boldsymbol{\mu}}_{\mathrm{s}} \cdot \boldsymbol{B}^{\mathrm{ext}} \tag{59b}$$

$$\hat{h}^{\mathrm{OP}} = \frac{1}{c^2} \sum_{A} \boldsymbol{\mu}_A \left(\frac{\boldsymbol{r}_A}{r_A^3} \times \hat{\boldsymbol{p}} \right) \tag{59c}$$

$$\hat{h}^{\mathrm{DS}} = \frac{1}{2c^2} \sum_{A} \left[(\boldsymbol{\mu}_A \cdot \boldsymbol{B}^{\mathrm{ext}}) \left(\frac{\boldsymbol{r}_A}{r_A^3} \cdot \boldsymbol{r} \right) - (\boldsymbol{\mu}_A \cdot \boldsymbol{r}) \left(\boldsymbol{B}^{\mathrm{ext}} \cdot \frac{\boldsymbol{r}_A}{r_A^3} \right) \right] \tag{59d}$$

$$\hat{h}^{\mathrm{FC}} + \hat{h}^{\mathrm{SD}} = \hat{\boldsymbol{S}} \cdot \boldsymbol{B}^{\mathrm{nuc}} = \frac{1}{c^2} \sum_{A} \hat{\boldsymbol{S}} \left[\boldsymbol{\mu}_A \left(\boldsymbol{\nabla} \cdot \frac{\boldsymbol{r}_A}{r_A^3} \right) - (\boldsymbol{\mu}_A \cdot \boldsymbol{\nabla}) \frac{\boldsymbol{r}_A}{r_A^3} \right] \tag{59e}$$

$$\hat{h}^{\mathrm{OD}} = \frac{1}{2c^4} \sum_{B \neq A} \frac{(\boldsymbol{\mu}_A \cdot \boldsymbol{\mu}_B)(\boldsymbol{r}_A \cdot \boldsymbol{r}_B) - (\boldsymbol{\mu}_A \cdot \boldsymbol{r}_B)(\boldsymbol{\mu}_B \cdot \boldsymbol{r}_A)}{r_A^3 r_B^3} \tag{59f}$$

Eq. (59a) is the orbital Zeeman term, Eq. (59b) spin Zeeman, Eq. (59c) paramagnetic orbital, Eq. (59d) diamagnetic shielding, Eq. (59e) Fermi-contact+spin-dipole, Eq. (59f) diamagnetic orbital term, respectively. The terms (59c)–(59f) are the hyperfine terms due to the presence of nuclear spins because they lead to a ('hyperfine') splitting of spectral lines. Their relative smallness as compared to the other terms can be seen from the additional c^{-2} or c^{-4} prefactors. These prefactors do not indicate relativistic corrections here but arise from the conversion to atomic units, as mentioned earlier. The individual FC and SD operators, in particular the well-known δ function for the FC term, are obtained by explicitly carrying out the differentiation of $\boldsymbol{r}_A/r_A^3$ in Eq. (59e). The first term on the right hand side of Eq. (59e), yields 3/2 of the FC operator, while the second term yields $-1/2$ of the FC plus the SD operator. One finally obtains the prehaps more familiar expressions

$$\hat{h}^{\mathrm{FC}} = \frac{8\pi}{3c^2} \delta(\boldsymbol{r}_A) \boldsymbol{\mu}_A \cdot \hat{\boldsymbol{S}} \tag{60a}$$

$$\hat{h}^{\mathrm{SD}} = \frac{1}{c^2} \cdot \frac{3(\hat{\boldsymbol{S}} \cdot \boldsymbol{r}_A)(\boldsymbol{\mu}_A \cdot \boldsymbol{r}_A) - r_A^2 \boldsymbol{\mu}_A \cdot \hat{\boldsymbol{S}}}{r_A^5} \tag{60b}$$

In Eq. (59a), $\hat{\boldsymbol{\mu}}_{\mathrm{e}} = -(1/2)(\boldsymbol{r} \times \hat{\boldsymbol{p}})$ is the magnetic moment operator for an electron's orbital motion. By

comparison of Eq. (59a) with Eq. (59b) the magnetic moment operator with respect to an electron spin degree of freedom appears to be $\hat{\boldsymbol{\mu}}_s = -\hat{\boldsymbol{S}}$. Since Eq. (56) is obtained from the Dirac equation of a single electron, transformation to two-component form and taking the nonrelativistic limit, the electronic g-factor is exactly 2 and not noted explicitly. Experimental evidence and more sophisticated theoretical treatments show that the correct value is rather 2.0023... The inclusion of the electronic g-factor in Eq. (58) can be achieved by replacing the spin magnetic moment operator of the electron, $\hat{\boldsymbol{\mu}}_s = -\hat{\boldsymbol{S}}$, with $\hat{\boldsymbol{\mu}}_s = -(g/2)\hat{\boldsymbol{S}}$ in the operators where necessary.

Relativistic corrections $\hat{H}^{\mathrm{rel}}$ in Eq. (54) can be formulated in many different ways, as already mentioned [51,52,57]. For a perturbational treatment in lowest order, for example, four-component ('Dirac') so-called 'direct' perturbation theory (DPT) [58–68] or two-component 'Pauli' perturbation theory (PPT) [50,69,70] can be employed. Again, we initially omit two-electron terms and concentrate on the one-electron operators arising from the field-free Dirac equation for one electron in a nuclear potential V_N. PPT yields to lowest order the well-known Pauli Hamiltonian [71]:

$$\hat{h}^{\mathrm{rel}'}_{\mathrm{PPT}} = -\frac{\hat{\boldsymbol{p}}^4}{8c^2} - \frac{(\hat{\boldsymbol{p}}^2 V_N)}{8c^2} + \frac{i}{2c^2}\hat{\boldsymbol{S}}[(\hat{\boldsymbol{p}}V_N)\times\hat{\boldsymbol{p}}]. \tag{61}$$

The first term in the last equation is the mass–velocity correction to the kinetic energy, the second term is the Darwin term, and the third term is the spin–orbit operator. The DPT approach yields instead (with $E^{(0)}$ being the unperturbed nonrelativistic energy)

$$\hat{h}^{\mathrm{rel}'}_{\mathrm{DPT}} = \frac{1}{4c^2}\hat{\boldsymbol{p}}(V_N - E^{(0)})\hat{\boldsymbol{p}} + \frac{i}{2c^2}\hat{\boldsymbol{S}}[(\hat{\boldsymbol{p}}V_N)\times\hat{\boldsymbol{p}}] \tag{62}$$

For an exact nonrelativistic one-electron wavefunction ψ, the expectation values (= first-order relativistic energy corrections) $\langle\psi|\hat{H}^{\mathrm{rel,PPT}}|\psi\rangle$ and $\langle\psi|\hat{H}^{\mathrm{rel,DPT}}|\psi\rangle$ yield the same result, however the DPT operator is more well behaved regarding numerical instabilities. In both operators, the last term

$$\hat{h}^{\mathrm{SO}} = \frac{i}{2c^2}\hat{\boldsymbol{S}}[(\hat{\boldsymbol{p}}V_N)\times\hat{\boldsymbol{p}}] \tag{63}$$

is responsible for the spin–orbit (SO) coupling due to the field of the nuclei, while the remaining terms are the scalar relativistic one-electron operators. The SO operator is also often written as $-(1/4c^2)\hat{\boldsymbol{S}}(\hat{\boldsymbol{p}}\times\boldsymbol{E}_N - \boldsymbol{E}_N\times\hat{\boldsymbol{p}})$, with $\boldsymbol{E}_N = \boldsymbol{\nabla}V_N = i\hat{\boldsymbol{p}}V_N$ being the electric field due to the nuclear potential. Excluding the SO operator from a relativistic perturbation computation retains the simple picture of real one-component orbitals or wavefunctions, which can facilitate interpretations of relativistic effects in molecules. It is also possible (in various different ways) to separate the four-component Dirac Hamiltonian into a scalar and a spin–orbit part [72]. For the important case of closed-shell systems, the SO operator does not contribute to the relativistic energy correction to first-order and is therefore often neglected. Relativistic Hamiltonians derived from perturbation theory, in particular the Pauli Hamiltonian, have frequently been used in variational calculations, even though this is generally not permissible. The problems arise due to the variational instability of the operators. In case very restricted basis sets in the atomic core regions and frozen core orbitals are employed, the variational instability can be somewhat kept under control. Even though the procedure is rather unsatisfactory from a theoretical point of view, in practice many useful results have been obtained from such Pauli-variational treatments (some of which are quoted in Section 3). In recent years, variationally stable two-component methods have become more available and diminished much of the former importance of this relativistic method. Due to the singular behavior of the Pauli Hamiltonian and its higher orders it is also not easily possible to study higher orders of relativistic corrections within this scheme. The DPT method has been much more successful in this respect. One of the most popular methods by which to treat relativistic effects is the use of relativistic effective corepotentials (ECPs) for heavy elements. Because there are no explicit corrections to the kinetic energy operator fot the valence electrons in this approach we do not present details and refer to Section 3.1.1 for further comments and applications.

Upon consideration of electromagnetic fields in the relativistic formalism relativistic field correction terms arise that are collected in $\hat{H}^{\mathrm{rel}''}$. For example, in the PPT scheme, one obtains the following kinetic energy and field correction to the spin Zeeman term (59b):

$$\hat{h}^{\mathrm{SZ}''} = -\frac{1}{2c^2}\hat{\boldsymbol{S}}\boldsymbol{B}(\hat{\boldsymbol{p}} + \boldsymbol{A})^2 \tag{64}$$

From the substitution $\hat{\boldsymbol{p}} \to \hat{\boldsymbol{\pi}}$ in the mass-velocity operator (the first term in Eq. (61)) or the scalar relativistic part of the DPT operator in Eq. (62), corrections to the orbital Zeeman term can be obtained. We refer to the literature for details [73–76]. The mass-velocity term can here lead to highly singular operators, e.g. in the case of fields due to nuclear spins [73]. Another term arises from the substitution $\hat{\boldsymbol{p}} \to \hat{\boldsymbol{\pi}}$ in the SO operator (63):

$$\hat{h}^{\mathrm{SO}''} = \frac{i}{2c^2}\hat{\boldsymbol{S}}[(\hat{\boldsymbol{p}}V_N)\times\boldsymbol{A}] \tag{65}$$

The latter has been denoted a 'gauge correction' to $\hat{h}^{\mathrm{SO}}$, while other authors refer to it as 'diamagnetic correction' because of the similarity of this operator to the diamagnetic shielding operator (59d). The similarity

becomes obvious upon substitution of $\boldsymbol{A} = (1/2)\boldsymbol{B} \times \boldsymbol{r}$ for a static homogeneous external magnetic field.

Finally, we want to briefly mention some of the two-electron terms in Eq. (54) that arise from a relativistic treatment of the electron–electron Coulomb interaction. Upon formal substitution of the electron-nuclear attraction potential V_N in the spin–orbit operator (65) by the electrostatic potential $V_{kl} = 1/r_{kl}$ between two electrons, one obtains the electron–electron SO operator

$$\hat{H}^{\mathrm{eeSO}} = \frac{i}{2c^2} \sum_{l \neq k} \hat{\boldsymbol{S}}_k [(\hat{\boldsymbol{p}}_k V_{kl}) \times \hat{\boldsymbol{p}}_k] \tag{66}$$

Here, $\hat{\boldsymbol{S}}_k$, $\hat{\boldsymbol{p}}_k$ act on the degrees of freedom of the kth electron A similar 'diamagnetic' or 'gauge correction' term as (65) but in two-electron form involving V_{kl} instead of V_N arises from Eq. (66) upon minimal substitution $\hat{\boldsymbol{p}} \rightarrow \hat{\boldsymbol{p}} + \boldsymbol{A}$. Likewise, in PPT there is also a two-electron Darwin operator and a corresponding term involving the potential within the DPT scheme. Note that these terms are in an approximate way accounted for if, in addition to the nuclear potential V_N, an effective electron-electron repulsion (e.g. the Coulomb potential of Eq. (27) plus an exchange term) is used in Eq. (61). Another important term is the spin–other-orbit operator

$$\hat{H}^{\mathrm{SOO}} = -\frac{i}{c^2} \sum_{l \neq k} \hat{\boldsymbol{S}}_k [(\hat{\boldsymbol{p}}_k V_{kl}) \times \hat{\boldsymbol{p}}_l] \tag{67}$$

which arises from the transformation of four-component relativistic corrections to $1/r_{kl}$ to to-component form and is again accompanied by an appropriate 'gauge correction' or 'diamagnetic' term. Further, we note that a term formally equivalent to Eq. (59e) is obtained for the spin–spin interaction $\hat{H}^{\mathrm{SS}}$ between pairs of electrons by replacing the magnetic moment $\boldsymbol{\mu}_A$ of the nuclei by its electronic counterpart $\boldsymbol{\mu}_s$ and considering distance vectors $\boldsymbol{r}_{kl}$ between two electrons instead of distances $\boldsymbol{r}_A$ between an electron and a nucleus as in Eq. (59e):

$$\hat{H}^{\mathrm{SS}} = -\frac{1}{c^2} \sum_{l \neq k} \hat{\boldsymbol{S}}_k \left[\hat{\boldsymbol{S}}_l \left(\boldsymbol{\nabla}_l \cdot \frac{\boldsymbol{r}_{kl}}{r_{kl}^3} \right) - (\hat{\boldsymbol{S}}_l \cdot \boldsymbol{\nabla}_l) \frac{\boldsymbol{r}_{kl}}{r_{kl}^3} \right] \tag{68}$$

Just as in Eq. (59e), Eq. (68) also leads to a contact term (now between pairs of electrons) upon differentiation of the $\boldsymbol{r}_{kl}/r_{lk}^3$ terms. $\hat{h}^{\mathrm{FC}} + \hat{h}^{\mathrm{SD}}$ arises from considering the interaction of an electron spin with a nuclear spin instead.

It has to be noted that the additional terms (58) in the Hamiltonian due to magnetic fields are based on a nonrelativistic treatment, and perturbational relativistic corrections have been obtained at the end of this section. Starting from a nonrelativistic energy expression, relativistic corrections to, say, NMR observables, or polarizabilities are third-order perturbational properties. When the treatment starts from a variational relativistic energy expression in zeroth-order, the relativistic corrections are, of course, included in the final results already in the second-order perturbational treatment. Therefore, it depends somewhat on the energy expression to start with which property is 'second-order', and which is 'third-order'. It is also important to note again that the terms in the Hamiltonian due to electromagnetic fields are of a different form if they are derived from a relativistic Hamiltonian that is correct to higher orders in c^{-2} or directly within the four-component scheme. The expressions given in Eqs. (59a)–(59f) are then recovered from these modified operators in the non-relativistic limit ($c^{-2} \rightarrow 0$), while the relativistic field corrections listed here can be obtained to first-order in c^{-2}. We refer to the literature for further details [50,56,73,77–88].

3. Applications of the theory

In this section we discuss a number of properties based on the general formulae given in the theoretical section. The properties are grouped into static properties (time-independent perturbation) and dynamic ones (time-dependent perturbation). As already mentioned in the introduction, emphasis will be put on DFT applications because of their current practical importance. Furthermore, if relativistic methods are available we will emphasize those in favor of more traditional nonrelativistic approaches because they allow, e.g. for detailed comparisons between molecules containing 3rd, 4th and 5th row transition metals. This is in particular the case for NMR properties because of their pronounced sensitivity to relativistic effects.

Most of the quantities discussed in the following are 2nd rank tensors, defined by the second derivative of the energy with respect to perturbations that have three vector components each. In most cases, only the isotropic value, i.e. the rotational average $a = (1/3)(a_{xx} + a_{yy} + a_{zz})$ of the tensor a is routinely determined in experiments. We will below use non-boldface symbols a for the isotropic value of a tensor quantity a.

3.1. Static properties

3.1.1. NMR chemical shifts

Classically, the interaction of a nuclear magnetic moment with an external magnetic field $\boldsymbol{B}$ is given by

$$E = -\boldsymbol{\mu}_A \cdot \boldsymbol{B} \tag{69}$$

where $\boldsymbol{B}$ is an external static homogeneous magnetic field, and $\boldsymbol{\mu}_A$ is the spin magnetic moment of the respective nucleus. For nuclei in atoms or molecules, however, it is experimentally observed that the external field is shielded by the electrons and the nucleus interacts with an effective field such that

$$E = -\boldsymbol{\mu}_A \cdot (1-\boldsymbol{\sigma})\boldsymbol{B} \tag{70}$$

Here, $\boldsymbol{\sigma}$ is the nuclear shielding tensor for a nucleus A in a given environment. Quantum mechanically, Eq. (70) can also be derived from a second-order perturbational treatment as in Section 2, considering the presence of an external magnetic field and nuclear spins. Since the nuclear Zeeman operator $-\boldsymbol{\mu}_A \cdot \boldsymbol{B}$ is usually not included in the zero-order quantum chemical computations, the nuclear shielding tensor is given by

$$\boldsymbol{\sigma}_A = \left.\frac{\partial^2 E}{\partial \boldsymbol{B} \partial \boldsymbol{\mu}_A}\right|_{\boldsymbol{B}=0,\boldsymbol{\mu}_A=0} \tag{71}$$

in formal agreement with Eq. (70). $\boldsymbol{\sigma}$ is dimensionless and is usually reported in units of 10^{-6} (part per million = ppm). Its rotational average σ is the isotropic shielding constant. Experimental data from nuclear magnetic resonance (NMR) spectroscopy usually refer to the chemical shift of a nucleus, i.e. the change of σ with respect to a reference nucleus in a reference compound. The chemical shift δ in terms of the shielding constants of the two nuclei is given by

$$\delta = \sigma^{\text{reference}} - \sigma \tag{72}$$

The nuclear shielding is a property that depends on the electronic structure very close around the nuclei. In a formalism based on orthogonal molecular orbitals, the valence orbitals necessarily influence this electronic structure close to the nuclei and are in fact largely responsible for the chemical shift. Because of the dependency of the nuclear shielding on the electronic structure close to the nuclei it is not very surprising that relativistic NMR effects are very large for heavy elements. In particular during the last decade, the computation of NMR shieldings based on relativistic methods has been very successful in explaining experimental trends such as the normal and inverse halogen dependence of chemical shifts in classes of compounds as different as organic halides and Pt complexes.

From the operators listed in Section 2.4, the ones linear in either $\boldsymbol{\mu}_A$ or $\boldsymbol{B}$ or bilinear in both of these quantities are responsible for the nuclear shielding based on Eq. (9). In a nonrelativistic formalism, from inspection of the operators in Section 2.4 it becomes obvious that these are the orbital Zeeman term (59a), the paramagnetic orbital term (59c) and the diamagnetic shielding term (59d). The spin Zeeman term also depends on the external field but does not contribute to the shielding tensor for nonrelativistic closed shell systems. The same holds for the Fermi-contact (FC) and spin-dipole (SD) operators (59e) which depend on $\boldsymbol{\mu}_A$. Generally, $\hat{H}^{(0,1)} = \hat{A}^{(0,0)} = \partial \hat{H}^{\text{OZ}}/\partial \boldsymbol{B}|_{\boldsymbol{B}=0}$ is used for the determination of the perturbed orbitals for reasons of effectiveness, since otherwise the set of perturbed orbitals with respect to $\partial \hat{H}^{\text{OP}}/\partial \boldsymbol{\mu}_A|_{\boldsymbol{\mu}_A=0}$ for each of the nuclei of interest needs to be calculated. The diamagnetic shielding term gives rise to a contribution from $\hat{H}^{(1,1)}$ in Eq. (9) which is simply evaluated as an expectation value with the ground state density. Additional terms arise within a relativistic treatment. In particular when spin–orbit coupling is included in the unperturbed wavefunction, non-zero contributions from the FC and SD operators occur that can cause large spin–orbit induced changes of the nuclear shielding. A prominent example is the proton shielding in the series HX, X = F, Cl, Br, I. The possibility of spin–orbit induced contributions of the FC and SD operators to the nuclear shielding has already been discussed in the late 1960s [89], and computational evidence has soon been provided [90,91]. The problem still receives attention [92–98]. Scalar relativistic corrections to nuclear shieldings, in particular for heavier nuclei, have attracted the attention of theoretical researchers mainly only during the last decade.

The computational methodology for nuclear shieldings has been reviewed several times in the past. See, e.g. Refs. [99–104] and the annual reviews by C. Jameson in Nucl. Mag. Res. There has been a tremendous interest in the computation of nuclear shieldings over the past decades. Theoretical studies, however, have long focused on small molecules with light main group atoms. Reviews with emphasis on transition metal complexes usually focus on DFT methods, such as Refs. [105–107], and the importance of relativistic effects (in particular spin–orbit coupling for ligand shieldings and scalar relativistic effects for metal shieldings) is frequently pointed out in these articles. Applications of DFT and/or relativistic methodology deal, e.g. with oxo-complexes [74,75,108,109], Mo chemical shifts [110,111], Ru complexes [112], transition metal carbonyls [74,93,113–119], Pt complexes [120], tungsten halides and oxides [121], Nb and Ti compounds [122,123], Hg compounds [124,125], ferrocene [107], uranium compounds [126] or W and Pb complexes [127]. An article specifically dedicated to the relativistic computation of NMR nuclear shieldings and spin–spin coupling constants has been recently prepared by the present authors [98].

Table 1 displays ^{13}C chemical shifts of 5d transition metal carbonyls, computed with some different relativistic methods. For light atomic ligand shieldings, the relativistic effects can be effectively treated by the use of 'effective core potentials' ECPs (the words 'effective' and 'effectively' in this sentence are not related to each other, but nevertheless the use of ECPs is often computationally less expensive than the usage of more direct relativistic methods). Spin–orbit effects can also be treated by ECPs which is much less common yet in standard applications. Recently, the authors of Ref. [97] have implemented the use of spin–orbit ECPs for the computation of nuclear magnetic shieldings, with good results as demonstrated by the data in Table 1. The

Table 1
^{13}C chemical shifts in 5d transition metal carbonyls, from DFT calculations

Compound	δ exp. [a]	Pauli [b]	Pauli-SO [c]	SO-ECP [d]
$[Hf(CO)_6]^{2-}$	244	228.3	234.5	228.2
$[Ta(CO)_6]^{-}$	211	211.8	214.8	206.0
$W(CO)_6$	192	197.7	196.7	188.6
$[Re(CO)_6]^{+}$	171	183.9	176.2	173.7
$[Os(CO)_6]^{2+}$	147	172.4	149.5	153.9
$[Ir(CO)_6]^{3+}$	121	153.6	125.8	130.9
$[Au(CO)_2]^{+}$	174		165.3	164.0
$[Hg(CO)_2]^{2+}$	169		158.2	154.0

[a] As compiled in Refs. [93,97], with respect to TMS.
[b] Scalar relativistic Pauli operator (variational procedure employing frozen cores), Ref. [118].
[c] Pauli operator including spin–orbit coupling (variational procedure employing frozen cores), Ref. [93].
[d] Spin–orbit ECPs, Ref. [97].

results are very similar to the two-component relativistic values obtained by Wolff and Ziegler in 1998 [93] with the Pauli Hamiltonian (61) (and frozen cores to keep the variational instability under control). In comparison, the scalar relativistic results are much less accurate, in particular for the metals with higher group numbers. This at first sight unintuitive trend for the magnitude of spin–orbit corrections has been explained in detail in Ref. [93].

So far, a consistent treatment of heavy nucleus shieldings within a pseudopotential formalism has not been presented, and therefore theoretical investigations of shielding constants for the metal atom in transition metal complexes have been carried out with all-electron or frozen-core methods either nonrelativistically, or by including relativistic effects directly. Table 2 lists the case of ^{199}Hg chemical shifts. For such a heavy nucleus, a relativistic formalism is vital. We are not aware of a currently implemented post-Hartree–Fock method by which nuclear shieldings of heavy elements could be computed in molecules, therefore the data that are presented here are based on relativistic Hartree–Fock and DFT computations. Generally, DFT methods are able to reproduce experimentally observed trends for chemical shifts with sufficient accuracy in order to allow for an interpretation of the results, since electron correlation is treated at least in an approximate manner. From Table 2 it can be seen that for Hg chemical shifts the Hartree–Fock method can yield satisfactory results as well. The last three rows of Table 2 indicate the importance of solvent effects in the experimental environment, that in principle need to be modeled in the computations. Ammonia has been used in the computations in order to simulate the experimentally used solvent pyridine. The effects on the chemical shifts are very substantial, and rather well reproduced in the computations at a quite simplified level regarding the consideration of solvent effects.

Table 2
^{199}Hg chemical shifts

Compound [a]	δ exp. [b]	DFT [c]	HF
$Hg(SiH_3)_2$	+196		+232 [d]
$Hg(GeH_3)_2$	−147		−289 [d]
HgMe(CN)	−766	−861	
$Hg(CN)_2$	−1386	−1724	
HgMeCl	−861	−943	
HgMeBr	−915	−1068	
HgMeI	−1097	−1025	
$HgCl_2$	−1519	−1556	(−1519) [e]
$HgBr_2$	−2213	−2684	−2134/−3191 [e]
HgI_2	−3447	−3506	−2371/−4130 [e]
$HgCl_2(NH_3)_2$ [f]	−1280 [g]	−1086	
$HgBr_2(NH_3)_2$ [f]	−1622 [g]	−1858	
$HgI_2(NH_3)_2$ [f]	−2355 [g]	−2836	

[a] (Me = CH_3).
[b] With respect to $HgMe_2$, as compiled in Refs. [86,125]. Solvent for HgX_2 has been THF (except for the last 3 rows).
[c] DFT calculations with the two-component relativistic ZORA [54,128] method, Ref. [86].
[d] Hartree–Fock computations based on the two-component Douglas–Kroll operator [51], Ref. [125].
[e] Hartree–Fock computations with the scalar relativistic Douglas–Kroll operator and the Pauli SO operator, Ref. [124]. Data reported with respect to $HgCl_2$, therefore, the value for $HgCl_2$ has been set equal to the experimental shift here. Results were obtained with two different basis sets. The shifts obtained with the 'external field projectors' (see Ref. [124]) are displayed.
[f] NH_3 to simulate the solvent pyridine in the computations.
[g] Experimental values for HgX_2 in pyridine.

Kaupp et al. [109] have compared DFT and ab-initio approaches for ^{17}O chemical shifts of transition metal oxo-complexes, employing scalar relativistic ECPs on the metal center. These properties have also been studied by a scalar relativistic DFT method in Ref. [74], again employing the Pauli operator and frozen cores. The data are summarized in Table 3. It can be seen that for these compounds the ab-initio computations produce unreasonable results that, in particular in the MP2 case, do not seem to have much physical meaning. The DFT methods perform rather well in comparison. This and other such examples reported in the literature have perhaps led the authors of a recently published textbook, Ref. [129], to the statement that "density functional approaches are probably the only means available today to obtain reasonably accurate results for NMR and ESR properties". The relativistic effects are rather pronounced for the 6th row metals (reducing, e.g. the oxygen shielding in WO_4^{2-} by $\sim$50%) and obviously well reproduced at the scalar relativistic level employed in the computations, since the agreement with experimental data is quite satisfactory for all the DFT methods.

As already mentioned, within the usual finite basis set approximations correction terms to the NMR shielding tensor arise that stem from a treatment of the so-called gauge dependency problem. This issue has been dis-

Table 3
^{17}O chemical shielding constants [$\times(-1)$] in transition metal oxo complexes [a]

Compound	δ exp. [b]	BP86 [c]	BP86 [d]	BP86 [e]	B3LYP [d]	HF [d]	MP2 [d]
WO_4^{2-}	129	140	157	138	183	194	21
MoO_4^{2-}	239	216	251	231	289	335	60
CrO_4^{2-}	544	446	508	490	640	1308	−2173
ReO_4^-	278	278	282	277	339	464	−3
TcO_4^-	458	405	421	410	518	819	−184
MnO_4^{2-}	939	778	832	821	1149	7248	−54485
OsO_4	505	521	517	503	657	1295	−1069
RuO_4	815	740	765	733	1037	3330	−8262

[a] Experimental data has been converted to absolute ^{17}O shieldings based on a value of 290.9 ppm for $\sigma(^{17}O)$ of liquid water at room temperature [109]. All values in the table have been multiplied by −1.
[b] As compiled in Ref. [109].
[c] Scalar relativistic DFT, Pauli operator with frozen core, GIAO, Ref. [74].
[d] Scalar relativistic ECP, GIAO, Ref. [109].
[e] Scalar relativistic ECP, IGLO, paramagnetic term semi-empirically scaled ('SOS-DFT'), Ref. [109].

cussed numerous times in review articles dealing with NMR [102–104], therefore we will not elaborate on details. In short, the vector potential $\boldsymbol{A}$ related to the external magnetic field by Eqs. (53a) and (53b) is not uniquely defined, since the gradient of any scalar function can be added to $\boldsymbol{A}$ without changing the $\boldsymbol{B}$-field. This can be translated to a gauge change for $\boldsymbol{A}$ upon different choices for the coordinate origin. In a complete basis set, expectation values with the exact and various types of model wavefunctions or within DFT methods do not depend on the coordinate choice, but this does no longer hold for finite basis sets. In order to enforce gauge invariance of the nuclear shieldings, basis functions can be introduced that are correct to first-order in the external magnetic field such that expectation values are no longer origin dependent, but at the same time the basis becomes dependent on the perturbation. This problem can be dealt with using standard methodology that has been developed in order to compute accurate nuclear gradients of the energy [8,37], which leads to additional terms in the expression for the shielding tensor that vanish for increasing basis set size. Compared to the nuclear gradients, the correction terms in NMR are rather small. Nevertheless they are very important in order to calculate reliable nuclear shieldings, since these quantities are extremely sensitive and small changes are significant for experimental and theoretical interpretations. As of today, most NMR implementation deal explicitly with the gauge invariance problem. Two popular methods are the 'gauge including/independent atomic orbitals' (GIAO) [12,13] and the 'independent gauge for localized orbitals' (IGLO) [14] methodologies. See reviews dedicated to NMR computations for details and further Refs. [102–104]. Gauge correction terms are further necessary in other computations of properties that are related to perturbations by an external magnetic field, such as ESR **g**-shift tensors (Section 3.1.3), magnetizabilities (Section 3.1.4), CD (Section 3.2.3), VCD (Section 3.3), and optical rotations (Section 3.2.3).

3.1.2. Nuclear spin–spin couplings

In analogy to Eq. (69), the nuclear spin-Hamiltonian describes the interaction between pairs of nuclear spins in a molecule as

$$E = \boldsymbol{\mu}_A \mathsf{K}_{AB} \boldsymbol{\mu}_B \tag{73}$$

for each pair of nuclei. The reduced nuclear spin–spin coupling tensor for two nuclei A and B in a molecule is in formal agreement with the last equation given by

$$\mathsf{K}_{AB} = \left.\frac{\partial^2 E}{\partial \boldsymbol{\mu}_A \partial \boldsymbol{\mu}_B}\right|_{\boldsymbol{\mu}_A=0,\boldsymbol{\mu}_B=0} \tag{74}$$

As in Eq. (71), $\boldsymbol{\mu}_A$ and $\boldsymbol{\mu}_B$ refer to nuclear magnetic moments. The spin–spin coupling is always present in a molecule independent of an external magnetic field but is usually observed in NMR chemical shifts measurements as the fine structure of the spectrum. However, there exist other valuable experimental sources for spin–spin coupling constants and chemical shieldings that have long been overlooked by many chemistry researchers [130]. The rotational average of K_{AB} is the isotropic reduced coupling constant K_{AB}. Theoretical data are usually reported in SI units of kg m^{-2} A^{-2} s^{-2} with a typical magnitude of 10^{19} to 10^{22}. Experimentally observed are the spin–spin coupling constants J_{AB} in units of Hertz. Their relation to the reduced coupling constants is

$$J_{AB} = \frac{h}{4\pi^2}\gamma_A\gamma_B K_{AB} \tag{75}$$

Since the J coupling constants depend on the nuclear magneto–gyric ratios γ, comparisons of spin–spin coupling constants for different types of nuclei are more straightforward when referring to the K values instead.

The spin–spin coupling tensor consists of a direct dipolar coupling between the nuclei, which is described by a Hamiltonian equivalent to the SD operator (60b) but with the electron's spin magnetic moment $\hat{\boldsymbol{\mu}}_s = -\hat{\boldsymbol{S}}$ (or $-(g/2)\hat{\boldsymbol{S}}$) replaced by the spin magnetic moment $\boldsymbol{\mu}_B$ of another nucleus, and $\boldsymbol{r}_A$ replaced by the distance vector $\boldsymbol{r}_{AB}$ between the nuclei. The resulting operator does not depend on the electronic coordinates and can therefore be evaluated without any knowledge of the wavefunction/orbitals. However, the direct coupling does not contribute to the coupling tensor in case of rapidly rotating molecules (solution/gas phase) and will not be considered further, since most experimental data up to date refers to measurements in solution or gas phase. If the molecules are not freely rotating, such as in solids or due to alignment in liquid crystals or by magnetic fields, the direct coupling becomes important [131].

Operators listed in Section 2.4 that are either linear or bilinear in the nuclear magnetic moments (and not depending on an external field) contribute to K_{AB}. Among the nonrelativistic operators are the OP term (59c), the FC and SD terms (59e), and the OD term (59f). Relativistic effects are very pronounced for nuclear spin–spin couplings and affect in particular the contributions due to the FC term.[3] This has early been recognized [132] and resulted in the use of semiempirical relativistic scaling factors for AO contributions to the Fermi-contact term in molecular calculations [133]. Spin–orbit coupling induces mainly cross terms between the FC and the OP term that are zero in the nonrelativistic or scalar relativistic limit [134–137]. The OD term is responsible for a 'diamagnetic' $\hat{H}^{(1,1)}$ contribution in Eq. (9) that is often completely negligible, but easy to compute. However, there are exceptions such as the proton–proton coupling in water, where the diamagnetic term is quite large. Likewise, the SD term is often negligible, and in practice often neglected because it is rather difficult and expensive to compute. Counter examples, for which the SD term is rather large, are interhalogen diatomics [138,130] or triple bonded molecules such as CO or N_2 [139,140]. In a nonrelativistic formalism, the Fermi-contact term, which often leads to the by far largest individual contribution to nuclear spin–spin couplings, probes the electron density at the nuclei. In order to obtain a non-negligible coupling constant, it is necessary that the densities of individual orbitals that contribute to the coupling[4] are large at both nuclei simultaneously, which illustrates why nuclear spin–spin coupling can be considered a valence shell property [141] since core shells do not have a significant electron density at other nuclei. It was previously found that accurate results can be obtained also within a frozen core formalism. However, the requirements on the basis set do not allow for a drastic reduction of the computation time as compared to all-electron calculations [87]. Only the contributions from s-type basis functions to a bond orbital yield density *at* the nuclei, therefore, the nuclear spin–spin coupling K_{AB} effectively probes the s-character of a chemical bond between A and B.[5] For couplings between nuclei that are separated by more than one bond, such a simple explanation does not necessarily hold. Likewise, the explanation is only meaningful if the coupling constant is indeed largely determined by the FC term. However, counter examples are known some of which have been analyzed in detail very recently [138].

In comparison to the nuclear shielding tensor, the spin–spin coupling has—despite its importance in experimental research—received far less attention. Overviews covering theoretical applications mostly to light atomic main group compounds can be found, e.g. in Refs. [101,104,130,139] and in the previously mentioned annual reviews by C. Jameson. First principles relativistic computations of K_{AB} involving heavy nuclei have only been carried out since 1999 [87,95,136–138,142,143], even though theoretical approaches have been outlined much earlier [81,85]. Not many applications to heavy transition metal complexes are available so far. Much has been learned from extended relativistic Hückel calculations [144–146], but the semiempirical nature and the drastic simplifications of the approach do not permit reliable calculations. However, the data that have been gathered so far with first-principles methods indicate that a relativistic formalism is vital in all cases where coupling constants to a heavier metal in metal complexes are to be studied. Already for 3d metals, the relativistic effects on the coupling constants can be of the magnitude of 10% of the total value, and they often exceed 100% for couplings of light elements to 5d metals. Therefore, we will focus on relativistic computations in the following, since future theoretical studies of spin–spin couplings in transition metal complexes will likely need to take relativistic effects into consideration. In case that only couplings between the ligands are of interest, scalar relativistic ECP can be used effectively, see Ref. [147] for an example (Os(II)-complexes). An application of a relativistic method based on the Pauli operator and frozen cores to metal–ligand couplings in a number of transition metal complexes can be found in Ref. [148]. This method is

[3] More precisely, in relativistic methods there is usually no actual 'contact' term due to a delta function but some analogue that heavily weights the close vicinity of the nuclei.

[4] Of course, such orbitals contributions are not uniquely defined since it is somewhat arbitrary how to split up an expectation value into individual contributions.

[5] A similar argument holds in the relativistic case, and/or for extended (not pointlike) nuclei.

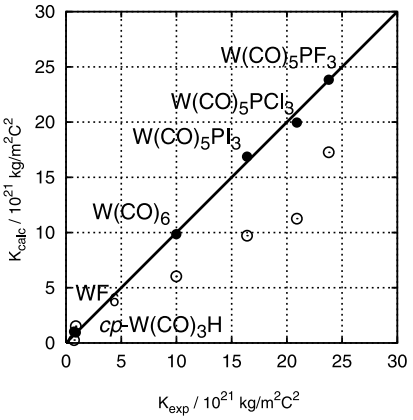

Fig. 1. One-bond metal–ligand spin–spin coupling constants (W–C, W–H and W–F, absolute values) in some tungsten complexes, in 10^{21} kg m^{-2} A^{-2} s^{-2}. Data based on nonrelativistic (open markers) and ZORA scalar relativistic (filled markers) DFT computations, from Ref. [87].

somewhat related to the use of scaling factors that we mentioned earlier. However, from the available applications to main group compounds it is known that a variationally stable all-electron method should preferably be used in case the coupling to a heavier nucleus is of interest. For applications and benchmark data, see e.g. Refs. [149–153] (semiempirical, scaling factors, Group 14 compounds), [154] (four component Hartree–Fock, H_2X (X = O–Te)), [95] (four component Hartree–Fock, HX (X = F–I)), [142] (four-component Hartree–Fock, Group 14 compounds), [134,155] (first-order spin–orbit corrections in Hartree–Fock and correlated ab-initio methods, HX (X = F–I), H_2X (X = O–Te), PbH_4). So far, mostly one-bond couplings have been studied theoretically. Fig. 1 displays some metal–ligand coupling constants that have been calculated for various tungsten complexes by a NMR implementation [87,136] based on a scalar relativistic DFT method (the so-called ZORA method [54,128]). The agreement with experiment is excellent and demonstrates the possible accuracy of the methodology. Spin–orbit corrections have shown to be of minor importance for couplings to transition metal elements, but they can be vital for heavy p-block elements (I, Tl, Pb) [136–138]. In a subsequent study [137], it was also resolved why a much less favorable accuracy had originally [87] been obtained for linear Hg and square planar Pt complexes. As in the previously mentioned case of Hg chemical shifts (see Table 2), coordination of solvent molecules to the metal has to be taken into account. In the case of spin–spin coupling constants, even such solvents that can be considered as 'inert' for chemical shifts have a substantial influence on the magnitude of the results. See Table 4 for some illustrative examples. The solvent effect has been analyzed in detail in Ref. [137] and can be attributed to charge donation from solvent lone-pairs into the metal–ligand bonds. It generally appears to increase the magnitude of the coupling constants of this type (dominated by a Fermi-contact mechanism), since the charge donation has its most significant influence on the magnitude of the sensitive Fermi-contact contribution which rises with increasing charge in binding metal–ligand σ-orbitals. For the test set of 23 metal–ligand coupling constants studied in Refs. [87,137], a comparison of theoretical and experimental data is displayed in Fig. 2. As can be seen, a quite uniformly good performance of the computations demonstrates the applicability of relativistic DFT methods to problems in transition metal NMR spectroscopy.

It has been demonstrated earlier, that the inclusion of electron correlation has a significant influence on spin–

Table 4
Computed Hg–C one-bond spin–spin couplings K for the solvated compounds HgMeX (Me = CH_3, X = Me, Cl, Br, I) and $Hg(CN)_2$, in 10^{20} kg m^{-2} A^{-2} s^{-2} (data taken from Ref. [137])

Compound	Solvent	+2 Solv. [a,b]	+3 Solv. [a,b]	+4 Solv. [a,b]	Expt.
HgMeCl	$CHCl_3$	223.5	233.5	277.1 261.5 [d]	263.1
	DMSO	260.3	295.2		307.8
HgMeBr	$CHCl_3$	218.9	227.2		256.3
	DMSO	253.8	293.6		299.9
HgMeI	$CHCl_3$	192.9	241.2		239.3
	DMSO	251.0	295.4		283.1
$HgMe_2$ [c]	$CHCl_3$	108.0	121.8		126.6
	DMSO	118.5	130.7		133.4
$Hg(CN)_2$ [c]	MeOH	513.1		576.2 560.7 [d]	577.8
	THF	511.5		581.8	558.5

[a] Coupling constant for the complex including the number of specified solvent molecules DFT, BP86 functional.
[b] Scalar ZORA computation, SD term neglected.
[c] Mean value of both Hg–C coupling constants.
[d] ZORA spin–orbit computation including the SD term.

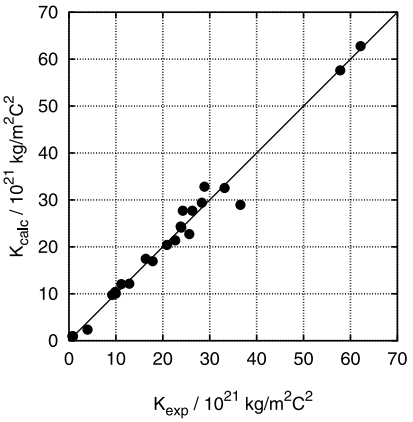

Fig. 2. Metal–ligand one-bond spin–spin coupling constants in complexes containing W, Pt, Hg and Pb, in 10^{21} kg m^{-2} A^{-2} s^{-2} (absolute values). Data based on scalar ZORA relativistic DFT computations, from Ref. [87,137]. For coordinatively unsaturated complexes (Hg, Pt), metal coordination by the solvent has been considered by completing the first coordination shell with solvent molecules.

spin couplings, and that Hartree–Fock calculations perform rather poorly [134,135,142]. Electron correlation is to some extent included in the DFT computations, and the accuracy of the NMR parameters is quite good in particular for the heavier elements where local density approximations (LDAs) perform already quite well. It should be noted, however, that spin–spin coupling constants in light atomic systems are much more sensitive to the choice of the functional, and it also appears that they are more sensitive towards the choice of the XC potential than nuclear shieldings (for some examples see Ref. [156]). For coordinatively unsaturated complexes, the computational data in Fig. 2 are based on optimized geometries in which the first coordination shell has been filled by solvent molecules. The overall agreement with experiment is favorable. In Ref. [143], a Pt–Tl cyano complex has been studied with the same computational approach. There, the effects of solvent complexation on the spin–spin couplings could rationalize some very unintuitive features in the experimental spectrum that had originally lead to a rather controversial, but nevertheless correct, assignment of the spectrum [157,158].

3.1.3. EPR observables

3.1.3.1. The g-tensor. Electron paramagnetic resonance (EPR) is observed when placing a paramagnetic molecule in an external magnetic field $\boldsymbol{B}$. If the effect is entirely due to a non vanishing spin magnetic moment $\boldsymbol{\mu}_s$ related to an effective spin vector $\boldsymbol{S}$ of the molecule, sometimes the term 'electron spin resonance' (ESR) is preferred [56]. We will entirely focus on the latter here. In analogy to the NMR shielding tensor, the ESR $\Delta\mathbf{g}$-tensor can be defined via an effective spin Hamiltonian that includes the interaction of the electron spins with an external magnetic field and with each other (note that we introduce here the factor $g/2$ that has already been mentioned in Section 2.4:

$$\hat{H}^{\text{eff}} = \frac{1}{2}\boldsymbol{B}(g + \Delta\mathbf{g})\hat{\boldsymbol{S}} + \hat{\boldsymbol{S}}D\hat{\boldsymbol{S}} \tag{76}$$

Eq. (76) follows the usual sign conventions for $\Delta\mathbf{g}$. The eigenvalues of the effective spin-Hamiltonian are intended to correspond to the experimentally observed energy levels. D is responsible for a zero-field splitting caused by the electron spin–spin interaction due to the operator (68) in analogy to the coupling K between nuclear spins, but it can be neglected from the discussion for the limit of a strong external field. The spin Zeeman term (59b) is related to the free electron g value and can therefore be omitted from the computations. In this case, the $\Delta\mathbf{g}$ tensor is in formal agreement with the eigenvalues of the spin-Hamiltonian (76) given as

$$\Delta\mathbf{g} = 2\frac{\partial^2 E}{\partial\boldsymbol{B}\partial\boldsymbol{S}}\bigg|_{\boldsymbol{B}=0,\boldsymbol{S}=0} \tag{77}$$

where the derivative with respect to a nuclear magnetic moment in the case of NMR shieldings is replaced here by the derivative with respect to the electronic spin vector $\boldsymbol{S}$ of the molecule (which is proportional to its spin magnetic moment). $\Delta\mathbf{g}$ is dimensionless just as the NMR shielding tensor, and results are typically reported in units of 10^{-6} (ppm) or 10^{-3} (part per thousand, ppt). Note that the spin $\boldsymbol{S}$ and the spin operators $\hat{\boldsymbol{S}}$ are dimensionless here, while the factor 1/2 in Eq. (76) stems from the Bohr magneton converted to atomic units.

A technical difficulty arises here as compared to the last paragraphs where the nuclear magnetic moments and the external field could be directly used as the perturbation parameters. This is because the electron spin in the operators in Section 2.4 are given in terms of the spin-operator $\hat{\boldsymbol{S}}$ whereas the derivative of the energy has to be taken with respect to the spin vector, not the operator. Suppose we write a spin-dependent one-electron operator for the z component of $\hat{\boldsymbol{S}}$ in the form $\Sigma_k\, \hat{h}(\boldsymbol{x}_k)$ with $\hat{h}(\boldsymbol{x}) = \hat{a}_z(\boldsymbol{r})\hat{S}_z$, its action on the wavefunction, after integration over spin, is

$$S_z\hat{a}_z(\boldsymbol{r})Q_z(\tilde{\boldsymbol{r}},\boldsymbol{r})|_{\tilde{\boldsymbol{r}}=\boldsymbol{r}} \tag{78}$$

with $Q_z(\tilde{\boldsymbol{r}},\boldsymbol{r})$ being the *normalized* spin density [6] and S_z the maximum value of the projection of the spin onto the quantization axis. Taking the derivative $\partial/\partial S_z$ is now straightforward and yields $\hat{a}_z(\boldsymbol{r})Q_z(\tilde{\boldsymbol{r}},\boldsymbol{r})|_{\tilde{\boldsymbol{r}}=\boldsymbol{r}}$. From this, it can be seen that the derivatives of the spin-dependent operators in Section 2.4 with respect to the spin result in the spin-free part of these operators acting on the normalized spin density. According to the procedure of 'spin-field reduction', the external field direction determines the axis of spin-quantization and

consequently by taking derivatives of spin-dependent operators with respect to the x, y or z-component of the spin will involve the action of each spatial component of the operator on the same spin density matrix $Q_z(\tilde{\boldsymbol{r}}, \boldsymbol{r})$, respectively [160]. In orbital-based methods, the normalized spin density and the spin density differ by a factor of $S_z = (n_\alpha - n_\beta)/2$, with n_γ being the number of occupied orbitals for spin γ. Recently, in Ref. [159], the density functional ESR formulation of Schreckenbach and Ziegler [160] could be extended to systems with $S > 1/2$. This simply leads to an additional factor of $(n_\alpha - n_\beta)^{-1}$ in the final equation of the original formulation in Ref. [160] which was based on Eq. (77) for the case $S = 1/2$, i.e. $(n_\alpha - n_\beta) = 1$. This can be easily rationalized from Eq. (78). We refer to the literature (e.g. Ref. [56,161]) for a discussion of the more conceptual problems related to the effective Hamiltonian, its eigenvalues, and their proper relation to experimentally determined values for the components of $\Delta\mathbf{g}$. It should also be noted that the '**g**-tensor' and some other tensors related to magnetic properties do not necessarily transform as proper (in a strict mathematical sense) tensors under spatial rotations, therefore the use of the word 'tensor' in this context can be somewhat misleading [161].

The **g** tensor relates the spin magnetic moment to the spin itself. In nonrelativistic quantum mechanics, these electronic spin degrees of freedom are completely independent from the electrons motions through space,[6] i.e. the electronic spin magnetic moment does not 'see' the molecular environment. It is thus evident that there needs to be spin–orbit coupling present in order to observe any change $\Delta\mathbf{g}$ as compared to the free electron g value when comparing the magnetic resonance of free electrons and electrons bound in a molecule. Therefore, no effect can be calculated from an entirely nonrelativistic formalism. Consequently, the contribution due to the one-electron SO operator (63) has been found to be the leading term in the $\Delta\mathbf{g}$-tensor. Operators listed in Section 2.4 that are linear in the electron spin operator or the external magnetic field or bilinear in both perturbations contribute to the $\Delta\mathbf{g}$-tensor within the second-order perturbation theoretical approach. This is on the one hand the $\boldsymbol{B}$-dependent OZ term, for which—as in the NMR shieldings case—the perturbed wavefunction/orbitals can be evaluated first (including necessary gauge correction terms, see Section 3.1.1). Linear in the electron spin operator, on the other hand, are the SO operator (63) and its two-electron counterpart (66), and the SOO operator (67). Bilinear in both perturbations are the $\hat{\boldsymbol{p}}^2$ part of the SZ″ term (64) as well as the 'gauge correction' or 'diamagnetic' terms due to the SO (65), eeSO (66), and SOO (67) operators. Often, in implementations not all of the two-electron terms are considered, or they are included in a mean-field sense. As already mentioned in Section 3.1.1 circumventing the guage problem for $\boldsymbol{B}$ can lead to additional terms in finite basis set calculations.

It has been shown that the machinery to calculate nonrelativistic NMR chemical shifts based on DFT can be used with few modifications in order to compute ESR $\Delta\mathbf{g}$ tensors [160]. Recently, a similar DFT approach including the two-electron spin–orbit terms explicitly has been published in Ref. [162], and was subsequently extended in order to include the popular hybrid functionals as well [163]. An implementation very similar to the one reported in Refs. [159,160] was published very recently [164] and is also applicable with hybrid functionals. As we have already pointed out, the question whether a quantity is a first-, second, etc. order energy perturbation depends on the choice for the zeroth-order. In case spin–orbit coupling is already present in zeroth-order, the $\Delta\mathbf{g}$ tensor (or more precisely: the squares of its elements and the sign of the product of its principle components) can be evaluated via an expectation value of the perturbation operators linear in the magnetic field [161] (orbital-, and spin-Zeeman operator and 'gauge correction' or 'diamagnetic' terms). This procedure has been implemented in a DFT code by van Lenthe et al. [165] and might prove more adequate for systems in which SO coupling is very large. However, applications of the first-order approach have so far employed a spin-restricted unperturbed solution because of technical difficulties with the description of spin density in a spin–orbit coupled context. A recent comparison of different methods can be found, e.g. in Ref. [164]. Earlier work on $\Delta\mathbf{g}$ tensors with ab-initio (Hartree–Fock, MCSCF, CI) or semiempirical methods has been reported, e.g. in Refs. [166–172]. For further references on these approaches we refer to the literature cited in Refs. [164,173]. Scalar relativistic corrections can in principle be included in all the aforementioned methods, either explicitly or via ECPs.

The code by Schreckenbach and Ziegler [160] has been applied to d^1 transition metal complexes of the type MEX_4^{n-}, with M = V, Cr, Mo, W, Tc, and Re, E = O, N, and X = F, Cl, and Br [174]. A scalar relativistic method employing the Pauli operator and frozen cores has been employed here to obtain the unperturbed Kohn–Sham orbitals. The results are displayed in Fig. 3. It can be seen that the correlation between the theoretically predicted and the experimental values is

[6] The electron spin is usually not regarded as a 'relativistic' property of the electron since it needs to be included also in a nonrelativistic theory because of empirical evidence. Relativistic theories for the electron automatically account for the electron spin. The equations can be transformed back to the nonrelativistic limit, which, e.g. results in the presence of the spin Zeeman term (59b) and the spin-dependent hyperfine terms. However, the coupling between the electron's spatial and spin degrees of freedom is a relativistic effect that vanishes for $c \to \infty$, see Eqs. (61) and (62).

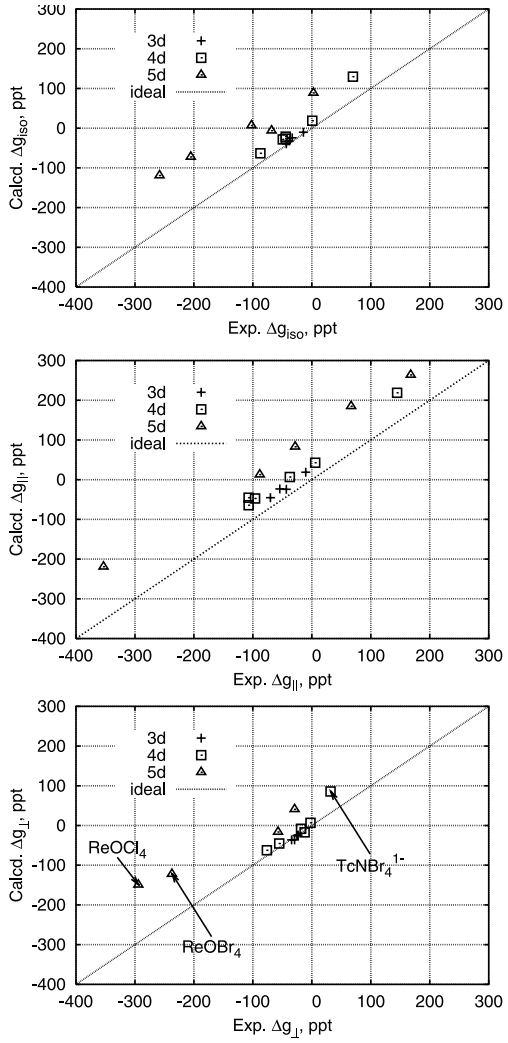

Fig. 3. Calculated vs. experimental **Δg** isotropic values and tensor components for a set of 3d to 5d transition metal complexes MEX_4^{n-}, in ppt, from Ref. [174]. $\Delta g||$ and $\Delta g_\perp$ refer to the principal components with respect to the C_4 symmetry axis of the complexes.

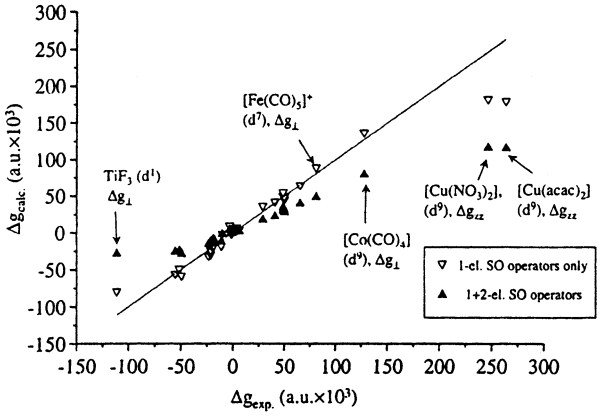

Fig. 4. Calculated vs. experimental **Δg** tensor components for a set of 3d transition metal complexes, reprinted with permission from Malkina et al., Ref. [162] © (2000) American Chemical Society.

quite reasonable for the 3d and 4d metals. The $\Delta g_{||}$ component is systematically overestimated, though, in particular for the 5d metals. While density functional computations appear to perform very well for the ESR of main group radicals, the performance of pure LDA or GGA density functionals is less satisfactory for transition metal complexes. This has been attributed in Ref. [174] to deficiencies of such density functionals that lead to an overestimation of covalent bonding between the metal and the ligands, a viewpoint that has recently been corroborated by Malkina et al. [162]. There is some evidence that hybrid density functionals perform slightly better in comparison [163,164], however, the restricted number of available data points makes a statistical evaluation difficult. Fig. 4 displays a comparison between theoretical and experimental results for various 3d transition metal complexes from Ref. [162], where the two-electron spin–orbit terms have been considered explicitly. While the inclusion of these operators resulted in an increasing accuracy for light atomic main group radicals, Fig. 4 shows clearly that this is not the case for transition metal complexes. Generally, the two-electron terms tend to reduce the effect due to the one-electron SO operator, in particular for light atomic (first and second row) compounds. Their relative importance decreases rapidly for increasing nuclear charge, as has previously been shown for total energies or NMR nuclear shieldings [175,176]. In Ref. [164], an approximate SO operator for the calculation g of **Δg** tensors has been employed that is based on effective nuclear charges in the one-electron operator (63). This corresponds to a screened nuclear potential due to the two-electron terms, which provides the desired reduction effect and very similar results to the ones explicitly based on one- and two-electron spin–orbit operators [162]. In previous applications by Ziegler and coworkers [159,160,174], some of the two-electron contributions have been simulated by the use of the effective Kohn–Sham potential in Eq. (63), but the SOO term has been neglected. At the same time, the usage of the two-electron operators in a Kohn–Sham procedure suffers from some theoretical inconsistencies the numerical consequences of which are yet unclear. In Ref. [164], the first-order ZORA approach by van Lenthe et al. [165] was also applied to the test set of 3d metal complexes, and resulted in very comparable overall accuracy compared to the other approaches (Refs. [162,174] and the data of Ref. [164]). Small linear molecules containing transition metal atoms have also been studied by the ZORA approach in Ref. [177], with reasonable agreement of the theoretical with experimental results.

Fig. 5 displays a comparison between calculated and experimental data for a number of spatially non degenerate diatomic high-spin radicals with more than one unpaired electron, containing both a main group

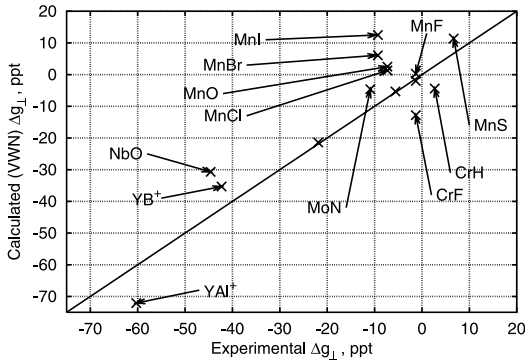

Fig. 5. Calculated vs. experimental $\Delta g_{\perp}$ values for a set of mixed main-group element–tranistion metal diatomic high spin radicals, from Ref. [156]. The $\Delta g_{||}$ values are generally very small and not displayed.

element and a transition metal [156]. It can be seen that the accuracy is not much different from what has been achieved with computations for metal complexes with one unpaired electron. In this study, reasonable accuracy has again been obtained for main-group—main-group diatomic radicals, while a significant deterioration of the results was observed for transition metal—transition metal diatomics, with a general trend of a strong overestimation of the calculated values in comparison with experiment. The case of mixed diatomics is probably more representative in order to assess the accuracy that could be expected in DFT applications to transition metal complexes with several unpaired electrons. The particular choice of a pure density functional was found to have only a very small influence on the results in this case [156]. An earlier application of ab-initio (MCSCF) methods to the calculation of diatomic nondegenerate high-spin triplet radicals can be found in Ref. [178].

Other more recent DFT applications of theoretical methods to $\Delta\mathbf{g}$ tensors of transition metal complexes include in particular studies on metal porphyrins [179,180], Fe, Ru, and Os nitrosyl complexes [181], model complexes for the active center of [NiFe]-hydrogenase [182], or biologically relevant vanadyl complexes [183].

3.1.3.2. The A-tensor. Another ESR analogue of nuclear spin–spin couplings is the A-tensor or hyperfine tensor. The effective Hamiltonian for the interaction of the electronic spin with one of the nuclear spins is [56,161]

$$\hat{H}^{\mathrm{eff}} = \boldsymbol{S}\mathsf{A}\boldsymbol{I}_A \tag{79}$$

As for the properties in previous sections, the A tensor is here in formal agreement with the eigenvalues of Eq. (79) given as

$$\mathsf{A} = \left.\frac{\partial^2 E}{\partial \boldsymbol{I}_A \partial \boldsymbol{S}}\right|_{\boldsymbol{I}_A=0,\boldsymbol{S}=0} \tag{80}$$

i.e. the effect of the presence of nuclear spin angular momentum $\boldsymbol{I}_A$ on the electronic spin in a molecular environment is investigated. Note that $\boldsymbol{\mu}_A = \gamma_A \boldsymbol{I}_A$. Eq. (80) follows a common convention for the definition of A. Values are typically given in SI units of MHz, or in c.g.s. units of G (Gauss, with a conversion factor of $\sim$ 2.8025 MHz/G [184]).

The same operators depending linearly on the electron spin as in the case of the $\Delta\mathbf{g}$ tensor, and the same operators that depend linearly on the nuclear spin magnetic moment as in the case of the nuclear spin–spin couplings, contribute to the A tensor. The FC+SD term (59e) yields the bilinear contribution due to $\hat{H}^{(1,1)}$ here, which is often very large in the case of A-tensors. As can be seen from the preceding discussion about g-shifts, the bilinear term results, due to the differentiation with respect to $\boldsymbol{S}$, in an expectation value of the FC+SD operator with the unperturbed normalized spin–density matrix. No spin–orbit coupling enters this expression if a nonrelativistic or scalar relativistic unperturbed solution is used as the starting point for the calculation. This $\hat{H}^{(1,1)}$-contribution is sometimes called 'first-order' [185–188], even though it is derived from second-order perturbation theory. The contribution due to the FC term based on a non- or scalar-relativistic spin–density matrix is isotropic, while the one due to the SD term is traceless and anisotropic. This distinction is frequently made in the literature (see, e.g. Ref. [184] and references cited therein). The remaining terms due to the OP and the spin–orbit operators then yield further isotropic 'pseudo-contact' and anisotropic contributions. As in the case of $\Delta\mathbf{g}$-tensors, it is possible to evaluate these terms within a first-order scheme in the case that the spin–orbit coupling has been included variationally in the unperturbed solution. This is the basis of the ZORA-DFT implementation of A-tensors by van Lenthe et al. [189]. Applications have so far been restricted to non-spin-polarized spin–orbit computations. From the nature of the bilinear contribution, in particular of the isotropic one due to the FC operator, it is seen that the A tensor effectively probes the spin density at the nucleus. This is in contrast to the nuclear spin–spin coupling, which probes the density at pairs of nuclei instead.

A comprehensive comparison between DFT and coupled-cluster ab-initio methods for the computation of A tensors has been recently carried out by Munzarová and Kaupp and is specifically geared towards applications to transition metal complexes [188]. They found that "none of the investigated functionals performs well for all complexes", including hybrid functionals. The coupled-cluster approach did yield very accurate results for the smaller molecules of the test set with a tendency for underestimation of the experimental reference values, but it is still prohibitively expensive for larger systems. The problems with the density functionals have

been attributed to difficulties in order to get the correct balance between core spin polarization (which determines the hyperfine coupling constants) and valence spin polarization, which causes problematic spin contamination [190]. The mechanism of ESR hyperfine coupling has been subsequently studied in detail in Ref. [191], outlining the leading role of overlap between the singly occupied orbital of a doublet system with certain doubly occupied valence orbitals. The results were within ~ 10–15% error for most of the complexes and most of the functionals, allowing for a reliable interpretation of the results in comparison with experiments. A similar range of accuracy has also been quoted by Belanzoni et al. [177], where a large set of linear molecules in a $^2\Sigma$ ground state (mostly diatomics) have been studied by the first-order approach of van Lenthe et al. [189]. In this work, the A tensors have also been analyzed in detail, based on Mulliken populations of the singly occupied molecular orbitals and semi-quantitative estimates of the orbital mixing due to spin–orbit coupling.

Based on elaborate studies of the fluorine A tensor in TiF_3, Belanzoni et al. [187,186] have also pointed out the difficulties regarding experimental reference values, since often theoretical assumptions are made in order to determine the experimental data. After re-considering the experimental analysis for TiF_3, good agreement between the theoretical approach [185,186] based on a semi-empirical spin–orbit operator and the experiments could be achieved.

3.1.4. Magnetizabilities

Magnetizability is the magnetic equivalent to the electric polarizability, i.e. it relates the first-order response of the magnetic moment $\mathscr{M}$ of a molecule to the strength of the applied magnetic field $\boldsymbol{B}$ by

$$\mathscr{M}^{(1)} = \boldsymbol{\kappa}\boldsymbol{B} \tag{81}$$

with $\boldsymbol{\kappa}$ being the magnetic susceptibility or magnetizability tensor. It is in turn related to the molecular energy by

$$\boldsymbol{\kappa} = -\left.\frac{\partial^2 E}{\partial \boldsymbol{B}\partial \boldsymbol{B}'}\right|_{\boldsymbol{B}'=\boldsymbol{B}=0} \tag{82}$$

since the interaction energy between a magnetic dipole $\mathscr{M}$ and the magnetic field is, $-\mathscr{M}\cdot\boldsymbol{B}$, and therefore $\mathscr{M}^{(0)} = -(\partial E/\partial \boldsymbol{B})_{\boldsymbol{B}=0}$, and $\mathscr{M}^{(1)}$ is consequently given by the second derivative of the energy. Values for $\boldsymbol{\kappa}$ are usually quoted in SI units of J/T^2 or in c.g.s. units of erg/G^2. As for the other tensor quantities discussed in this article, the symbol κ will denote the rotational average of the magnetic susceptibility tensor.

From Eq. (82) is can be seen that, in a nonrelativistic approach, the derivative of the OZ operator (59a) with respect to the magnetic field yields both perturbation operators $\hat{A}$ and $\hat{B}$ of Section 2. The magnetic field that perturbs the magnetic moment can be time-dependent, therefore the magnetic susceptibility is a frequency dependent quantity just as the electric polarizability. However, applications to molecules have so far focused on static magnetic fields.

First-principles computations of magnetic susceptibilities have been carried out with Hartree–Fock and correlated ab-initio methods and with DFT. A relatively large number of applications to diamagnetic organic compounds is available at various ab-initio levels of theory. Density functional calculations of magnetic susceptibilities are also possible. However, with standard functionals they result in an 'uncoupled' approach, i.e. there are no contributions due to a first-order effective potential in Eq. (42) (i.e. $\mathsf{K}=0$). The reason for this is that a static external magnetic field induces no density change in the molecule but only a change in the current density. Most density functionals so far depend only on the density, but not on the current density, therefore the effective potential is not perturbed. It has been argued that this might be a bad approximation, and a current density functional approach for the computation of magnetic susceptibilities has been suggested [192]. It should be noted here that the same 'uncoupled' restriction applies to NMR nuclear shieldings, ESR g-shifts, and other properties related to external magnetic field perturbations.[7] It has been shown in a subsequent implementation of the formalism suggested in Ref. [192] for nuclear shieldings, that the effect of a current–density functional is negligible [193]. However, this study was based on a local (current) density approximation to DFT, therefore the importance of the current related terms for more generalized types of functionals remains an open question. If the magnetic field becomes time-dependent, it also induces time-dependent density changes in the molecule. Therefore, a time-dependent magnetic field perturbation always leads to an additional first-order potential perturbation both in ab-initio and conventional (i.e. neglecting the current dependence) DFT methods. Regarding the performance of Hartree–Fock and DFT, it has been frequently noted that correlation effects are negligible for the computation of magnetizabilities except for rare cases [194]. However, unless the GIAO methodology is employed, the convergence of the results with respect to the basis set size is very slow.

Magnetism is an enormously important research field. Most applications to transition metal systems, however, focus on the technologically important collective effects

[7] The same considerations regarding the origin dependence of the results obtained from finite basis set calculations apply, and consequently GIAOs or the IGLO methodology can be employed for κ, also.

(ferromagnetism etc.) of condensed matter. It is beyond the scope of the present article to deal with the incorporation of magnetism in computational methods originating from solid state physics. For paramagnetic transition metal complexes, the magnetism due to spin- and orbitals magnetic moments is discussed in detail in textbooks such as Ref. [195]. Currently, by far the most benchmark computations on molecules have dealt with magnetic susceptibilities of diamagnetic light-atomic molecules see, e.g. Refs. [194,196–213]. In order to present an application of such computations to transition metal complexes here, we remind that the magnetic susceptibility has been used in the context of defining a criterion for aromaticity. We do not wish to enter the ongoing debate about the definition of aromaticity and respective quantitative criteria but refer to the many excellent articles in the May 2001 special issue of Chemical Reviews about this topic. Different quantitative aromaticity criteria are, e.g. reviewed in Ref. [214]. Applications of DFT to aromaticity measures are covered by Ref. [215]. The term 'magnetic susceptibility exaltation' (MSE) has been coined in order to describe the 'aromatic' contributions to κ due to the ring currents [216] in aromatic systems as compared to hypothetical non-aromatic species built from an increment system (benzene vs. a hypothetical non-aromatic cyclohexatriene, for example). The value κ' for the hypothetical system is generated from increment systems and is therefore experimentally accessible as well. In case of aromatic systems, the MSE

$$\Lambda = \kappa - \kappa' \tag{83}$$

is usually found to be negative (diamagnetic), whereas it is found to be positive (paramagnetic) for systems described as antiaromatic. Experimentally, the range of proton and ^{13}C chemical shifts often indicates the aromatic or antiaromatic character of a compound [217].

In the complex η^6-$(C_6H_6)Cr(CO)_3$, the aromatic protons are experimentally found to be more shielded by about 2 ppm as compared to benzene. This causes the question of whether the benzene moiety in the complex is significantly less aromatic than free benzene. The complexation of benzene to Cr goes along with significant changes in the geometric and electronic structure of the benzene subunit. Experimental evidence (in particular the increase in the H–C spin–spin coupling constants) indicates that electronic charge is transferred from Cr to the benzene ligand. Simion and Sorensen [218] have calculated the MSE for this complex as $\Lambda = +12.3 \times 10^{-6}$ erg/G^2, as compared to the calculated value for benzene of $\Lambda = -15.1 \times 10^{-6}$ erg/G^2 (experimental value: -13.2 [219]). The experimental value of $-113 \pm 22 \times 10^{-6}$ erg/G^2 for κ of the complex η^6-$(C_6H_6)Cr(CO)_3$ has also been well reproduced in the calculations (-109.3×10^{-6} erg/G^2). The result for the MSE is in intuitive agreement with the large NMR upfield shift of the benzene protons in the Cr complex (which was also quantitatively reproduced in the calculations). Further, the aromatic stabilization energy (ASE), another measurement for aromaticity conceptionally related to the MSE criterion but based on binding energies instead, was found to be 18.5 kcal/mol as compared to 34.1 kcal mol^{-1} for benzene itself [220]. Therefore, the authors of Ref. [218] have concluded that benzene in the complex is actually antiaromatic, based on the sign of the MSE. However, from an NMR study, Mitchell et al. had earlier concluded that $Cr(CO)_3$ in fact increases the aromaticity of the benzene moiety [221]. Later [220], it has been argued based on the so-called 'nuclear independent chemical shift' (NICS, i.e. the chemical shift is evaluated with respect to the position of a hypothetical nucleus in order to draw conclusions about the aromatic ring currents) that the aromaticity of benzene in the η^6-$(C_6H_6)Cr(CO)_3$ complex is not reduced. Both the MSE criterion employed in Ref. [218] as well as the NICS criterion [220] agree that cyclobutadiene in η^4-$(C_4H_4)Cr(CO)_3$ is aromatic due to the electron transfer from the metal into the π-system.

3.1.5. Harmonic force constants

Assuming, to lowest order, a quadratic form for the potential energy surface in the vicinity of the equilibrium structure for a molecule, the molecular energy as a function of the mass-weighted nuclear displacements $\boldsymbol{X}^\dagger = (\boldsymbol{X}_A^\dagger, \boldsymbol{X}_B^\dagger \ldots) = (X_1, Y_1, Z_1, \ldots, X_M, Y_M, Z_M)$ can be written as

$$E = (1/2)\boldsymbol{X}^\dagger \mathsf{Q} X \tag{84}$$

The energy scale has been chosen here such that $E = 0$ when the nuclei are in their equilibrium positions, $\boldsymbol{X}^e$, while $\boldsymbol{X}$ refers to displacements from these equilibrium positions. The X_A, Y_A and Z_A are the Cartesian coordinates for nucleus A multiplied by $\sqrt{M_A}$, with M_A being its mass. The $3M \times 3M$ matrix Q contains the second derivatives of the molecular energy with respect to these nuclear displacements $\boldsymbol{X}$, i.e.

$$\mathsf{Q} = \left.\frac{\partial^2 E}{\partial \boldsymbol{X} \partial \boldsymbol{X}'}\right|_{\boldsymbol{X}'=\boldsymbol{X}=0} \tag{85}$$

The normal modes [222] $\boldsymbol{q}_\alpha$ are the eigenvectors of Q, while its eigenvalues k_α are the mass-weighted force constants associated with the $\boldsymbol{q}_\alpha$. From this, the vibrational spectrum of the molecule in the harmonic approximation can be calculated, since the frequency of a harmonic oscillation is related to the mass-weighted force constant by

$$\omega_\alpha = \sqrt{k_\alpha} \tag{86}$$

Zero frequencies are obtained for the overall translational and rotational motion of the molecule. The

second derivatives of the energy with respect to nuclear displacements are, in principle, obtained by Eq. (9). As already mentioned, with standard quantum chemical basis sets correction terms in addition to Eq. (9) occur that take into account the dependence of the basis set on the nuclear positions [8,223–225]. It has early been recognized [8] that it is impossible for all but the smallest molecules to compute reliable forces based on the (Hellmann–Feynman [3,226]) force expression (6) with approximate wave function/orbitals expressed in nuclear-centered basis functions. In case that other basis set types such as plane waves or floating basis functions [227] are employed, no correction terms are necessary for variational methods.

"It is fair to say that it is virtually impossible to interpret and correctly assign the vibrational spectra of larger polyatomic molecules without quantum chemical calculations" (P. Pulay, in Ref. [9]). Nowadays, the computation of harmonic frequencies is a standard quantum chemical task, and many program codes have implemented the computation of second derivatives of the energy with respect to nuclear displacements by means of analytic methods (i.e. by explicit evaluation of the perturbed orbitals/wavefunction with respect to nuclear displacements). In case such methods are not available but only analytic gradients it is always possible to replace the second derivative in Eq. (85) by a finite difference, i.e.

$$\mathsf{Q} = \left.\frac{\partial^2 E}{\partial \boldsymbol{X}\partial \boldsymbol{X}'}\right|_{\boldsymbol{X}'=\boldsymbol{X}=0} \approx \frac{\Delta(\partial E/\partial \boldsymbol{X})|_{\boldsymbol{X}=0}}{\Delta \boldsymbol{X}'} \tag{87}$$

for small $\boldsymbol{X}'$ in the sense of Eq. (52). (Of course, in principle, the gradients can be calculated by finite differences as well.) However, the computational expense due to the gradient calculations for each displacement scales unfavorably with the number of nuclei in the molecule.

An important application of second energy derivatives with respect to nuclear displacements is related to the classification of stationary points on the potential energy surface (PES), in particular of minima as well as of transition states which are first-order saddle points on the PES. A transition state affords a negative force constant associated with one of the normal modes, which results according to Eq. (86) in an imaginary frequency and therefore the characterization of a molecular structure as a transition state is in principle straightforward. However, the transition state has to be found first, which is generally not as simple. From a knowledge of the PES, detailed information about the dynamics of a reaction can be extracted. Because of the large amount of literature available for this type of applications of second energy derivatives we refer to Refs. [1,229–231] for further details and original papers.

The accuracy of various computational approaches and in particular of DFT for the calculation of harmonic force constants of transition metal carbonyls and carbonyl hydrides has been investigated, e.g. in a series of papers by Jonas and Thiel [232–235]. An overview of applications to transition metal complexes is also presented in the textbook Ref. [129]. It was found that DFT performs generally well for such molecules and properties, while Hartree–Fock and MP2 did not yield very satisfactory results. With ECPs and the BP86 functional, typical deviations for vibrational frequencies compared to experiment were found to be in the range of 0–30 cm^{-1} with a tendency to overestimate metal–carbon stretching frequencies and to underestimate the C–O stretching frequencies [232]. Trends for the change in the C–O frequencies upon complexation were also well reproduced. The remaining errors are well within what one might expect from anharmonicity corrections or frequency shifts due to a surrounding matrix. For the carbonyl hydrides, the metal–H stretching frequencies were typically overestimated by 30–50 cm^{-1} for the 3d metals and by 10 cm^{-1} for the other metals. It has previously been found that for many light atomic main group compounds DFT methods, in particular with hybrid functionals, perform very well for the computation of vibrational frequencies [236] even in comparison with highly accurate ab-initio methods. The accuracy can be further improved by applying scaling factors for each particular method and basis set. See also Ref. [237] for an alternative scaling approach.

That the effective core potential approach is suitable even for elements as heavy as U, Np, and Pu, has been demonstrated in Ref. [238]. Experimental values were overestimated by 9–14% in Hartree–Fock calculations, whereas density functional calculations performed much better. Calculations of vibrational frequencies of transition metal complexes with DFT (both with nonrelativistic and relativistic methods) have also been performed by Ehlers et al. [118] and by Bérces and Ziegler [239] who have also later reported the analytic solution of the coupled perturbed Kohn–Sham equations for nuclear displacements within DFT [240,241] for the analytic computation of vibrational frequencies based on numerical integration. See the next paragraph for further applications.

3.1.6. Infrared intensities

The harmonic frequencies discussed in the last paragraph can be combined with a computation of the respective intensities that would be observed for the absorption of an infrared light beam of the respective energy in order to simulate infrared (IR) vibrational spectra. The intensities I_α are (in the double harmonic approximation [223]) proportional to the square of the derivative of the electric dipole moment $\mathscr{D}$ of the molecule with respect to nuclear displacements along

the normal coordinates [242], i.e. this leads to another second energy derivative of the form

$$\mathrm{I}_\alpha \propto \left|\frac{\partial \mathscr{D}}{\partial \boldsymbol{q}_\alpha}\right|^2_{\boldsymbol{q}_\alpha=0} = \left|\frac{\partial^2 E}{\partial \boldsymbol{q}_\alpha \partial \boldsymbol{E}}\right|^2_{\boldsymbol{E}=0,\boldsymbol{q}_\alpha=0} \quad (88)$$

since the lowest order energy change of a molecule in an electric field $\boldsymbol{E}$ is given by $-\mathscr{D}^{(0)}\cdot\boldsymbol{E}$, and therefore $\mathscr{D}^{(0)} = -(\partial E/\partial \boldsymbol{E})_{\boldsymbol{E}=0}$. The electronic contribution to the electric dipole moment operator does not depend on the nuclear coordinates, therefore there are no cross terms due to $\hat{H}^{(1,1)}$ in Eq. (9) to evaluate. The constant of proportionality in Eq. (88) is $(4\pi\varepsilon_0)^{-1}(N_A\pi)/(3c^2)d_\alpha$, with d_α being the degeneracy of the normal mode [223,224]. IR intensities are usually reported in units of km/mol.

The perturbed wavefunction $\partial\Psi/\partial\boldsymbol{X}|_{\boldsymbol{X}=0}$ (or the set of orbitals) with respect to the nuclear Cartesian displacements $\boldsymbol{X}$ is already available from the determination of Q for the respective IR frequencies, therefore a simple linear transformation yields $\partial\Psi/\partial\boldsymbol{q}_\alpha|_{\boldsymbol{q}_{\alpha=0}}$. From this, the intensities are readily computed from Eq. (9).

Since the dipole integrals are available in most quantum chemical codes, the calculation of the intensities does not cause any significant increase in the computational effort once the vibrational frequencies have been evaluated. Several of the aforementioned papers dealing with vibrational spectra of transition metal complexes have therefore also compared the computed intensities to experimental data. Due to certain difficulties in the experimental determination of absolute intensities, often only relative values are given. In Ref. [238] absolute experimental IR intensities for the strong absorption bands ν_3 of UF_6, NpF_6 and PuF_6 (and also of the weaker ν_4 for UF_6) have been reported. Using a larger basis set 6-31+G*, the experimental intensities for UF_6 and PuF_6 could be reproduced by the DFT methods within 15% error. An early application of DFT to IR intensities has been carried out in Ref. [243] for $Ni(CO)_4$ and $Cr(CO)_6$, in good agreement with the available experimental data both for relative and absolute intensities. In case spectra are simulated from theoretical calculations, the usual pragmatic procedure is to superimpose the calculated line spectrum with Gaussian or Lorentz curves, and to directly compare the experimental and the simulated spectrum. Fig. 6 displays some simulated IR spectra of metal tris-acetylacetonates, from Ref. [244]. As can be seen, the agreement of the experimental spectra with theoretical predictions is excellent and allows for a complete assignment of the spectra. Because of the good overall agreement, the authors of Ref. [244] concluded that the experimentally observed band at around 800 cm^{-1} that is not present in the theoretical simulations is not a fundamental frequency. As further examples, Mg and Zn porpyrin spectra have been investigated in Ref. [245],

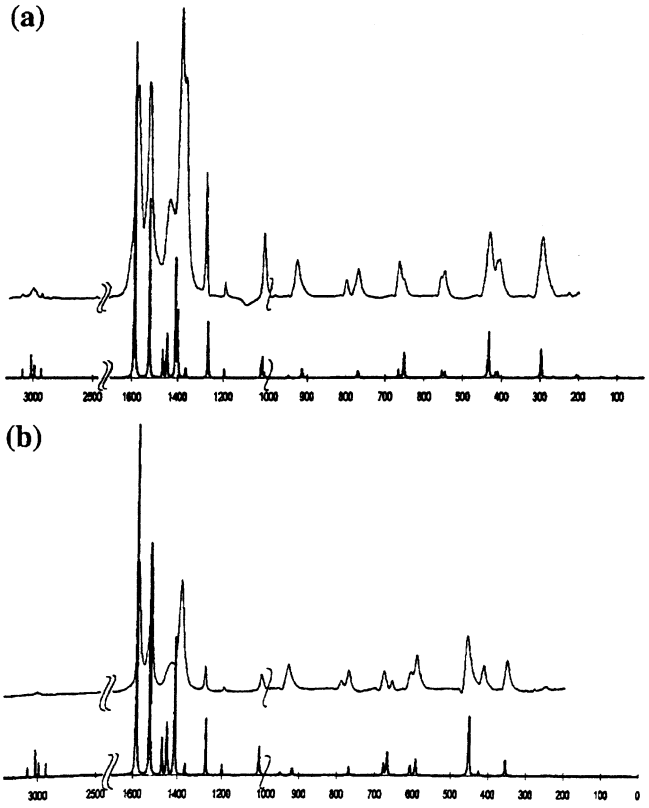

Fig. 6. Simulated and experimental (KBr) IR spectrum of $Fe(acac)_3$ (a) and $Cr(acac)_3$ (b), from density functional calculations. acac = acetylacetonate. Reprinted with permission from Diaz-Acosta et al., Ref. [244]© (2001) American Chemical Society.

and Ni porphyrin spectra in Ref. [246], with similar success in the assignment of the experimental spectra. Limitations in the first-principles calculation of IR spectra along with examples have been discussed, e.g. in Ref. [247]. Theoretical approaches, related technical details and further applications have been reviewed, e.g. in Ref. [9]. As in the previous section, the derivative of the dipole moment can also quite easliy be calculated from a finite difference. Analytical methods can greatly benefit from developments such as the '**Z**-vector' method [225,228] by which the expensive solution of a coupled perturbed problem, similar to an iterative solution of the zero-frequency limit of Eq. (42), with respect to *all* $3M$ nuclear coordinates is avoided, and only one modified coupled perturbed problem has to be solved explicitly for a set of simultaneous perturbations. It becomes intuitively clear that this must in principle be possible, since also the RPA Eq. (42) and its generalizations can be solved for any type of perturbation (the right hand side vector) once A and B are known (which do not depend on the perturbation, but usually they are too large to store explicitly). In the **Z**-vector method, the problem is re-cast in such a way that it is solved for an intermediate quantity $\boldsymbol{Z}$ which is then used to determine the actual perturbed density matrix related to a specific

perturbation. If an iterative solution, e.g. of Eq. (36), is directly attempted, this needs instead to be done for each perturbation individually (i.e. all $3M$ coordinate displacements).

3.1.7. Relativistic force changes

So far we have dealt with second derivatives of the energy where E refers either to a nonrelativistic value (appropriate for light atomic compounds) or a value obtained from a relativistic treatment (often necessary for heavy element compounds). 'Relativity' (i.e. the effect on various properties that stems from the difference between a treatment according to Einstein's or Galilei's relativity principle) can be treated as a perturbation as well. In this case, c^{-2} with c being the speed of light serves as a convenient perturbation parameter which we will label 'r' (for relativity) in the following for simplicity. For $c \to \infty$, $r \to 0$, the nonrelativistic (i.e. Galilei-relativistic) formalism is recovered. In Section 2.4 we have already presented the terms (61) or (62) from which frequently employed lowest order perturbation operators $\hat{H}^{(1,0)} = \hat{H}^r = c^2\hat{H}^{\mathrm{rel}}$ are obtained simply by omitting the c^{-2} prefactors. In this context, the relativistic change of intramolecular forces has created some confusion for some time. The property[8] under discussion is here the lowest-order change of the energy gradient due to relativistic effects, i.e.

$$\boldsymbol{F}^r_A = -\left.\frac{\partial^2 E}{\partial r \partial \boldsymbol{X}_A}\right|_{\boldsymbol{X}_A=0, r=0} \tag{89}$$

with $\boldsymbol{X}_A$ again being a displacement of nucleus A from its nonrelativistic equilibrium position. For non vanishing $\boldsymbol{F}^r_A$, the system will undergo relativity-induced geometry changes which can be quite large for molecules containing 6th row atoms such as Pt, Au, Hg, Tl, and Pb. In a large number of cases, relativistic bond contractions are observed in the computations. Such structural effects lead to pronounced irregularities in periodic trends for increasing atomic numbers within the groups of the periodic table. Relativity also contributes significantly to phenomena such as the 'second periodicity' [248]. We refer to Refs. [249–251] for detailed overviews regarding relativistic effects in chemistry.

The aforementioned confusion arises upon interpretation of the relativistic force change within a first-order perturbational treatment of the relativistic effects. It is well known that atoms contract relativistically, i.e. their relativistic radius is smaller than predicted by a nonrelativistic computation. This can therefore serve as a straightforward explanation for the relativistic bond contraction [249]. However, the case is not as simple. Since the order in which the derivatives are taken in Eq. (89) is arbitrary, one might at first compute the first-order relativistic energy change

$$E^r = \langle \Psi^{(0,0)} | \hat{H}^r | \Psi^{(0,0)} \rangle \tag{90}$$

The relativistic force that causes the geometry change is qualitatively correctly reproduced at this first-order by computing the gradient of $E^{(r)}(\boldsymbol{X}_A, \boldsymbol{X}_B, \ldots)$ with respect to the nuclear displacements, i.e.

$$\boldsymbol{F}^r_A = -\left.\frac{\partial E^r}{\partial \boldsymbol{X}_A}\right|_{\boldsymbol{X}_A=0} \tag{91}$$

Consequently, since the zeroth-order wavefunction in Eq. (90) does not contain any contribution due to the relativistic contraction of the atoms, one has to conclude that $\boldsymbol{F}^r_A$ in Eq. (91) is not at all related to the relativistic atomic contractions. This undoubtedly correct view has been put forward by several authors based upon numerical studies of $E^r(R)$ as a function of bond distance R in heavy diatomics [262,264–266].

On the other hand, by reversing the order of differentiation in Eq. (89) and considering the energy gradient as the first perturbation, it is easy to show that (in a four-component formalism or DPT)

$$\boldsymbol{F}^{\mathrm{rr}}_A = \int \mathrm{d}\boldsymbol{r} \cdot \hat{\boldsymbol{F}}_A \rho^r \tag{92}$$

where $\hat{H}^{(0,1)} = \hat{\boldsymbol{F}}_A$ is the nonrelativistic (Hellmann–Feynman) force operator and $\rho^r = \rho^{(1,0)}$ is the lowest order relativistic change of the electron density [267–270]. In a two-component formalism, a small [271] contribution from $\hat{H}^{(1,1)}$ occurs in addition that we can omit from the discussion. The electron density is often partitioned into a sum of atomic contributions (the promolecular density), and a deformation density due to bond formation and overlap effects. Similarly, ρ^r can be split up as

$$\rho^r = \sum_A \rho^r_A + \Delta\rho^r \tag{93}$$

Therefore, in this interpretation the (promolecular) relativistic change of the atomic densities (atomic contractions ρ^r_A) directly contributes to $\boldsymbol{F}^r_A$ which then causes relativistic structure changes, and an apparent paradox has been created by the two different interpretation schemes. Due to the numerical difficulties with the evaluation of forces based on Eq. (92) in many-electron heavy nucleus systems, this paradox could only recently be resolved [257,272]. There it was shown that in heavy atom compounds the relativistic change of the deformation density $\Delta\rho^r$ is responsible for most of the magnitude of $\boldsymbol{F}^r_A$ even in the second interpretation scheme (93), and that the promolecular contribution is rather small but not negligible. It has also been

[8] It has to be emphasized once more that 'property' in this context is not to be understood as a physically observable property of the system but as a theoretical construct from which nonetheless much can be learned about the differences between observable properties of light and heavy elements.

Table 5
Experimental and some calculated spectroscopic constants of the AuH molecule (δ = relativistic corrections)

	D_e (eV)	δ	R_e (Å)	$-\delta$	W_e (cm^{-1})	δ
Experiment [a]	3.36		1.52		2305	
DPT–DFT LDA [b]	3.44	0.78	1.55	0.16	2231	525
DPT–DFT GGA [b]	3.00	0.72	1.56	0.17	2162	541
DPT–DFT LDA [c]	3.44	0.80	1.54	0.16	2233	505
DPT–DFT GGA [c]	3.00	0.73	1.56	0.17	2157	516
Hartree–Fock+ECP [d]	1.58	0.63	1.58	0.25	2061	601
DK–CC [e]	2.92		1.53	0.22	2288	723
DK–MRDCI [f]	3.13	0.94	1.52	0.20	2381	816
DFT GGA Pauli [g]	3.27	1.61	1.53	0.20	2306	696
DFT X& Pauli [g]	2.95	1.35	1.55	0.23	2241	537
MP2+ECP [h]	2.91	1.01	1.51	0.20	2373	678
ZORA–DFT LDA [i]	3.78	1.14	1.53	0.18	2340	630
ZORA–DFT GGA [i]	3.33	1.05	1.54	0.20	2290	660

[a] Experimental data from Ref. [252].
[b] DFT implementation of scalar relativistic first-order DPT, using Slater-type basis functions. LDA is the VWN functional [253], GGA is BP86 [254–256]. Ref. [257].
[c] DFT implementation of scalar relativistic first-order DPT, using Gaussian-type basis functions. Ref. [258].
[d] Hartree–Fock with ECPs, Ref. [259].
[e] Douglas–Kroll coupled cluster, Ref. [260].
[f] Douglas–Kroll multi-reference CI, Ref. [260].
[g] Pauli operator (scalar rel.) with frozen cores, Refs. [261] (GGA) and [262] (Xα functional).
[h] MP2 with ECPs, Ref. [263].
[i] Zeroth-order relativistic approximation (ZORA), Ref. [54].

demonstrated that the same results for $\boldsymbol{F}^r_A$ are obtained from Eqs. (91) and (92) in actual computations, as required, despite the nonintuitive and somewhat paradoxical explanations. Generally, regarding double-perturbation properties it is often possible to derive quite different, correct, and numerically equivalent formulae, which can lead to quite different and apparently paradoxical—but not to contradictory—complementary explanations.

As an example, the theoretically well studied molecule AuH has relativistically a much shorter (approx. 0.2 Å) bond than what is predicted from nonrelativistic computations. See Table 5 for experimental and some calculated spectroscopic constants. To first-order in the relativistic formalism, only about 3/4 of the total relativistic effects on bond energies or internuclear distances can be obtained; the missing quarter is due to relativistic corrections of higher order (in particular c^{-4} and c^{-6}) that are already very important for sixth row compounds and in particular for Au(I). In order to evaluate the relativistic force change based on Eq. (92), the relativistic density change to first-order in c^{-2} needs to be available. This has been analytically implemented by one of us with respect to the scalar relativistic part of the DPT operator (62) [257,272]. The relativistic force change in the AuH molecule is graphically displayed in Fig. 7 for both schemes, Eqs. (91) and (92). It is thereby numerically demonstrated that both schemes yield the same answer in a heavy element compound, even though they cause very different interpretations of the effect. The promolecular contribution to the relativistic force change F^r_H according to Eq. (92) amounts to -0.45 eV Å^{-1}, whereas the total computed value (at the nonrelativistic equilibrium distance) is -1.84 eV Å^{-1} (from LDA DFT calculations).

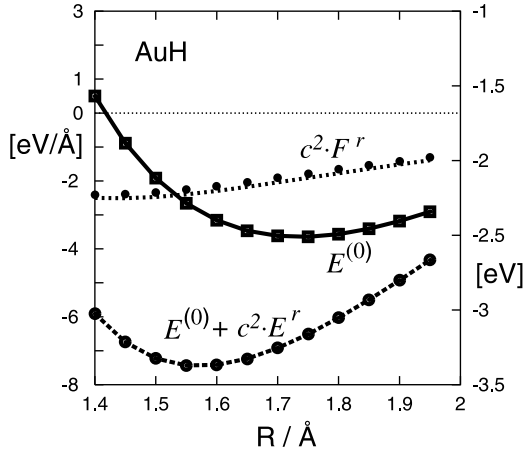

Fig. 7. Nonrelativistic ($E^{(0)}$) and first-order relativistic binding energy $E^{(0)}+c^2 \cdot E^r$, and relativistic force change $c^2 \cdot F^r$ of the AuH molecule as a function of internuclear distance R, from LDA density functional calculations [257]. For numerical reasons, the force on the H nucleus, $c^2 \cdot F^r_H$, has been computed. The relativistic force change is responsible for the bond length contraction. The dotted line refers to Eq. (91) and has been obtained from a differentiation of the $c^2 \cdot E^r(R)$ curve with respect to R. The filled markers for the $c^2 \cdot F^r_H$ refer to a direct evaluation of Eq. (92) from the analytically computed first-order scalar relativistic density change ρ^r. The promolecular contribution amounts to approx 25%.

3.2. Dynamic properties

3.2.1. Polarizabilities

The polarizability of a molecule relates a perturbation of its dipole moment $\mathscr{D}$ to an applied external electric field $\boldsymbol{E}$ by

$$\mathscr{D}^{(1)} = \boldsymbol{\alpha}\boldsymbol{E} \tag{94}$$

As mentioned previously, since the dipole moment in turn is related to the first-order energy change of a molecule in an electric field, the polarizability tensor $\boldsymbol{\alpha}$ is given as

$$\boldsymbol{\alpha} = -\left.\frac{\partial^2 E}{\partial \boldsymbol{E}\partial \boldsymbol{E}'}\right|_{\boldsymbol{E}'=\boldsymbol{E}=0} \tag{95}$$

Molecular polarizabilities are conveniently expressed in atomic units (a.u.), with a conversion factor to SI units of $\approx 1.648 \times 10^{-41}$ C^2 m^2 J^{-1}/a.u. [273]. The frequency dependence of $\boldsymbol{\alpha}$ is the prime textbook example for the introduction of frequency dependent response properties and has been used numerous times in order to illustrate applications of the RPA Eq. (42) within the Hartree–Fock and semiempirical approaches and time dependent DFT, and applications of more sophisticated generalizations of the RPA equation within ab-initio methods. In contrast to magnetizabilities the frequency dependence of atomic and molecular polarizabilities has received very much attention, also as benchmark values for code implementations, since a rather large body of experimental data in particular for small molecules is available. Another reason for the interest in polarizabilities is, as mentioned in many of the references cited below, their sensitivity to correlation effects. Thus, the computation of polarizabilities is also a stringent test of the capability of a particular method to treat the correlation problem. Static polarizabilities have frequently been computed by a finite field method (see Section 2.3.3) in case an analytic treatment of the linear response of the dipole moment was not available. However, there has been considerable progress during the past decades in methodological developments and code implementations, therefore analytic treatments of static and frequency dependent polarizabilities are nowadays available for many correlated ab-initio methods as well as for DFT. Only the operator (55) in Section 2.4 needs to be considered for both the perturbation from the electric field as well as for the perturbed observable, the electric dipole moment. No mixed contribution due to $\hat{H}^{(1,1)}$ arises, and no correction terms due to basis set incompleteness have to be evaluated. Since the polarizability does not depend on features of the wavefunction/orbitals near the nuclei, ECPs can effectively be used in order to incorporate relativistic effects.

The computation of polarizabilities in particular for small and light atomic molecules has been reviewed many times in the past. We refer to Refs. [6,27,43,49,129,223,224,274] for details on the methodology and/or original references and benchmark data. A number of papers dealing with new methodology and results in particular for small molecules have been published during recent years [275–302], many of them employing correlated ab-initio methods [303–322] or DFT [17–19,323–332]. A few studies have been specifically directed towards relativistic methods, such as Refs. [333–335]. It appears that applications of already well established and computationally efficient methodology often deal with small clusters, since their polarizabilities are experimentally important in order to deduce information about the shape of the clusters. See Refs. [267,277,281,282,287,288,293,302,325,329,332] for examples. A number of the previously cited references are dealing with nonlinear optical (NLO) properties, for the computation of which the availability of reliable dipole polarizabilities is a first prerequisite.

Not very many computational studies on polarizabilities of transition metal complexes are available so far. As an example, Cundari et al. have studied the static polarizability and second hyperpolarizability of transition metal oxo complexes and tiometalates [336]. In particular, the influence of a solvent has been of interest for the authors, the effect of which has been modeled with the PCM methodology (polarizable continuum model). The results are displayed in Fig. 8. So far, no experimental data are available for comparison [336]. The inclusion of solvent effects has been found to be particularly necessary for the highly negatively charged species, since otherwise the polarizability and even more

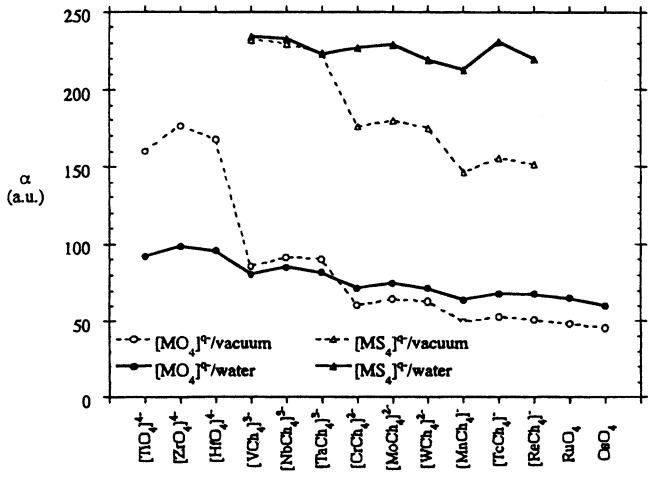

Fig. 8. Static dipole polarizabilities for metalates and thiometalates of various 3d to 5d transition metals, from Hartree–Fock computations, reprinted with permission from Cundari et al., Ref. [336] © (2000) American Chemical Society. The solid lines refer to computations including solvent effects via the PCM, the dashed lines refer to computations excluding solvent effects.

the NLO properties tend to be systematically overestimated. For the less charged species, the polarizability is seen to increase upon solvation (Fig. 8). By comparison to MP2 calculations it was found that a modeling of solvent effects is more important than inclusion of correlation in the calculations. Other computational studies treating solvent effects on polarizabilities can be found, e.g. in Refs. [294,296,323].

A well studied transition metal complex for which a direct comparison between theory and experiment has been made is ferrocene ($Fe(C_5H_5)_2$). Experimental data for the Group 8 metallocenes have been published in Ref. [337], and theoretical values have been provided in Ref. [273]. Fig. 9 displays the frequency dependent polarizability for the metallocenes together with the theoretical data of Ref. [273]. It can be seen that reasonable agreement with experiment could be achieved from the density functional calculations.

The response function of a system that ultimately determines properties such as polarizabilities is related to the reaction of a molecule M to a small external perturbation. It has been recognized that the perturbation can also be due to the electric potential of another molecule N at some distance R_{MN}. In fact, the van der Waals dispersion coefficients can be theoretically related to dipole and higher multipole polarizabilities at imaginary frequencies. The leading interaction term proportional to R^{-6} involves only dipole polarizabilities and can therefore be computed from already available code for polarizabilities or accurate experimental data for a range of frequencies. Most important here is the isotropic coefficient C_6, which is related to the isotropic polarizability by

$$C_6(M,N) = \frac{3}{\pi}\int_0^\infty \mathrm{d}\omega \cdot \alpha_M(i\omega)\alpha_N(i\omega) \tag{96}$$

Similar expressions involving the polarizability anisotropy are obtained for the anisotropic contributions to the R^{-6} term. As an example, Goebel and Hohm have calculated a lower limit of the respective C parameters for $M = N$ from the experimental data for the frequency dependent polarizabilities of metallocenes, see Fig. 9. The untypically high isotropic values (0.004 (ferrocene) to 0.007 (osmocene) a.u.) are in agreement with the fact that a rather high concentration of metallocene dimers has been observed in their respective vapors. See Ref. [337] for details.

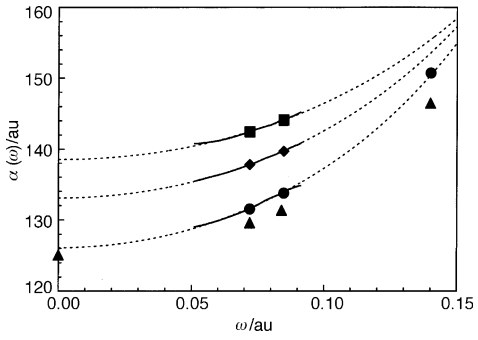

Fig. 9. Frequency dependent electric polarizability of ferrocene (lower line), ruthenocene (middle line) and osmocene (upper line). Reprinted from Goebel and Hohm, Ref. [337] with permission from the Royal Society of Chemistry. The triangle markers refer to previously computed values for ferrocene (DFT B3LYP) [273], the other markers refer to experimental data.

We briefly note at the end of this paragraph that Raman intensities are proportional to the square of the change of the polarizability along the normal mode [242]. Therefore, they can be obtained from a third-order perturbational treatment that includes the change of the wavefunction with respect to nuclear displacements in addition. Likewise, finite difference methods are frequently used for this purpose. The calculation of Raman intensities as polarizability derivatives is in close analogy to the computation of dipole moment derivatives in order to obtain IR intensities, see Section 3.1.6.

3.2.2. Electronic excitation spectra

By combining the two terms of Eq. (19) for $\eta \to 0$ with the operators $\hat{\boldsymbol{D}} = \Sigma_k\, \hat{\boldsymbol{d}}(\boldsymbol{x}_k)$ for the dipole moment and $-\hat{\boldsymbol{D}}\boldsymbol{E}(\omega)$ for the external electric field, the SOS equation for electric dipole polarizabilities is obtained as [338]

$$\alpha = \frac{2}{3}\sum_j \frac{(E_j - E_0)|\langle \Psi_0|\hat{\boldsymbol{D}}|\Psi_j\rangle|^2}{(E_j - E_0)^2 - \omega^2} = \sum_j \frac{f_{0j}}{(E_j - E_0)^2 - \omega^2} \tag{97}$$

The spectroscopic oscillator strengths

$$f_{0j} = \frac{2}{3}(E_j - E_0)|\langle \Psi_0|\hat{\boldsymbol{D}}|\Psi_j\rangle|^2 \tag{98}$$

are the quantities related to the intensities of vertical electronic excitations at frequencies $\omega_{0j} = (E_j - E_0)$. They afford the Thomas–Reiche–Kuhn (TRK) sum rule

$$\sum_{j\neq 0} f_{0j} = N \tag{99}$$

with N being the number of electrons. The quantities

$$\boldsymbol{D}_{0j} = \langle \Psi_0|\hat{\boldsymbol{D}}|\Psi_j\rangle \tag{100}$$

are the electric transition dipole moments for the excitation $0 \to j$. The corresponding formula for the electric transition dipoles obtained from a treatment by RPA Eq. (42) based upon a solution of the equation system (50) has already been given in Eq. (51a). The computation of oscillator strengths and excitation energies is an important field because it allows for the simulation and interpretation of electronic excitation spectra of molecules (UV–vis spectra). Experimentally,

the dimensionless oscillator strengths are obtained from the spectra as the integrated intensities of individual absorption bands:

$$f_{0j} \approx 3.48 \times 10^{-5} \int_{\text{Band } j} \mathrm{d}E \cdot \frac{\varepsilon_0(E)}{\mathrm{eV} \cdot l/(\mathrm{mol} \cdot \mathrm{cm})} \qquad (101)$$

Here, $\varepsilon_0(E)$ is the absorption coefficient for the reference state '0' (not to be confused with the dielectric constant of the vacuum) at energy E. Because in the experimental spectra absorption bands may overlap and an assignment of individual bands is not always easy, theoretically simulated spectra from computations of excitation energies and oscillator strengths can be very useful. Often, the computations are based on the RPA Eq. (42) (or its generalizations) and the resulting pseudo-eigenvalue Eq. (50) in order to avoid the explicit calculation of many excited states wavefunctions. Recent investigations have shown that in particular a time-dependent DFT treatment based on Eqs. (42) and (50) yields simulated spectra that are often reliable enough in order to allow a direct comparison with experimental data, at least for excitation energies well below the negative energy of the HOMO [17,20]. In order to obtain information about the PES of the excited states, a procedure to obtain gradients of the time-dependent DFT excitation energies with respect to nuclear displacements has been devised [339]. For this purpose, and for the computation of low lying excitation energies, ΔSCF methods are also popular in which the excited state is approximated by replacing occupied orbitals of the ground state (Kohn–Sham- or Hartree–Fock- or semiempirical) determinant with virtual orbitals. As previously mentioned, accurate ab-initio CI methods (single- or multi-reference) play an important role in the determination of excitation spectra. For heavy element compounds in particular those involving heavy p-block elements, an efficient treatment of spin–orbit coupling is vital in order to obtain accurate results. Applications typically involve small molecules. We refer to Refs. [48,340] for further details and references.

A comparison between the computationally efficient semiempirical INDO/S CI [342] and the time-dependent DFT method (based on the RPA Eq. (42)) with hybrid density functionals) for various ruthenium diimine complexes has recently been made in Ref. [343]. The authors conclude that both methods yield 'remarkably accurate' results, with an average deviation of the excitation energies as compared to experimental data of 0.14 eV (INDO/S) and 0.11 eV (DFT), respectively. Since the interpretation of the results were similar with both methods, and they also quantitatively agreed quite well, the authors suggest that the computationally cheaper semiempirical method might be reliable for large complexes for which a DFT treatment is still not feasible. An application of the semiempirical methodology to binuclear Ru complexes can, e.g. be found in [344]. Recent developments in so-called 'linear scaling' techniques will help to reduce the computational effort of the DFT methods [326]. However, it has frequently been found that in particular Rydberg excitations of small molecules are very sensitive to defects in various common density functionals (because of their wrong asymptotic behavior), and functionals specifically designed to overcome these limitations are now in use [327,345].

Table 6
Vertical excitation energies of $Ni(CO)_4$ and MnO_4^-, in eV (all data from Ref. [341])

Method	Band I	Band II	Band III	Band IV
$Ni(CO)_4$				
Experiment	4.5	5.4	5.5	6.0
CASSCF	7.3	7.5	7.6	7.7
CASPT2	4.3	5.2	5.6	6.3
SAC-CI	4.8	5.5	5.7	5.8
TDDFT	4.7	4.8	5.4	5.8
MnO_4^-				
Experiment	2.27	3.47	3.99	5.45
SAC-CI	2.57	3.58	3.72	5.82
DFT-ΔSCF	2.57	3.42	3.76	5.99
TDDFT	2.63	3.60	4.52	5.46

The excitation spectrum of small metal complexes such as $Ni(CO)_4$ and MnO_4^- has been studied by various theoretical methods. Table 6 shows a comparison of DFT and ab-initio methods for these two compounds. In particular MnO_4^- provides a stringent test for any computational method. Even though all the methods displayed in Table 6 reproduce the excitation energies reasonably well, the assignment (not displayed) of the four bands in the spectrum are not consistent between the methods for MnO_4^- [341]. The DFT approach performs surprisingly well in comparison to the much more expensive correlated ab-initio approaches. See also Refs. [346–350] and literature cited therein for further applications to transition metal complexes, also with respect to the direct inclusion of scalar relativistic effects [349].

It is possible nowadays to calculate the electronic excitation (and CD spectrum, see below) of a rather large molecule very efficiently based on the RPA Eq. (42), either with Hartree–Fock or, more accurately, with time-dependent DFT. An advantage over some of the older semi-empirical approaches is that all the orbitals in the system are treated on the same footing and they can all contribute to the excitations spectrum to an extent that is determined by the solution of the equation system (50). A convenient analysis of the excitation in terms of contributions of individual MOs is possible, since the contributions are determined by the respective coefficient belonging to the composite index (ak) (a = virtual,

k = occupied orbital) in the solution vectors $\boldsymbol{F}_{0j}$. We have already mentioned certain approximations to the RPA treatment in Section 2.3.1. From an inspection of Eqs. (49) and (50) it can be seen that, if all the contributions from K to Ω are neglected, this yields the uncoupled approach in which the Ω is diagonal and thus the vectors $\boldsymbol{F}_{0j}$ contain only one nonzero element each. In this approximation, the excitation energies are just the orbital energy differences. A slightly better approximation would be to use the diagonal part of A. In the full RPA treatment, an electronic excitation is described by a mixture of such 'uncoupled' occupied-virtual orbital excitations which manifests itself in different (ak) elements in each vector $\boldsymbol{F}_{0j}$, but often there is one dominant contribution which allows a convenient and intuitive assignment of UV and CD spectra based on the orbital model.

3.2.3. Optical rotation and circular dichroism

3.2.3.1. Optical rotation. Optical rotation is related to perturbations of the electric dipole moment $\mathscr{D}$ of a molecule by a time-dependent magnetic field, or alternatively to the perturbation of the magnetic moment $\mathscr{M}$ by an electric field. The optical rotation tensor $\boldsymbol{\beta}$ is defined here by [338,351–354]

$$\mathscr{D}^{(1)} = -\boldsymbol{\beta}\dot{\boldsymbol{B}} \tag{102a}$$

$$\mathscr{M}^{(1)} = \boldsymbol{\beta}\dot{\boldsymbol{E}} \tag{102b}$$

i.e. the net effect of the influence of the electric field on the magnetic moment or vice versa is proportional to the time derivative of the respective perturbing field. Therefore, no perturbation takes place if the external fields are static. This is intuitively clear since a static external electric field does only induce changes of the electron density but does not induce a current density which would contribute to the magnetic moment. Likewise, a static magnetic field induces only a current density in the molecule but no density change. If the perturbing fields are time dependent, they induce both density and current–density changes. The respective effect of $\boldsymbol{E}$ on $\mathscr{D}$ has already been discussed in Section 3.2.1, and the effect of $\boldsymbol{B}$ on $\mathscr{M}$ has been discussed in Section 3.1.4. In the framework of double perturbation theory, the optical rotation parameter is evaluated based upon consideration of the quantity

$$\left.\frac{\partial^2 E}{\partial \boldsymbol{B}\partial \boldsymbol{E}}\right|_{\boldsymbol{B}=0,\boldsymbol{E}=0} \tag{103}$$

and the result is recast in the form of either Eq. (102a) or Eq. (102b) [338]. As for the computation of frequency dependent electric polarizabilities, the RPA Eq. (42) or more sophisticated ab-initio counterparts can be used in order to compute $\boldsymbol{\beta}$. The macroscopically observed optical rotation is usually reported in experimental work in form of the specific rotation $[\alpha]_\lambda$ in degrees per (g cm^{-3}) and per dm (length of the cuvette) for wavelength λ of the perturbing field. Gaussian units are still commonly used in theoretical work related to optical activity, in which case the optical rotation parameter β is in units of cm^4. The conversion factor to specific rotations is then

$$[\alpha]_\lambda = 28800 \cdot \frac{\pi^2 N_\mathrm{A}}{\lambda^2 M}\beta \tag{104}$$

with N_A being Avogadro's number, M the molecular weight in g mol^{-1}, λ the wavelength in cm. It should be noted that even though the perturbations in Eq. (102) as well as the specific rotation $[\alpha]_\lambda$ vanish for the zero-frequency limit, the optical rotation parameter stays finite and has a well defined limit for $\omega \to 0$. This has previously been used in order to avoid an explicit frequency dependent perturbational treatment for the calculations of optical rotations, by calculating β at zero frequency employing standard 'static' methodology, and conversion to specific rotation for a specified wavelength (usually the Na D line) [355,356].

The operators needed for the perturbational treatment are the 'electric ' operator, Eq. (55) in Section 2.4, and the orbital Zeeman term (59a). No mixed contribution due to $\hat{H}^{(1,1)}$ occurs. In case a gauge dependence of results obtained with finite basis sets due to the external magnetic field is explicitly avoided by the usage of GIAOs or IGLOs, for example, additional correction terms arise. It has been demonstrated, however, that high quality basis sets have to be employed in order to compute reliable optical rotation parameters, in which case the gauge dependence is not very pronounced [356,357]. Due to the symmetry properties of the operators involved it can be shown [358] that the optical rotation parameter is necessarily zero in case the molecular symmetry group has an improper rotation $\mathscr{S}_n$ as one of its elements. Therefore, only chiral molecules exhibit optical rotation, and no effect is observed in particular when the molecule has a mirror plane $\mathscr{S}_1$ or an inversion center $\mathscr{S}_2$.

3.2.3.2. Circular dichroism. Circular dichroism is the chirality effect on the excitation spectra discussed in Section 3.2.2 and is observed as the difference $\Delta\varepsilon$ of the absorption intensities for left- and right-hand circular polarized light. In close analogy to the relation between the oscillator strengths and the polarizability in the SOS Eq. (97), the SOS expression for the optical rotation parameter β contains the quantities that determine the magnitude of the CD effect:

$$\beta = \frac{2}{3}\sum_j \frac{\mathrm{Im}[\langle\Psi_0|\hat{\boldsymbol{D}}|\Psi_j\rangle\langle\Psi_j|\hat{\boldsymbol{M}}|\Psi_0\rangle]}{(E_0 - E_j)^2 - \omega^2}$$

$$= \frac{2}{3}\sum_j \frac{R_{0j}}{(E_j - E_0)^2 - \omega^2} \quad (105)$$

The quantities

$$R_{0j} = \mathrm{Im}[\langle\Psi_0|\hat{\boldsymbol{D}}|\Psi_j\rangle\langle\Psi_j|\hat{\boldsymbol{M}}|\Psi_0\rangle] \quad (106)$$

are the rotatory strengths for the excitation $0 \rightarrow j$. The corresponding expression obtained from the RPA Eq. (42) is given by substituting Eqs. (51a) and (51b), accordingly, for the electric and magnetic transition dipole moments. Similar to the oscillator strengths, the rotatory strengths are related to the integrated intensity of the experimentally observed signal $\Delta\varepsilon$ for the reference state '0':

$$R_{0j} = \mathrm{const.}\int_{\mathrm{CD\ \ Band}\ j} \frac{\mathrm{d}E}{E}\cdot\frac{\Delta\varepsilon_0(E)}{l/(\mathrm{mol}\cdot\mathrm{cm})} \quad (107)$$

The constant of proportionality in the last equation is approx 22.97×10^{-40} esu cm erg/G, referring to c.g.s. units in which the rotatory strengths are usually reported. The conversion to SI units is 3.336×10^{-15} C·m·J/T/c.g.s-unit. It is also common to report dimensionless 'reduced' rotatory strengths, which are obtained from the R values in 10^{-40} c.g.s.-units units by multiplication with 1.07827. As for optical rotations, CD is only observed when the molecule's symmetry group does not contain a $\mathscr{S}_n$.

For the practically most important case of real wavefunctions it can be seen that, since $\hat{\boldsymbol{D}}$ is a real operator and $\hat{\boldsymbol{M}}$ is purely imaginary, the rotatory strengths as real quantities must be related to the imaginary part of the product of the electric transition dipole and the magnetic one $\langle\Psi_j|\hat{\boldsymbol{M}}|\Psi_0\rangle$. Mathematically, this comes about out due to the fact that the perturbation is proportional $\dot{\boldsymbol{E}}$ or $\dot{\boldsymbol{B}}$ instead of $\boldsymbol{E}$ or $\boldsymbol{B}$, which introduces imaginary prefactors in Eq. (19) upon Fourier transformation. The rotatory strengths afford the sum rule

$$\sum_{j\neq0} R_{0j} = 0 \quad (108)$$

i.e. the CD spectrum necessarily consists of positive and negative bands at different excitation energies. The rotatory strengths can either be computed explicitly from the knowledge of reference- and excited state wavefunctions and their energies, or alternatively from a consideration of the solutions of the RPA Eq. (42) (or its ab-initio generalizations), which again leads to the pseudo-eigenvalue Eq. (50). Both the electric and the magnetic transition dipole moments can in this case be obtained from the eigenvectors $\boldsymbol{F}_{0j}$ of Ω, as shown in Eq. 51. As in the case of the simulation of UV–vis spectra, time-dependent density functional methods yield more accurate excitation energies and rotatory strengths than the Hartree–Fock approach. Because of the fact that neighbor excitations with rotatory strengths of different sign can cancel, an assignment of CD bands and an extraction of individual experimental rotatory strengths based on Eq. (107) is often difficult except in unambiguous cases where it is obvious that the CD band is due to a single transition.

CD and optical rotations are intimately related to each other by the so-called Kronig–Kramers transformations [352]. Also, from the inspection of the SOS formula for the optical rotation parameter it is clear that the optical rotation parameter can be calculated once all the excitation frequencies and the rotatory strengths are known. Likewise, by the Kronig–Kramers transformations the CD spectrum can be computed from the knowledge of the optical rotatory dispersion (ORD) over the whole frequency range and vice versa. Some earlier experimental data for CD spectra have in fact been calculated from the ORD spectrum [352].

3.2.3.3. Applications. The calculation of optical rotations (OR) and circular dichroism (CD) by time-dependent DFT has in the past few years received attention from several research groups, and implementations into various codes have been reported quite recently [357,359–370]. Methodology involving ab-initio codes and earlier semiempirical approaches is described, e.g. in Refs. [274,352,354–356,370–380]. We refer to Ref. [381] and references therein for more detailed overviews regarding applications to organic molecules, and to Ref. [382] in particular for an overview of common computational methodology until 1994. The first-principles computation of OR and CD for transition metal complexes has not received much attention so far due to the computational effort involved and due to the need for accurate wavefunctions/orbitals within high quality basis sets because of the cancellation of large contributions of opposite sign that have thus to be computed very precisely. Further, CD and OR is only observed for molecules with no or very low symmetry, which means that the popular set of small but highly symmetric molecules that is so often studied regarding polarizabilities is not suitable for this type of application. Twisted ethylene has therefore been studied in a number of pioneering implementations for CD, e.g. as a model compound for *trans*-cyclooctene which is still a small molecule as compared to most transition metal complexes.

However, much has been learned about optical activity of metal complexes from semi-empirical treatments based on the ligand field model [383–385]. It allows a qualitative understanding of the CD effect of the lowest-energy excitations in terms of small deviations from non chiral parent symmetries and the associated mixing of orbitals of different parent symme-

tries upon the chiral distortion of a complex. Due to the small number of excitations that are treated by this approach, a reliable estimate of the OR by employing the SOS equation can not be given. A very well studied system is here the complex $[Co(en)_3]^{3+}$ (en = ethylenediamine), which has D_3 symmetry. The absorption and the CD spectrum of this complex are displayed in Fig. 10 together with an illustration of how a trigonal distortion of the octahedral symmetry splits the metal $t_{2g}^5 e_g^1$ excited states in the complex. The singlet–singlet d–d transitions are symmetry but forbidden in O_h symmetry become allowed in D_3 symmetry and give rise to the weak absorption bands at 21 000 and 29 000 cm^{-1}. In fact, the deviation from the achiral octahedral symmetry is not very large ($E(^1A_2) - E(^1E) \approx 500\ cm^{-1}$ [386]), therefore the the two excitations around 21 000 cm^{-1} are not resolved experimentally, and only the (small) sum of their CD is observed in the spectrum. We note that the deviation of a chiral geometry from a given symmetry can be quantitatively expressed in form of so-called 'continuous symmetry measurements' CSM (or continuous chirality measurements), either based upon discrete sets of points [387–390] or wave-function based [391], that often correlate well with the observed strength of the optical activity. The d–d transitions in this and similar complexes have been studied by several semiempirical approaches based on the ligand field model [392–395]. We refer to the overviews about transition metal CD in Refs. [383,385] for details. The ligand field theory for d–d transitions has also been extended to f–f transitions [396,397]. In the case of ligands such as phenanthroline (phen) or bipyridyl (bipy), chiral complexes exhibit CD of the ligand's π–π* excitations. This mechanism has been studied by the 'exciton theory' of optical activity. Examples (Fe, Ru, Os $phen_3$ and $bipy_3$) can be found in Refs. [398,399] along with theoretical estimates of the rotatory strengths. Alternative calculations employing the coupled chromophor model have lead to somewhat different interpretations of the spectrum [400,401].

The present authors have recently implemented the DFT computation of CD and OR [366–368], and currently applications to chiral closed-shell transition metal complexes are carried out. Fig. 11 displays a computation for the CD-spectrum of the *lel*$_3$-conformation of Λ-$[Co(en)_3]^{3+}$, employing the full D_3 symmetry of the complex. The computed rotatory strengths and the excitation energies are indicated by the vertical lines in Fig. 11. The calculated line spectrum has been converted to a simulated spectrum by representing each transition by a Gaussian function that reproduces the computed oscillator- and rotatory strengths of each transition upon integration. The line width has been chosen proportional to the square root of the excitation energy in order to match the magnitudes of the experimentally observed spectra over the range of frequencies. The results for other conformers of the complex are very similar and not shown. The following interpretation is tentative. The absorption spectrum is qualitatively well reproduced. The good performance of DFT for this type of applications has already been noted

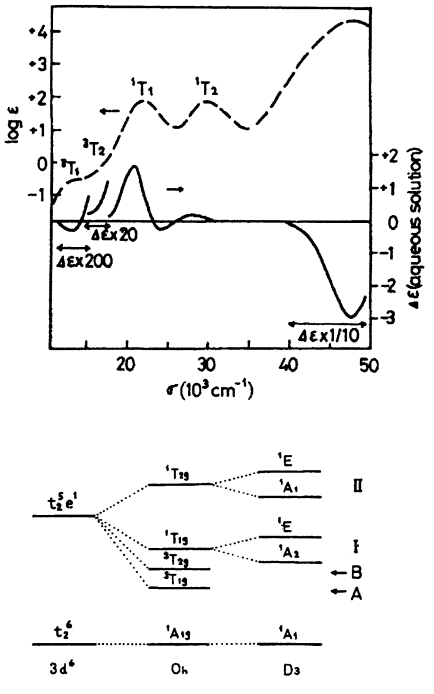

Fig. 10. Experimental absorption (dashed line) and CD spectrum (straight line) of Λ-$[Co(en)_3]^{3+}$ (upper figure). Lower figure: relative energies of excited states of a d^6 metal ion in the octahedral and the D_3 crystal field. Both graphics reprinted from Kuroda and Saio, Ref. [383] with permission from Wiley-VCH.

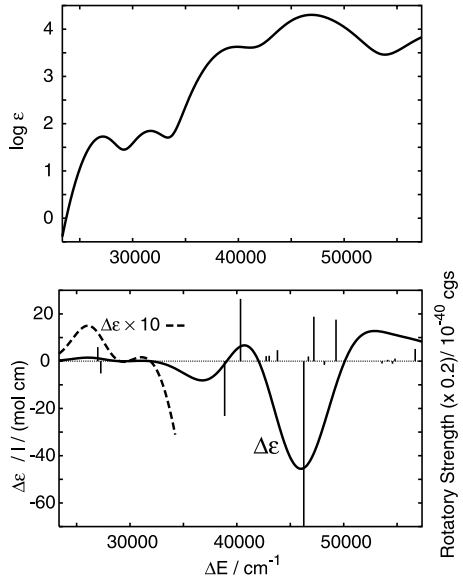

Fig. 11. Simulated absorption and CD spectrum of the *lel*$_3$ conformer of Λ-$[Co(en)_3]^{3+}$, from density functional calculations [402]. The computed rotatory strengths and the excitation energies are indicated as vertical lines.

in Ref. [343]. However, the excitation energies predicted from the BP86 functional appear to be in less good agreement with the experimental data as compared to the B3LYP hybrid functional that has been employed to calculate the excitation energies of some Ruthenium complexes [343]. The computed individual rotatory strengths for the two lowest d–d transitions are somewhat smaller than experimentally determined values and previous estimates based on the ligand-field model [383], but the resulting magnitude of the simulated spectrum in the frequency range of the d–d transitions agrees well with the experimental one. Computationally, the d–d transitions are shifted to higher energies. At the same time, the first charge-transfer (CT) band, experimentally observed at 48 000 cm^{-1}, is somewhat too low in energy. The existence of the second charge-transfer CD band with positive $\Delta\varepsilon$ at higher energies has been experimentally observed in vacuum UV CD measurements at $\sim$ 58 000 cm^{-1} and is also predicted somewhat too low in energy in the computation. To some extent, this is a known defect of the density functional that has been used (BP86), since it overestimates the covalent character of the metal–ligand bonds, resulting in a too large HOMO–LUMO gap. At the same time, the ligand-to-d charge transfer excitations are underestimated in energy. Therefore, quantitative agreement with the experimental spectrum can not be achieved by simply shifting all calculated value by a constant. A problem might also be the fact that the complex has a high charge, and solvent effects and coordination by the counter ion will certainly be of some importance. However, apart from these deviations, the $\Delta\varepsilon$ values of the simulated spectrum agree reasonably well with the experimental spectrum. The computation predicts a second pair of (much weaker) CD bands between 35 000 and 45 000 cm^{-1} due to linand-to-d charge transfer, that are not visible in the experimental spectrum. This could be due to an overestimation of the energy splitting between the two excitations in the computations. If the CD bands were much closer in energy, they would not necessarily be observed at the experimental resolution. Another possibility is that this first pair of CD bands in the charge-transfer region in the simulated spectrum corresponds to the CT band that is visible in the experimetal spectrum at 48 000 cm^{-1}, but is strongly underestimated in energy due to the missing treatment of solvent effects in combination with deficiencies of to the density functional. It has already been noted that the BP86 functional leads to rather good agreement of the computed and the experimentally observed shape of the CD spectrum [367], which appears to be the case here as well. Based on the contributions of occupied and virtual orbitals to the $\boldsymbol{F}_{0j}$-vectors, an assignment of each transition can be made which is in qualitative agreement with predictions from a simple ligand field model. Further details on the CD spectrum of $[Co(en)_3]^{3+}$ and other metal complexes will be published elsewhere [402].

3.3. Related properties

3.3.1. VCD

The CD effect that we have discussed in Section 3.2.3 is not necessarily restricted to electronic transitions and excitation wavelengths in the UV–vis range. An important experimental technique for the investigation of chiral molecules is in fact based on the CD effect for vibrational transitions usually at infrared wavelengths which has been termed 'vibrational CD' (VCD). Generally, the rotatory strengths are defined as in Eq. (106), but refer to the complete (nuclear+electronic) wavefunctions and the respective operators instead. Likewise, the electric and magnetic dipole moment operators include the nuclear contributions as well. When working in the Born–Oppenheimer approximation, the nuclear and electronic transition dipole moments are completely separated, and there are no contributions from the electrons to the VCD and from the nuclear motion to the CD. If we write the electric and magnetic dipole moment operators as a sum over electronic $\hat{\boldsymbol{D}}^{\mathrm{e}}$ and nuclear $\hat{\boldsymbol{D}}^{\mathrm{N}}$ contributions, and the total wavefunction $\Psi_{0v}(\boldsymbol{\tau},\boldsymbol{q})$ as a simple product of electronic $\Psi_0^{\mathrm{e}}(\boldsymbol{\tau})$ and nuclear wavefunction $\Phi_{0v}(\boldsymbol{q})$ for an electronic reference state '0' and an associated vibrational state 'v', we have for a transition dipole moment for the vibrational transition $0\rightarrow 1$

$$\begin{aligned}\mathscr{O}_{01} &= \langle \Psi_0^{\mathrm{e}}\Phi_{00}|\hat{\mathscr{O}}^{\mathrm{e}} + \hat{\mathscr{O}}^{\mathrm{N}}|\Psi_0^{\mathrm{e}}\Phi_{00}\rangle \\ &= \langle \Psi_0^{\mathrm{e}}|\hat{\mathscr{O}}^{\mathrm{e}}|\Psi_0^{\mathrm{e}}\rangle\langle\Phi_{00}|\Phi_{01}\rangle + \langle \Psi_0^{\mathrm{e}}|\Psi_0^{\mathrm{e}}\rangle\langle\Phi_{00}|\hat{\mathscr{O}}^{\mathrm{N}}|\Phi_{01}\rangle \end{aligned} \quad (109)$$

where $\hat{\mathscr{O}}$ is either the electric or the magnetic dipole moment. Since the ground and excited state nuclear wavefunctions are orthogonal, the electronic contribution vanishes, and the only term left is the purely nuclear term $\langle\Phi_{00}|\hat{\mathscr{O}}^{\mathrm{N}}|\Phi_{01}\rangle$.

In order to obtain meaningful results it is necessary to consider both electronic and nuclear contributions to the VCD effect. The former arise from the dependence of the electronic structure on the nuclear coordinates and the effect of electronic states on the nuclear motion. The reason for the importance of the vibronic contributions lies in the fact that the nuclear rotatory strengths are smaller by several orders of magnitude as compared to the electronic CD because of their dependence on the inverse nuclear masses. In order to obtain the electronic contributions, it is necessary to introduce some degree of coupling between the electronic and the nuclear degrees of freedom, because otherwise the electronic contributions to the VCD vanish as shown above. This is achieved through vibronic coupling, i.e. the total wavefunction of the reference state depends on all the Born–Oppenheimer nuclear and electronic wavefunc-

tions. The coupling comes through the action of the nuclear kinetic energy operator $\hat{T}_N$. Also, the dependence of the electronic wavefunction on the nuclear displacements will be considered explicitly by an additional linear term of the form $(\partial\Psi_0^e/\partial\boldsymbol{q})\boldsymbol{q}$.

We follow closely the detailed derivation of Ref. [403] (see also Refs. [404,405]). As in Section 2, one can apply first-order perturbation theory in order to obtain the total reference wavefunction $\Psi_{0v}(\boldsymbol{\tau},\boldsymbol{q}_\alpha)$ ($\boldsymbol{q}_\alpha$ indicates a dependence on the nuclear positions in terms of the normal modes) from the complete set of Born–Oppenheimer (BO) wavefunctions $\Psi_j^e(\boldsymbol{\tau},\boldsymbol{q}_\alpha)\cdot\Phi_{jv}(\boldsymbol{q}_\alpha)$ (the electronic wavefunctions Ψ of Section 2 have been renamed to Ψ^e) as

$$\Psi_{0v}(\boldsymbol{\tau},\boldsymbol{q}_\alpha)=\Psi_0^e(\boldsymbol{\tau},\boldsymbol{q}_\alpha)\Phi_{0v}(\boldsymbol{q}_\alpha)+\left.\frac{\partial\Psi_0^e}{\partial\boldsymbol{q}_\alpha}\right|_{\boldsymbol{q}_\alpha=0}\boldsymbol{q}_\alpha\Phi_{0v}+\sum_{jv'\neq 0v}C_{jv'}^{0v}\Psi_j^e(\boldsymbol{\tau},\boldsymbol{q}_\alpha)\Phi_{jv'}(\boldsymbol{q}_\alpha) \tag{110}$$

Here, v is the vibrational level in the electronic state j. The electronic wavefunctions depend parametrically on the $\boldsymbol{q}_\alpha$ values, which we will not always write explicitly. From a similar argument that leads to Eq. (21), the coefficients C are obtained as

$$C_{jv'}^{0v}=\frac{\langle\Psi_j^e\Phi_{jv'}|\hat{\mathscr{K}}|\Psi_0^e\Phi_{0v}\rangle}{E_{0v}-E_{jv'}} \tag{111}$$

with the perturbation operator

$$\hat{\mathscr{K}}=-(\partial/\partial\boldsymbol{q}_\alpha)^{\Psi}(\partial/\partial\boldsymbol{q}_\alpha)^{\Phi}-\frac{1}{2}(\partial^2/\partial\boldsymbol{q}_\alpha^2)^{\Psi} \tag{112}$$

where the superscripts Ψ and Φ indicate the function on which the operator acts. The set of nuclear wavefunctions is obtained from the harmonic oscillator approximation. This is consistent with simulating the vibrational spectrum from the harmonic approximation in Section 3.1.5. Restricting the dependence of the electronic wavefunction on the nuclear coordinates to the linear term in Eq. (110) is further consistent with neglecting the second derivative in Eq. (112). The total wavefunctions for the reference electronic state thus read

$$\Psi_{0v}(\boldsymbol{\tau},\boldsymbol{q}_\alpha)=\Psi_0^e\Phi_{0v}+\frac{\partial\Psi_0^e}{\partial\boldsymbol{q}_\alpha}|_{\boldsymbol{q}_\alpha=0}\boldsymbol{q}_\alpha\Phi_{0v}-\sum_{jv'\neq 0v}\frac{\langle\Psi_j^e|\dfrac{\partial\Psi_j^e}{\partial\boldsymbol{q}_\alpha}\rangle_{\boldsymbol{q}_\alpha=0}\langle\Phi_{jv'}|\dfrac{\partial\Phi_{0v}}{\partial\boldsymbol{q}_\alpha}\rangle_{\boldsymbol{q}_\alpha=0}}{E_{0v}-E_{jv'}}\Psi_j^e\Phi_{jv'} \tag{113}$$

We will focus on the electronic contributions in the following, and assume real wavefunctions. The nuclear contributions to the transition dipole moments are analytically obtained from the harmonic approximation and do not involve further integration upon electronic degrees of freedom. The energy denominators in Eq. (113) are approximated by (E_0-E_j), i.e. the splitting of the vibrational levels is neglected compared to the electronic excitation energies. The electronic contribution to the electric or magnetic transition dipole moments reads then

$$\begin{aligned}\mathscr{O}_{01}^e&=\langle\Psi_{00}(\boldsymbol{\tau},\boldsymbol{q}_\alpha)|\hat{\mathscr{O}}^e|\Psi_{01}(\boldsymbol{\tau},\boldsymbol{q}_\alpha)\rangle\\&\approx\left[\langle\Psi_0^e|\hat{\mathscr{O}}^e|\frac{\partial\Psi_0^e}{\partial\boldsymbol{q}_\alpha}\rangle+\langle\frac{\partial\Psi_0^e}{\partial\boldsymbol{q}_\alpha}|\hat{\mathscr{O}}^e|\Psi_0^e\rangle\right]_{\boldsymbol{q}_\alpha=0}\langle\Phi_{0,0}|\boldsymbol{q}_\alpha|\Phi_{0,1}\rangle\\&\quad-\sum_{j\neq 0}\frac{\langle\Psi_0^e|\hat{\mathscr{O}}^e|\Psi_j^e\rangle\langle\Psi_j^e|\dfrac{\partial\Psi_0^e}{\partial\boldsymbol{q}_\alpha}\rangle}{(E_0-E_j)}\langle\Phi_{00}|\frac{\partial\Phi_{01}}{\partial\boldsymbol{q}_\alpha}\rangle\\&\quad-\sum_{j\neq 0}\frac{\langle\Psi_j^e|\hat{\mathscr{O}}^e|\Psi_0^e\rangle\langle\Psi_0^e|\dfrac{\partial\Psi_j^e}{\partial\boldsymbol{q}_\alpha}\rangle}{(E_0-E_j)}\langle\Phi_{01}|\frac{\partial\Phi_{00}}{\partial\boldsymbol{q}_\alpha}\rangle\\&\quad+\text{higher order terms}\end{aligned} \tag{114}$$

The following equations are needed in order to obtain the final results for the electronic contributions:

$$\langle\Phi_{00}|\boldsymbol{q}_\alpha|\Phi_{01}\rangle=\sqrt{1/(2\omega_\alpha)} \tag{115a}$$

$$\langle\Phi_{00}|\frac{\partial\Phi_{01}}{\partial\boldsymbol{q}_\alpha}\rangle=\sqrt{\omega_\alpha/2} \tag{115b}$$

In the case of the electric dipole moment, the last two terms on the right hand side of Eq. (114) cancel while the first two are equal. With Eq. (115a), the electronic contribution to the electric transition dipole moment reads, therefore

$$\boldsymbol{D}_{01}^e=2\sqrt{1/(2\omega_\alpha)}\langle\Psi_0^e|\hat{\boldsymbol{D}}^e|\frac{\partial\Psi_0^e}{\partial\boldsymbol{q}_\alpha}\rangle_{\boldsymbol{q}_\alpha=0} \tag{116}$$

for normal mode α. In the case of the magnetic transition dipole moment, the first two terms on the right hand side of Eq. (114) cancel, and one obtains instead from the last two terms with Eq. (115b)

$$\boldsymbol{M}_{01}^e=2\sqrt{\omega_\alpha/2}\sum_{j\neq 0}\frac{\langle\Psi_0^e|\hat{\boldsymbol{M}}^e|\Psi_0^e\rangle_{\boldsymbol{q}_\alpha=0}}{E_0-E_j}\langle\Psi_j^e|\frac{\partial\Psi_0^e}{\partial\boldsymbol{q}_\alpha}\rangle_{\boldsymbol{q}_\alpha=0} \tag{117}$$

for normal mode α. Upon consideration of the nuclear contributions to the transition dipole moments, one obtains the final equations for the VCD effect within the 'vibronic coupling theory' [404–409].

Upon comparison of Eq. (117) with the expression for the time-independent perturbed electronic wavefunction in Eq. (21) for a perturbation by an external magnetic field, with $\hat{A}=-\hat{\boldsymbol{M}}^e$, it becomes obvious that the sum over states in Eq. (117) can be replaced by this first-

order perturbed wavefunction in a magnetic field. This is the 'magnetic field perturbation' formalism of VCD by Stephens [404]. The magnetic transition dipole moment reads accordingly

$$\boldsymbol{M}_{01}^{e} = 2\sqrt{\omega_\alpha/2} \cdot \left\langle \frac{\partial \Psi_0^e}{\partial \boldsymbol{B}} \middle| \frac{\partial \Psi_0^e}{\partial \boldsymbol{q}_\alpha} \right\rangle_{\boldsymbol{B}=0,\boldsymbol{q}_\alpha=0} \quad (118)$$

From this it can be seen that the VCD effect is readily computed once the first-order perturbed wavefunctions (or orbitals) with respect to an external magnetic field and nuclear displacements, respectively, are made available, the normal modes and frequencies are known, and the nuclear contributions to the VCD have been evaluated. Standard methodology can be employed for the task of computing the perturbed wavefunctions/orbitals, since the respective quantities are already necessary on the one hand in calculations of harmonic force constants and IR frequencies (which are in any case necessary for a simulation of a VCD spectrum), and on the other hand for NMR or ESR or magnetizability computations (this also includes necessary gauge correction terms). See Sections 3.1.1, 3.1.3, 3.1.4 and 3.1.5.

Applications of first-principles theories of VCD have been of considerable interest during the past two decades [408,409,411–415]. As with most other properties being discussed so far, more recent developments and applications have mostly concentrated on DFT because of its computational efficiency [416–421]. The first calculation for a molecule containing a transition metal has appeared only very recently [410], employing DFT and the magnetic field perturbation formalism. The VCD of the complex $Zn(sp)_2Cl_2$, with sp = 6*R*,7*S*,9*S*,11*S*-(−)-sparteine, has been investigated experimentally and by DFT computations (B3LYP). Fig. 12 displays the results that have been obtained for the vibrational spectrum. It can be seen that the theoretical results are in good agreement with the experimental spectra. The same authors have also recently studied the VCD spectrum of Λ-$Co(en)_3^{3+}$ (en = ethylenediamine), with similar success [422]. In this study, in particular the role of the anion in the stabilization of the various conformers has been investigated. The computations predicted the *ob*$_3$ conformer to be most stable for the isolated cation, whereas previous theoretical estimates [423] and experimental data suggests a predominance of *lel* conformations. Concerning the free energies, the mixed conformations are favored by the entropy term. The authors have suggested that it might be the interaction with solvent molecules or with the counter ion that stabilizes the *lel* conformations.

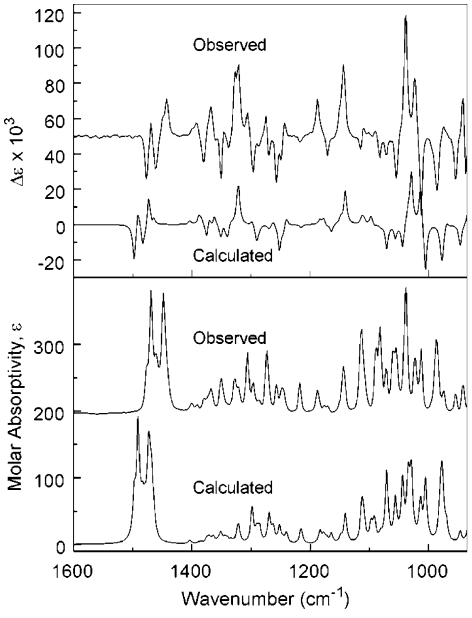

Fig. 12. Experimental and calculated (DFT) IR and VCD spectra of $Zn(sp)_2Cl_2$, reprinted with permission from He et al., Ref. [410] © (2001) American Chemical Society. The observed spectra have been offset for better readability.

We briefly note that there exists also a corresponding Raman CD effect. See, e.g. Ref. [353] for details and literature references.

3.3.2. MCD, MORD

Optical rotations and the CD and VCD effects are only observed for chiral molecules. However, by applying an external magnetic field, it is possible to induce an 'amount of chirality' in the electronic wavefunctions such that the electronic transitions exhibit a CD effect. This is called magnetic circular dichroism (MCD). The corresponding optical rotation in a magnetic field is, in case its frequency dependence is also concerned, called magneto optical rotatory dispersion (MORD). The theoretical description involves initially the knowledge of the wavefunction/orbitals in a magnetic field, which can be considered, e.g. on a perturbational level leading to 3rd order formalism. MCD and MORD can conceptually also be understood on the basis of a second-order perturbational treatment in case the first-order magnetically perturbed wavefunction/orbitals are first calculated from Eq. (21) and used as part of the zero order quantities. It is beyond the scope of this paper to present the formalism, and we refer to the literature for details [424,425].

4. Concluding remarks

We have outlined the theoretical approach to the computation of various second-order energy derivatives that are of considerable importance in chemical research. Examples together with applications to transition metal complexes have been discussed in detail in Section 3, such as NMR and ESR properties, electronic and vibrational spectra, relativistic effects, and obser-

vables related to optical activity. The methodologies are implemented in various popular quantum chemical program codes that are available for researchers worldwide. In recent years, many applications to coordination compounds have successfully been carried out with density functional methods. Most of the research fields are still under active development in order to incorporate a better correlation treatment or relativistic effects, or to establish the usefulness of DFT within the field and develop better suited functionals for specific purposes.

Acknowledgements

This work has received financial support from National Science and Engineering Research Council of Canada (NSERC). We thank Prof. Dr. F.E. Jorge for carrying out the CD calculations on $[Co(en)_3]^{3+}$ in Section 3.2.3. We further thank Prof. Dr. M. Kaupp for pre- and reprints of his recent work and Prof. Dr. W.H.E. Schwarz for comments on Section 3.1.7.

References

[1] T. Ziegler, J. Chem. Soc. Dalton Trans. (2002) 642.
[2] R.G. Parr, W. Yang, Density Functional Theory of Atoms and Molecules, Oxford University Press, New York, 1989.
[3] H. Hellmann, Z. Phys. 85 (1933) 180.
[4] A. Willetts, J.E. Rice, D.M. Burland, D.P. Shelton, J. Chem. Phys. 97 (1992) 7590.
[5] S.T. Epstein, The Variation Method in Quantum Chemistry, Academic Press, New York, 1974.
[6] R. McWeeny, Methods of Molecular Quantum Mechanics, 2nd ed., Academic Press, London, 1992.
[7] F.W. Byron, R.W. Fuller, The Mathematics of Classical and Quantum Physics, Addison-Wesley, Reading, MA, 1969.
[8] P. Pulay, Mol. Phys. 17 (1969) 197.
[9] P. Pulay, Analytical derivative techniques and the calculation of vibrational spectra, in: D.R. Yarkony (Ed.), Modern Electronic Structure Theory Part II, vol. 2, World Scientific, Singapore, 1995, pp. 1191–1240.
[10] J. Gerratt, I.M. Mills, J. Chem. Phys. 49 (1968) 1719.
[11] J. Gerratt, I.M. Mills, J. Chem. Phys. 49 (1968) 1730.
[12] F. London, J. Phys. Radium 8 (1937) 397.
[13] R. Ditchfield, Mol. Phys. 27 (1974) 789.
[14] W. Kutzelnigg, Isr. J. Chem. 19 (1980) 193.
[15] E.K.U. Gross, J.F. Dobson, M. Petersilka, Top. Curr. Chem. 81 (1996) 181.
[16] E.K.U. Gross, W. Kohn, Adv. Quant. Chem. 21 (1990) 255.
[17] M.E. Casida, Time-dependent density functional response theory for molecules, in: D.P. Chong (Ed.), Recent Advances in Density Functional Methods, vol. 1, World Scientific, Singapore, 1995.
[18] S.J.A. van Gisbergen, J.G. Snijders, E.J. Baerends, J. Chem. Phys. 103 (1995) 9347.
[19] C. Jamorski, M.E. Casida, D.R. Salahub, J. Chem. Phys. 104 (1996) 5134.
[20] R. Bauernschmitt, R. Ahlrichs, Chem. Phys. Lett. 256 (1996) 454.
[21] J.F. Dobson, Time-dependent density functional theory, in: J.F. Dobson, G. Vignale, M.P. Das (Eds.), Electronic Density Functional Theory. Recent Progress and New Directions, Plenum Press, New York, 1998, pp. 43–53.
[22] F. Furche, J. Chem. Phys. 114 (2001) 5982.
[23] R. Van Leeuwen, Int. J. Mod. Phys. B 15 (2001) 1969.
[24] A.D. McLachlan, M.A. Ball, Rev. Mod. Phys. 36 (1964) 844.
[25] P.W. Langhoff, S.T. Epstein, M. Karplus, Rev. Mod. Phys. 44 (1972) 602.
[26] A. Szabo, N.S. Ostlund, J. Chem. Phys. 67 (1977) 4351.
[27] J. Oddershede, Propagator methods, in: K.P. Lawley (Ed.), Ab initio Methods in Quantum Chemistry, vol. II, Wiley, New York, 1987, pp. 201–239.
[28] A. Dalgarno, G.A. Victor, Proc. R. Soc. Lond. A 291 (1966) 291.
[29] J.-M. André, et al., Exploring Aspects of Computational Chemistry, vol. 1, Presses Universitaires Namur, Namur, 1997.
[30] D.P. Santry, J. Chem. Phys. 70 (1979) 1008.
[31] D.P. Santry, Chem. Phys. Lett. 61 (1979) 417.
[32] D.P. Santry, T.E. Raidy, Chem. Phys. Lett. 61 (1979) 413.
[33] P.E.S. Wormer, F. Visser, J. Paldus, J. Comput. Phys. 48 (1982) 23.
[34] K. Wolinski, J.F. Hinton, P. Pulay, J. Am. Chem. Soc. 112 (1990) 8251.
[35] J.H. van Lenthe, P. Pulay, J. Comput. Chem. 11 (1990) 1164.
[36] M.R. Hestenes, E. Stiefel, J. Res. Natl. Bur. Stand. 49 (1952) 498.
[37] J.A. Pople, K. Raghavachari, H.B. Schlegel, J.S. Binkley, Int. J. Quantum Chem. S 13 (1979) 225.
[38] E.R. Davidson, J. Comput. Phys. 17 (1975) 87.
[39] B. Roos, Chem. Phys. Lett. 15 (1972) 153.
[40] R.J. Bartlett, E.J. Brändas, J. Chem. Phys. 56 (1972) 5467.
[41] P. Pulay, Chem. Phys. Lett. 73 (1980) 393.
[42] P. Pulay, J. Comput. Chem. 3 (1982) 556.
[43] P. Jørgensen, J. Simons, Second Quantization-Based Methods in Quantum Chemistry, Academic Press, New York, 1981.
[44] J.B. Foresman, M. Head-Gordon, J.A. Pople, M.J. Frisch, J. Phys. Chem. 96 (1992) 135.
[45] M.E. Casida, et al., J. Chem. Phys. 113 (2000) 7062.
[46] B. Champagne, B. Kirtman, Theoretical approach to the design of organic molecular and polymeric nonlinear optical materials, in: H.S. Nalwa (Ed.), Handbook of Advanced Electronic and Photonic Materials and Devices, vol. 9, Academic Press, New York, 2001.
[47] B. Champagne, P. Fischer, A.D. Buckingham, Chem. Phys. Lett. 331 (2000) 83.
[48] S.D. Peyerimhoff, Spectroscopy: computational methods, in: P. von Ragué Schleyer (Ed.), Encyclopedia of Computational Chemistry, Wiley, Chichester, 1998, pp. 2646–2664.
[49] J. Oddershede, Adv. Quantum Chem. 11 (1978) 275.
[50] R.E. Moss, Advanced Molecular Quantum Mechanics, Chapman and Hall, London, 1973.
[51] B.A. Hess, Relativistic theory and applications, in: P. von Ragué Schleyer (Ed.), Encyclopedia of Computational Chemistry, Wiley, Chichester, 1998, pp. 2499–2508.
[52] A.J. Sadlej, Methods of relativistic quantum chemistry, in: B.O. Roos (Ed.), Lecture Notes in Chemistry II, vol. 64, Springer, Berlin, 1994, pp. 203–230.
[53] C. Chang, M. Pelissier, M. Durand, Phys. Scr. 34 (1986) 394.
[54] E. van Lenthe, E.J. Baerends, J.G. Snijders, J. Chem. Phys. 99 (1993) 4597.
[55] K. Dyall, E. van Lenthe, J. Chem. Phys. 111 (1999) 1366.
[56] J.E. Harriman, Theoretical Foundations of Electron Spin Resonance, Academic Press, New York, 1978.
[57] W.H.E. Schwarz, Fundamentals of relativistic effects in chemistry, in: Z.B. Masic (Ed.), The Concept of the Chemical Bond, vol. 2, Springer, Berlin, 1990, pp. 559–643.
[58] G.L. Sewell, Proc. Cambridge Philos. Soc. 45 (1949) 631.

[59] R.A. Moore, Can. J. Phys. 53 (1975) 1240.
[60] R.A. Moore, Can. J. Phys. 53 (1975) 1247.
[61] R.A. Moore, Can. J. Phys. 53 (1975) 1251.
[62] A. Rutkowski, J. Phys. B 19 (1986) 149.
[63] A. Rutkowski, J. Phys. B 19 (1986) 3431.
[64] A. Rutkowski, J. Phys. B 19 (1986) 3443.
[65] W. Kutzelnigg, Z. Phys. D 11 (1989) 15.
[66] W. Kutzelnigg, Z. Phys. D 15 (1990) 27.
[67] W. Kutzelnigg, E. Ottschofski, R. Franke, J. Chem. Phys. 102 (1995) 1740.
[68] J. Autschbach, W.H.E. Schwarz, Theor. Chem. Acc. 104 (2000) 82.
[69] R.E. Moss, Mol. Phys. 38 (1979) 1611.
[70] J.D. Morrison, R.E. Moss, Mol. Phys. 41 (1980) 491.
[71] W. Pauli, Die allgemeinen prinzipien der wellenmechanik, in: Handbuch der Physik, vol. 5, Springer, Berlin, 1958.
[72] L. Visscher, E. van Lenthe, Chem. Phys. Lett. 306 (1999) 357.
[73] H. Fukui, T. Baba, H. Inomata, J. Chem. Phys. 105 (1996) 3175.
[74] G. Schreckenbach, T. Ziegler, Int. J. Quantum Chem. 61 (1997) 899.
[75] R. Bouten, et al., J. Chem. Phys. 104 (2000) 5600.
[76] W. Kutzelnigg, J. Comput. Chem. 20 (1999) 1199.
[77] N.C. Pyper, Chem. Phys. Lett. 96 (1983) 204.
[78] N.C. Pyper, Chem. Phys. Lett. 96 (1983) 211.
[79] Z.C. Zhang, G.A. Webb, J. Mol. Struct. 104 (1983) 439.
[80] P. Pyykkö, Chem. Phys. 74 (1983) 1.
[81] P. Pyykkö, Chem. Phys. 22 (1977) 289.
[82] M.M. Sternheim, Phys. Rev. 128 (1962) 676.
[83] H. Akai, et al., Prog. Theor. Phys. Suppl. 101 (1990) 11.
[84] S. Blügel, H. Akai, R. Zeller, P.H. Dederichs, Phys. Rev. B 35 (1987) 3271.
[85] G.A. Aucar, J. Oddershede, Int. J. Quantum Chem. 47 (1993) 425.
[86] S.K. Wolff, T. Ziegler, E. van Lenthe, E.J. Baerends, J. Chem. Phys. 110 (1999) 7689.
[87] J. Autschbach, T. Ziegler, J. Chem. Phys. 113 (2000) 936.
[88] H. Fukui, T. Baba, J. Chem. Phys. 108 (1998) 3854.
[89] Y. Nomura, Y. Takeuchi, N. Nakagawa, Tetrahedron Lett. 8 (1969) 639.
[90] I. Morishima, K. Endo, T. Yonezawa, J. Chem. Phys. 59 (1973) 3356.
[91] M.I. Volodicheva, T.K. Rebane, Teor. Éksp. Khim. (Theor. Exp. Chem.) 14 (1978) 348.
[92] J. Vaara, K. Ruud, O. Vahtras, H. Ågren, J. Jokisaari, J. Chem. Phys. 109 (1998) 1212.
[93] S.K. Wolff, T. Ziegler, J. Chem. Phys. 109 (1998) 895.
[94] T. Baba, H. Fukui, J. Chem. Phys. 110 (1999) 131.
[95] L. Visscher, T. Enevoldsen, T. Saue, H.J.A. Jensen, J. Oddershede, J. Comput. Chem. 20 (1999) 1262.
[96] M. Hada, Y. Ishikawa, J. Nakatani, H. Nakatsuji, Chem. Phys. Lett. 310 (1999) 342.
[97] J. Vaara, O.L. Malkina, H. Stoll, V.G. Malkin, M. Kaupp, J. Chem. Phys. 114 (2001) 61.
[98] J. Autschbach, T. Ziegler, Computation of NMR shieldings and spin–spin coupling constants, in: D.M. Grant, R.K. Harris (Eds.), Encyclopedia of Nuclear Magnetic Resonance, vol. 9, Wiley, Chichester, 2002, pp. 306–323.
[99] H. Fukui, Magn. Res. Rev. 11 (1987) 205.
[100] D.B. Chesnut, Ann. Rep. NMR Spectrosc. 29 (1994) 71.
[101] V.G. Malkin, O.L. Malkina, L.A. Eriksson, D.R. Salahub, The calculation of NMR and ESR spectroscopy parameters using density functional theory, in: J.M. Seminario, P. Politzer (Eds.), Modern Density Functional Theory: a Tool for Chemistry, vol. 2, Elsevier, Amsterdam, 1995, pp. 273–347.
[102] D.B. Chesnut, The ab initio computation of nuclear magnetic resonance chemical shielding, in: K.B. Lipkowitz, D.B. Boyd (Eds.), Reviews in Computational Chemistry, Ch. 5, vol. 8, VCH, New York, 1996, pp. 245–297.
[103] U. Fleischer, C. van Wüllen, W. Kutzelnigg, NMR chemical shift computation: ab initio, in: P. von Ragué Schleyer (Ed.), Encyclopedia of Computational Chemistry, Wiley, Chichester, 1998, pp. 1827–1835.
[104] T. Helgaker, M. Jaszuski, K. Ruud, Chem. Rev. 99 (1999) 293.
[105] M. Bühl, M. Kaupp, O.L. Malkina, V.G. Malkin, J. Comput. Chem. 20 (1998) 91.
[106] M. Kaupp, O.L. Malkina, V.G. Malkin, P. Pyykkö, Chem. Eur. J. 4 (1998) 118.
[107] G. Schreckenbach, S.K. Wolff, T. Ziegler, Covering the entire periodic table: relativistic density functional calculations of NMR chemical shifts in diamagnetic actinide compounds, in: J.C. Facelli, A.C. de Dios (Eds.), Modeling NMR Chemical Shifts. ACS Symposium Series 732, American Chemical Society, Boston, MA, 1999, pp. 101–114.
[108] (a) M. Kaupp, V.G. Malkin, O.L. Malkina, D.R. Salahub, J. Am. Chem. Soc. 117 (1995) 1851;
(b) M. Kaupp, V.G. Malkin, O.L. Malkina, D.R. Salahub, J. Am. Chem. Soc. 117 (1995) 8492 (Erratum).
[109] M. Kaupp, O.L. Malkina, V.G. Malkin, J. Chem. Phys. 106 (1997) 9201.
[110] M. Bühl, Chem. Eur. J. 5 (1999) 3514.
[111] H. Nakatsuji, M. Sugimoto, S. Saito, Inorg. Chem. 29 (1990) 3095.
[112] M. Bühl, S. Gaemers, C.J. Elsevier, Chem. Eur. J. 6 (2000) 3272.
[113] M. Kaupp, V.G. Malkin, O.L. Malkina, D.R. Salahub, Chem. Phys. Lett. 235 (1995) 382.
[114] M. Kaupp, V.G. Malkin, O.L. Malkina, D.R. Salahub, Chem. Eur. J. 2 (1996) 24.
[115] M. Kaupp, Chem. Ber. 129 (1996) 535.
[116] M. Kaupp, Chem. Ber. 129 (1996) 527.
[117] M. Kaupp, Chem. Eur. J. 2 (1996) 348.
[118] A.W. Ehlers, Y. Ruiz-Morales, E.J. Baerends, T. Ziegler, Inorg. Chem. 36 (1997) 5031.
[119] Y. Ruiz-Morales, G. Schreckenbach, T. Ziegler, J. Phys. Chem. 100 (1996) 3359.
[120] T.M. Gilbert, T. Ziegler, J. Phys. Chem. A 103 (1999) 7535.
[121] M. Hada, H. Kaneko, H. Nakatsuji, Chem. Phys. Lett. 261 (1996) 7.
[122] Y. Ishikawa, T. Nakajima, M. Hada, H. Nakatsuji, Chem. Phys. Lett. 283 (1998) 119.
[123] H. Nakatsuji, Z.-M. Hu, T. Nakajima, Chem. Phys. Lett. 275 (1997) 429.
[124] H. Nakatsuji, M. Hada, H. Kaneko, C.C. Ballard, Chem. Phys. Lett. 255 (1996) 195.
[125] J. Wan, R. Fukuda, M. Hada, H. Nakatsuji, J. Phys. Chem. A 105 (2001) 128.
[126] G. Schreckenbach, S.K. Wolff, T. Ziegler, J. Phys. Chem. A 104 (2000) 8244.
[127] A. Rodriguez-Fortea, P. Alemany, T. Ziegler, J. Phys. Chem. A 103 (1999) 8288.
[128] E. van Lenthe, The ZORA Equation, PhD thesis, Vrije Universiteit Amsterdam, Netherlands, 1996.
[129] W. Koch, M.C. Holthausen, A Chemist's Guide to Density Functional Theory, Wiley–VCH, Weinheim, 2000.
[130] D.L. Bryce, R.E. Wasylishen, J. Am. Chem. Soc. 122 (2000) 3197.
[131] R.E. Wasylishen, Dipolar and indirect coupling tensors in solids, in: D.M. Grant, R.K. Harris (Eds.), Encyclopedia of Nuclear Magnetic Resonance, Wiley, Chichester, 1996, pp. 1685–1695.
[132] G. Breit, Phys. Rev. 35 (1930) 1447.
[133] P. Pyykkö, E. Pajanne, M. Inokuti, Int. J. Quantum Chem. 7 (1973) 785.
[134] S. Kirpekar, J.A. Jensen, J. Oddershede, Theor. Chim. Acta 95 (1997) 35.

[135] S. Kirpekar, S.P.A. Sauer, Theor. Chem. Acc. 103 (1999) 146.
[136] J. Autschbach, T. Ziegler, J. Chem. Phys. 113 (2000) 9410.
[137] J. Autschbach, T. Ziegler, J. Am. Chem. Soc. 123 (2001) 3341.
[138] D.L. Bryce, R.E. Wasylishen, J. Autschbach, T. Ziegler, J. Am. Chem. Soc. 124 (2002) 4894.
[139] J. Kowalewski, Ann. Rep. NMR Spectrosc. 12 (1982) 81.
[140] V. Sychrovský, J. Gräfenstein, D. Cremer, J. Chem. Phys. 113 (2000) 3530.
[141] J. Khandogin, T. Ziegler, Spectrochim. Acta A55 (1999) 607.
[142] T. Enevoldsen, L. Visscher, T. Saue, H.J.A. Jensen, J. Oddershede, J. Chem. Phys. 112 (2000) 3493.
[143] J. Autschbach, T. Ziegler, J. Am. Chem. Soc. 123 (2001) 5320.
[144] P. Pyykkö, L. Wiesenfeld, Mol. Phys. 43 (1981) 557.
[145] N. Rösch, P. Pyykkö, Mol. Phys. 57 (1986) 193.
[146] P. Pyykkö, J. Organomet. Chem. 232 (1982) 21.
[147] G.B. Bacskay, I. Bytheway, N.S. Hush, J. Am. Chem. Soc. 118 (1996) 3753.
[148] J. Khandogin, T. Ziegler, J. Phys. Chem. A 104 (2000) 113.
[149] G.A. Aucar, R.H. Contreras, J. Magn. Res. 93 (1991) 413.
[150] G.A. Aucar, E. Botek, S. Gómez, E. Sproviero, R.H. Contreras, J. Organomet. Chem. 524 (1996) 1.
[151] J.A. Gonzaléz, G.A. Aucar, M.C. Ruiz de Azúa, R.H. Contreras, Int. J. Quantum Chem. 61 (1997) 823.
[152] R.M. Lobayan, G.A. Aucar, J. Mol. Struct. 452 (1998) 1.
[153] R.M. Lobayan, G.A. Aucar, J. Mol. Struct. 452 (1998) 13.
[154] G.A. Aucar, T. Saue, L. Visscher, H.J.A. Jensen, J. Chem. Phys. 110 (1999) 6208.
[155] J. Vaara, K. Ruud, O. Vahtras, J. Comput. Chem. 20 (1999) 1314.
[156] S. Patchkovskii, J. Autschbach, T. Ziegler, J. Chem. Phys. 115 (2001) 26.
[157] K.E. Berg, J. Glaser, M.C. Read, I. Tóth, J. Am. Chem. Soc. 117 (1995) 7550.
[158] M. Maliarik, K. Berg, J. Glaser, M.C. Read, I. Tóth, Inorg. Chem. 37 (1998) 2910.
[159] S. Patchkovskii, T. Ziegler, J. Phys. Chem. A 105 (2001) 5490.
[160] G. Schreckenbach, T. Ziegler, J. Phys. Chem. A 101 (1997) 3388.
[161] A. Abragam, B. Bleany, Electron Paramagnetic Resonance for Transition Ions, Clarendon Press, Oxford, 1970.
[162] O.L. Malkina, et al., J. Am. Chem. Soc. 122 (2000) 9206.
[163] M. Kaupp, et al., J. Comput. Chem. 23 (2002) 794.
[164] F. Neese, J. Chem. Phys. 115 (2001) 11080.
[165] E. van Lenthe, P.E.S. Wormer, A. van der Avoird, J. Chem. Phys. 107 (1997) 2488.
[166] G.H. Lushington, F. Grein, Theor. Chim. Acta 93 (1996) 259.
[167] G.H. Lushington, F. Grein, Int. J. Quantum Chem. 106 (1997) 3292.
[168] G.H. Lushington, J. Phys. Chem. A 104 (2000) 2969.
[169] W.H. Moores, R. McWeeny, Proc. R. Soc. Lond. A 332 (1973) 365.
[170] M. Ishii, K. Morihashi, O. Kikuchi, J. Mol. Struct. (Theochem.) 325 (1991) 99.
[171] O. Vahtras, B. Minaev, H. Ågren, Chem. Phys. Lett. 281 (1997) 186.
[172] D. Jayatilaka, J. Chem. Phys. 108 (1998) 7587.
[173] M. Kaupp, Ab initio and density functional calculations of electronic g-tensors for organic radicals, in: A. Lund, M. Shiotani (Eds.), EPR Spectroscopy of Free Radicals in Solids. Trends in Methods and Applications, Kluwer, Dordrecht, in press.
[174] S. Patchkovskii, T. Ziegler, J. Chem. Phys. 111 (1999) 5730.
[175] S. Okada, M. Shinada, O. Matsuoka, J. Chem. Phys. 93 (1990) 5013.
[176] O.L. Malkina, et al., Chem. Phys. Lett. 296 (1998) 93.
[177] P. Belanzoni, E. van Lenthe, E.J. Baerends, J. Chem. Phys. 114 (2001) 4421.
[178] M. Engström, B. Minaev, O. Vahtras, H. Ågren, Chem. Phys. 237 (1998) 149.
[179] S. Patchkovskii, T. Ziegler, J. Am. Chem. Soc. 122 (2000) 3506.
[180] E. van Lenthe, A. van der Avoird, W.R. Hagen, E.J. Reijerse, J. Phys. Chem. A 104 (2000) 2070.
[181] M. Wanner, T. Scheiring, W. Kaim, Inorg. Chem. 40 (2001) 5704.
[182] M. Stein, E. van Lenthe, E.J. Baerends, W. Lubitz, J. Phys. Chem. A 105 (2001) 416.
[183] M. Munzarová, M. Kaupp, J. Phys. Chem. B 105 (2001) 12644.
[184] L.A. Eriksson, ESR hyperfine calculations, in: P. von Ragué Schleyer (Ed.), Encyclopedia of Computational Chemistry, Wiley, Chichester, 1998, pp. 952–958.
[185] P.J.M. Geurts, P.C.P. Bouten, A. van der Avoird, J. Chem. Phys. 73 (1980) 1306.
[186] P. Belanzoni, E.J. Baerends, S. van Asselt, P.B. Langeven, J. Phys. Chem. 99 (1995) 13094.
[187] P. Belanzoni, E.J. Baerends, M. Gribnau, J. Phys. Chem. A 103 (1999) 3732.
[188] M. Munzarová, M. Kaupp, J. Phys. Chem. A 103 (1999) 9966.
[189] E. van Lenthe, A. van der Avoird, P.E.S. Wormer, J. Chem. Phys. 108 (1998) 4783.
[190] H.B. Schlegel, Spin contamination, in: P. von Ragué Schleyer (Ed.), Encyclopedia of Computational Chemistry, Wiley, Chichester, 1998, pp. 2665–2671.
[191] M.L. Munzarová, P. Kubáček, M. Kaupp, J. Am. Chem. Soc. 111 (2000) 11900.
[192] S.M. Colwell, N.C. Handy, Chem. Phys. Lett. 217 (1994) 271.
[193] A.M. Lee, N.C. Handy, S.M. Colwell, J. Chem. Phys. 103 (1995) 10095.
[194] K. Ruud, P.-O. Åstrand, P.R. Taylor, J. Phys. Chem. A 105 (2001) 9926.
[195] F.E. Mabbs, D.J. Machin, Magnetism and Transition Metal Complexes, Chapman and Hall, London, 1973.
[196] U. Fleischer, W. Kutzelnigg, P. Lazeretti, V. Mühlenkamp, J. Am. Chem. Soc. 116 (1994) 5298.
[197] H. Jiao, P. von Ragué Schleyer, Angew. Chem. Int. Ed. Engl. 32 (1993) 1763.
[198] K. Ruud, T. Helgaker, K.L. Bak, P. Jørgensen, H.J.A. Jensen, J. Chem. Phys. 99 (1993) 3847.
[199] K. Ruud, T. Helgaker, P. Jørgensen, K.L. Bak, Chem. Phys. Lett. 223 (1994) 12.
[200] K. Ruud, H. Skaane, T. Helgaker, K.L. Bak, P. Jørgensen, J. Am. Chem. Soc. 116 (1994) 10135.
[201] A. Rizzo, et al., J. Chem. Phys. 102 (1995) 8953.
[202] K. Ruud, P.-O. Åstrand, T. Helgaker, K.V. Mikkelsen, J. Mol. Struct. (Theochem.) 388 (1997) 231.
[203] C. van Wüllen, W. Kutzelnigg, J. Chem. Phys. 104 (1996) 2230.
[204] P.-O. Åstrand, K.V. Mikkelsen, K. Ruud, T. Helgaker, J. Phys. Chem. 100 (1996) 19771.
[205] P.-O. Åstrand, K. Mikkelsen, J. Chem. Phys. 104 (1996) 648.
[206] S.M. Cybulski, D.M. Bishop, J. Chem. Phys. 100 (1994) 2019.
[207] S.M. Cybulski, D.M. Bishop, J. Chem. Phys. 106 (1997) 4082.
[208] M.B. Ferraro, M.C. Caputo, J. Mol. Struct. (Theochem.) 335 (1995) 69.
[209] M.B. Ferraro, M.C. Caputo, J. Chem. Phys. 110 (1999) 10706.
[210] P.W. Fowler, E. Steiner, B. Cadioli, R. Zanasi, J. Phys. Chem. A 102 (1998) 7297.
[211] P.A. Hyams, J. Gerratt, D.L. Cooper, M. Raimondi, J. Chem. Phys. 100 (1994) 4417.
[212] T.A. Keith, Chem. Phys. 213 (1996) 123.
[213] K. Voges, D.H. Sutter, K. Ruud, T. Helgaker, Zeitschr. Naturforsch. Teil A 53 (1998) 67.
[214] A.R. Katritzky, K. Jug, D.C. Oniciu, Chem. Rev. 101 (2001) 1421.
[215] F. De Proft, P. Geerlings, Chem. Rev. 101 (2001) 1451.
[216] J.A.N.F. Gomes, R.B. Mallion, Chem. Rev. 101 (2001) 1349.

[217] R.H. Mitchell, Chem. Rev. 101 (2001) 1301.
[218] D.V. Simion, T.S. Sorensen, J. Am. Chem. Soc. 118 (1996) 7345.
[219] H.J. Dauben, Jr, J.D. Wilson, J.L. Laity, in: J.P. Synder (Ed.), Nonbenzenoid Aromaticity, vol. 2, Academic Press, New York, 1971.
[220] P. von Ragué Schleyer, J. Am. Chem. Soc. 122 (2000) 510.
[221] R.H. Mitchell, P. Zhou, S. Venugopalan, T.W. Dingle, J. Am. Chem. Soc. 112 (1990) 7812.
[222] W. Cornell, S. Louise-May, Normal modes, in: P. von Ragué Schleyer (Ed.), Encyclopedia of Computational Chemistry, Wiley, Chichester, 1998, pp. 1904–1913.
[223] R.D. Amos, Adv. Chem. Phys. 67 (1987) 99.
[224] R.D. Amos, J.E. Rice, Comp. Phys. Rep. 10 (1989) 147.
[225] Y. Yamaguchi, Y. Osamura, J.D. Goddard, H.F. Schaefer, III, A New Dimension to Quantum Chemistry: Analytic Derivative Methods in Ab-initio Molecular Electronic Structure Theory, Oxford University Press, New York, 1994.
[226] R.P. Feynman, Phys. Rev. 56 (1939) 340.
[227] H. Nakatsuji, K. Matsuda, T. Yonetzawa, Chem. Phys. Lett. 54 (1978) 347.
[228] N.C. Handy, H.F. Schaefer, J. Chem. Phys. 81 (1984) 5031.
[229] H.B. Schlegel, Adv. Chem. Phys. 67 (1987) 249.
[230] F. Bernardi, M.A. Robb, Adv. Chem. Phys. 67 (1987) 155.
[231] C.W. Bauschlicher, Jr, S.R. Langhoff, H. Partridge, The application of ab initio electronic structure calculations to molecules containing transition metal atoms, in: D.R. Yarkony (Ed.), Modern Electronic Structure Theory Part II, vol. 2, World Scientific, Singapore, 1995, pp. 1280–1374.
[232] V. Jonas, W. Thiel, J. Chem. Phys. 102 (1995) 8474.
[233] V. Jonas, W. Thiel, J. Chem. Phys. 105 (1996) 3636.
[234] V. Jonas, W. Thiel, Organomatetallics 17 (1998) 353.
[235] V. Jonas, W. Thiel, J. Phys. Chem. A 103 (1999) 1381.
[236] A.P. Scott, L. Radom, J. Phys. Chem. 100 (1996) 16502.
[237] J. Baker, A.A. Jarzecki, P. Pulay, J. Phys. Chem. A 102 (1998) 1412.
[238] P.J. Hay, R.L. Martin, J. Chem. Phys. 109 (1998) 3875.
[239] A. Bérces, T. Ziegler, Top. Curr. Chem. 182 (1996) 42.
[240] A. Bérces, et al., Comp. Phys. Comm. 100 (1997) 247.
[241] H. Jacobsen, A. Bérces, D. Swerhone, T. Ziegler, Comp. Phys. Comm. 100 (1997) 263.
[242] E.B. Wilson, J.C. Decious, P.C. Cross, Molecular Vibrations. The Theory of Infrared and Raman Vibrational Spectra, McGraw-Hill, New York, 1955.
[243] L. Fan, T. Ziegler, J. Chem. Phys. 96 (1992) 9005.
[244] I. Diaz-Acosta, J. Baker, W. Cordes, P. Pulay, J. Phys. Chem. A 105 (2001) 238.
[245] A.A. Jarzęcki, P.M. Kozlowski, P. Pulay, B.-H. Ye, X.-Y. Li, Spectrochim. Acta A 53 (1997) 1195.
[246] P.M. Kozlowski, et al., J. Phys. Chem. A 103 (1999) 1357.
[247] P. Pulay, J. Mol. Struct. 347 (1995) 293.
[248] P. Pyykkö, J. Chem. Res. S (1979) 380.
[249] P. Pyykkö, J.P. Desclaux, Acc. Chem. Res. 12 (1979) 276.
[250] P. Pyykkö, Chem. Rev. 88 (1988) 563.
[251] P. Pyykkö, Effects on periodic trends, in: The Effects of Relativity in Atoms, Molecules and Solids, Plenum, New York, 1991.
[252] K.P. Huber, G. Herzberg, Molecular Spectra and Molecular Structure, Van Nostrand Reinhold, New York, 1979.
[253] S.H. Vosko, L. Wilk, M. Nusair, Can. J. Phys. 58 (1989) 1200.
[254] A.D. Becke, Phys. Rev. A 38 (1988) 3098.
[255] J.P. Perdew, Phys. Rev. B 33 (1986) 8822.
[256] J.P. Perdew, Phys. Rev. B 34 (1986) 7406.
[257] J. Autschbach, About the calculation of relativistic effects, and about the interpretation of their trends in atoms and molecules (in German), PhD thesis, University of Siegen, Siegen, Germany, 1999.
[258] C. van Wüllen, J. Chem. Phys. 103 (1995) 3589.
[259] P. Schwerdtfeger, M. Dolg, W.H.E. Schwarz, G.A. Bowmaker, P.W. Boyd, J. Chem. Phys. 91 (1989) 1762.
[260] U. Kaldor, B.A. Heß, Chem. Phys. Lett. 230 (1994) 1.
[261] S.G. Wang, Relativistische effekte und chemische bindung, PhD thesis, Universität Siegen, Shaker Verlag, Aachen, 1994.
[262] T. Ziegler, J.G. Snijders, E.J. Baerends, J. Chem. Phys 74 (1981) 1271.
[263] C.L. Collins, K.G. Dyall, H.F. Schaefer, III, J. Chem. Phys. 102 (1995) 2024.
[264] J.G. Snijders, P. Pyykkö, Chem. Phys. Lett. 75 (1980) 5.
[265] T. Ziegler, J.G. Snijders, E.J. Baerends, Chem. Phys. Lett. 75 (1980) 1.
[266] P.A. Christiansen, W.C. Ermler, Mol. Phys. 55 (1985) 1109.
[267] W.H.E. Schwarz, Phys. Scr. 36 (1987) 403.
[268] W.H.E. Schwarz, S. Chu, Mol. Phys. 50 (1983) 603.
[269] A. Rutkowski, D. Rutkowska, W.H.E. Schwarz, Theor. Chim. Acta 84 (1992) 105.
[270] A. Rutkowski, W.H.E. Schwarz, Theor. Chim. Acta 76 (1990) 391.
[271] W.H.E. Schwarz, A. Rutkowski, G. Collignon, Nonsingular relativistic perturbation theory and relativistic changes of molecular structure, in: The Effects of Relativity in Atoms, Molecules and the Solid State, Plenum, New York, 1991, pp. 135–146.
[272] J. Autschbach, W.H.E. Schwarz, in preparation.
[273] U. Hohm, D. Goebel, S. Grimme, Chem. Phys. Lett. 272 (1997) 328.
[274] J. Olsen, P. Jørgensen, Time-dependent response theory with applications to self-consistent field and multiconfigurational self-consistent field wave functions, in: D.R. Yarkony (Ed.), Modern electronic Structure Theory Part II, vol. 2, World Scientific, Singapore, 1995, pp. 857–990.
[275] S.P. Apell, J.R. Sabin, S.B. Trickey, J. Oddershede, Int. J. Quantum Chem. 86 (2002) 35.
[276] D.S. Yakovlev, A.P. Mirgorodskiibreve, A.V. Tulub, B.F. Shchegolev, Opt. Spectrosc. 92 (2002) 449.
[277] L. Jensen, P.-O. Åstrand, A. Osted, J. Kongsted, K.V. Mikkelsen, J. Chem. Phys. 116 (2002) 4001.
[278] L. Jensen, P.-O. Åstrand, K.V. Mikkelsen, Int. J. Quantum Chem. 84 (2001) 513.
[279] K. Ruud, D. Jonsson, P.R. Taylor, J. Chem. Phys. 114 (2001) 4331.
[280] F.L. Gu, D.M. Bishop, B. Kirtman, J. Chem. Phys. 115 (2001) 10548.
[281] S. Millefiori, A. Alparone, J. Phys. Chem. A 105 (2001) 9489.
[282] P.P. Korambath, S.P. Karna, J. Phys. Chem. A 104 (2000) 4801.
[283] A. Derevianko, W.R. Johnson, M.S. Safronova, J.F. Babb, Phys. Rev. Lett. 82 (1999) 3589.
[284] J.M. Luis, B. Champagne, B. Kirtman, Int. J. Quantum Chem. 80 (2000) 471.
[285] M.F. Costa, T.L. Fonseca, O.A.V. Amaral, M.A. Castro, Phys. Lett. 263 (1999) 186.
[286] G. Schurer, P. Gedeck, M. Gottschalk, T. Clark, Int. J. Quantum Chem. 75 (1999) 17.
[287] H. Reis, M.G. Papadopoulos, I. Boustani, Int. J. Quantum Chem. 78 (2000) 131.
[288] K. Deng, J. Yang, C.T. Chan, Phys. Rev. A 61 (2000) 25201.
[289] L. Jensen, P.-O. Åstrand, K.O. Sylvester-Hvid, K.V. Mikkelsen, J. Phys. Chem. A 7 (104) 1563.
[290] P.T. van Duijnen, M. Swart, F. Grozema, Quantum Mechanical–Molecular Mechanical Calculations of (Hyper-)Polarizabilities with the Direct Reaction Field Approach. ACS Symposium Series, vol. 712, American Chemical Society, Boston, MA, 1999, pp. 220–233.
[291] B. Champagne, D.H. Mosley, J.G. Fripiat, J.-M. Andre, Adv. Quantum Chem. 35 (1999) 95.

[292] G. Maroulis, C. Makris, U. Hohm, U. Wachsmuth, J. Phys. Chem. A 103 (1999) 4359.
[293] K. Jackson, M. Pederson, C.-Z. Wang, K.-M. Ho, Phys. Rev. A 59 (1999) 3685.
[294] B. Champagne, B. Mennucci, M. Cossi, R. Cammi, J. Tomasi, Chem. Phys. 238 (1998) 153.
[295] P. Norman, Y. Luo, D. Jonsson, H. Ågren, J. Chem. Phys. 106 (1997) 8788.
[296] R. Cammi, M. Cossi, B. Mennucci, J. Tomasi, J. Chem. Phys. 105 (1996) 10556.
[297] Y. Luo, H. Ågren, H. Koch, P. Jørgensen, T. Helgaker, Phys. Rev. B 51 (1995) 14949.
[298] J.M. Stout, C.E. Dykstra, J. Am. Chem. Soc. 117 (1995) 5127.
[299] C.L. Darling, H.B. Schlegel, J. Phys. Chem. 98 (1994) 5855.
[300] S. Karna, Chem. Phys. Lett. 214 (1994) 186.
[301] P. Lazzeretti, M. Malagoli, L. Turci, R. Zanasi, J. Chem. Phys. 99 (1993) 6027.
[302] M.K. Harbola, B. Bhattacharya, H.M. Upadhyaya, S. Chandra, Solid State Commun. 98 (1996) 1629.
[303] M. Cafiero, L. Adamowicz, J. Chem. Phys. 116 (2002) 5557.
[304] M. Jaszunski, A. Rizzo, P. Jørgensen, Theor. Chem. Acc. 106 (2001) 251.
[305] M. Medved, M. Urban, V. Kellö, G.H.F. Diercksen, J. Mol. Struct. (Theochem.) 547 (2001) 219.
[306] G. Maroulis, P. Karamanis, Chem. Phys. 269 (2001) 137.
[307] G.L. Bendazzoli, V. Magnasco, G. Figari, M. Rui, Chem. Phys. Lett. 330 (2000) 146.
[308] M. Jaszunski, W. Klopper, J. Noga, J. Chem. Phys. 113 (2000) 71.
[309] H.L. Larsen, et al., J. Chem. Phys. 111 (1999) 1917.
[310] O. Christiansen, J. Gauss, J.F. Stanton, Chem. Phys. Lett. 305 (1999) 147.
[311] O. Christiansen, C. Hättig, J. Gauss, J. Chem. Phys. 109 (1998) 4745.
[312] O. Christiansen, J. Gauss, J.F. Stanton, Chem. Phys. Lett. 292 (1998) 437.
[313] O. Christiansen, A. Halkier, P. Jørgensen, Chem. Phys. Lett. 281 (1998) 438.
[314] O. Christiansen, A. Halkier, H. Koch, P. Jørgensen, T. Helgaker, J. Chem. Phys. 108 (1998) 2801.
[315] P. Piecuch, V. Spirko, J. Paldus, Pol. J. Chem. S 72 (1998) 1635.
[316] A. Cartier, M.T.C. Martins-Costa, D. Rinaldi, Int. J. Quantum Chem. 60 (1996) 883.
[317] C. Hättig, B.A. Hess, J. Phys. Chem. 100 (1996) 6243.
[318] C. Hättig, B.A. Hess, J. Chem. Phys. 105 (1996) 9948.
[319] F. Aiga, R. Itoh, Chem. Phys. Lett. 251 (1996) 372.
[320] B. Datta, P. Sen, D. Mukherjee, J. Phys. Chem. 99 (1995) 6441.
[321] R. Kobayashi, H. Koch, P. Jørgensen, Chem. Phys. Lett. 219 (1994) 30.
[322] S.P.A. Sauer, J. Oddershede, Int. J. Quantum Chem. 50 (1994) 317.
[323] W. Zhu, G.-S. Wu, Y. Jiang, Int. J. Quantum Chem. 86 (2002) 347.
[324] F.C. Grozema, R. Telesca, H.T. Jonkman, L.D.A. Siebbeles, J.G. Snijders, J. Chem. Phys. 115 (2001) 10014.
[325] S.J.A. van Gisbergen, J.M. Pacheco, E.J. Baerends, Phys. Rev. A 63 (2001) 63201.
[326] S.J.A. van Gisbergen, C. Fonseca-Guerra, E.J. Baerends, J. Comput. Chem. 21 (2000) 1511.
[327] P.R.T. Schipper, O.V. Gritsenko, S.J.A. van Gisbergen, E.J. Baerends, J. Chem. Phys. 112 (2000) 1344.
[328] P. Calaminici, K. Jug, A.M. Koster, J. Chem. Phys. 109 (1998) 7756.
[329] P. Fuentealba, O. Reyes, J. Phys. Chem. A 103 (1999) 1376.
[330] A.G. Ioannou, S.M. Colwell, R.D. Amos, Chem. Phys. Lett. 278 (1997) 278.
[331] S.M. Colwell, N.C. Handy, A.M. Lee, Phys. Rev. A 53 (1996) 1316.
[332] J. Guan, M.E. Casida, A.M. Koster, D.R. Salahub, Phys. Rev. B 52 (1995) 2184.
[333] I.S. Lim, et al., Phys. Rev. A 60 (1999) 2822.
[334] W. Cencek, K. Szalewicz, B. Jeziorski, Phys. Rev. Lett. 86 (2001) 5675.
[335] L. Visscher, T. Saue, J. Oddershede, Chem. Phys. Lett. 274 (1997) 181.
[336] T.R. Cundari, H.A. Kurtz, T. Zhou, J. Phys. Chem. A 104 (2000) 4711.
[337] D. Goebel, U. Hohm, J. Chem. Soc. Faraday Trans. 93 (1997) 3467.
[338] W. Kauzmann, Quantum Chemistry, Academic Press, New York, 1957.
[339] C. van Caillie, R.D. Amos, Chem. Phys. Lett. 291 (1998) 71.
[340] P. Jensen, P.R. Buenker (Eds.), Computatonal Molecular Spectroscopy, Wiley, Chichester, 2000.
[341] E.I. Solomon, A.B.P. Lever (Eds.), Inorganic Electronic Structure and Spectroscopy, vols. 1–2, Wiley, New York, 1999.
[342] M.C. Zerner, in: D.B. Boyd, K.B. Lipkowitz (Eds.), Reviews in Computational Chemistry, Ch. 2, vol. 8, VCH, New York, 1991.
[343] S.I. Gorelsky, A.B.P. Lever, J. Organomet. Chem. 635 (2001) 187.
[344] O.V. Sizova, V.I. Baranovski, N.V. Ivanova, A.I. Panin, Int. J. Quantum Chem. 65 (1997) 183.
[345] M. Grüning, O.V. Gritsenko, S.J.A. van Gisbergen, E.J. Baerends, J. Chem. Phys. 114 (2001) 652.
[346] G. Ricciardi, A. Rosa, E.J. Baerends, J. Phys. Chem. A 105 (2001) 5242.
[347] A. Rosa, G. Ricciardi, E.J. Baerends, S.J.A. van Gisbergen, J. Phys. Chem. A 105 (2001) 3311.
[348] G. Ricciardi, A. Rosa, S.J.A. van Gisbergen, E.J. Baerends, J. Phys. Chem. A 104 (2000) 635.
[349] A. Rosa, et al., J. Am. Chem. Soc. 121 (1999) 10356.
[350] S.J.A. van Gisbergen, J.A. Groeneveld, A. Rosa, J.G. Snijders, E.J. Baerends, J. Phys. Chem. A 103 (1999) 6835.
[351] E.U. Condon, Rev. Mod. Phys. 9 (1937) 432.
[352] A. Moscowitz, Adv. Chem. Phys. 4 (1962) 67.
[353] E. Charney, The Molecular Basis of Optical Activity, Wiley, New York, 1979.
[354] A.E. Hansen, T.D. Bouman, Adv. Chem. Phys. 44 (1980) 545.
[355] R.D. Amos, Chem. Phys. Lett. 87 (1982) 23.
[356] P.L. Polavarapu, D.K. Chakraborty, J. Am. Chem. Soc. 120 (1998) 6160.
[357] S. Grimme, Chem. Phys. Lett. 339 (2001) 380.
[358] D.J. Caldwell, H. Eyring, The Theory of Optical Activity, New York: Wiley–Interscience, 1971.
[359] K. Yabana, G.F. Bertsch, Phys. Rev. A 60 (1999) 1271.
[360] F. Furche, et al., J. Am. Chem. Soc. 122 (2000) 1717.
[361] J.R. Cheeseman, M.J. Frisch, F.J. Devlin, P.J. Stephens, J. Phys. Chem. A 104 (2000) 1039.
[362] P.L. Polavarapu, D.K. Chakraborty, K. Ruud, Chem. Phys. Lett. 319 (2000) 595.
[363] P.J. Stephens, et al., Tetrahedron: Asymmetry 11 (2000) 2443.
[364] P.J. Stephens, F.J. Devlin, J.R. Cheeseman, M.J. Frisch, J. Phys. Chem. A 105 (2001) 5356.
[365] F. Furche, R. Ahlrichs, J. Chem. Phys. 114 (2001) 10362.
[366] J. Autschbach, T. Ziegler, J. Chem. Phys. 116 (2002) 891.
[367] J. Autschbach, T. Ziegler, S.J.A. van Gisbergen, E.J. Baerends, J. Chem. Phys. 116 (2002) 6930.
[368] J. Autschbach, T. Ziegler, S. Patchkovskii, S.J.A. van Gisbergen, E.J. Baerends, J. Chem. Phys. 117 (2002) 581.
[369] S. Grimme, M. Waletzke, J. Chem. Phys. 111 (1999) 5645.
[370] K. Ruud, T. Helgaker, Chem. Phys. Lett. 352 (2002) 533.
[371] R. Nunez Miguel, J.A. Lopez Sastre, D. Galiesto, A. Gordaliza Ramos, J. Mol. Struct. 522 (2000) 219.

[372] T.B. Pedersen, H. Koch, Chem. Phys. Lett. 293 (1998) 251.
[373] P.L. Polavarapu, C. Zhao, Chem. Phys. Lett. 296 (1998) 105.
[374] F. Pulm, J. Schramm, J. Hormes, S. Grimme, S. Peyerimhoff, Chem. Phys. 224 (1997) 143.
[375] A. Rauk, A.F. Drake, S.F. Mason, J. Am. Chem. Soc. 101 (1979) 2284.
[376] K.D. Bak, et al., Theor. Chim. Acta 90 (1995) 441.
[377] A.E. Hansen, B. Voigt, S. Rettrup, Int. J. Quantum Chem. 23 (1983) 595.
[378] J.-P. Flament, H.-P. Gervais, Theor. Chim. Acta 61 (1982) 149.
[379] A. Rauk, J. Am. Chem. Soc. 103 (1981) 1023.
[380] A. Rauk, J.M. Barriel, Chem. Phys. 25 (1977) 409.
[381] K. Nakanishi, N. Berova, R.W. Woody (Eds.), Circular Dichroism: Principles and Applications, VCH, New York, 1994.
[382] A. Volosov, R.W. Woody, Theoretical approach to natural electronic optical activity, in: K. Nakanishi, N. Berova, R.W. Woody (Eds.), Circular Dichroism. Principles and Applications, VCH, New York, 1994.
[383] R. Kuroda, Y. Saito, Circular dichroism of inorganic complexes: interpretation and applications, in: K. Nakanishi, N. Berova, R.W. Woody (Eds.), Circular Dichroism. Principles and Applications, VCH, New York, 1994.
[384] C.J. Ballhausen, Molecular Electronic Structures of Transition Metal Complexes, McGraw-Hill, London, 1979.
[385] B.E. Douglas, Y. Saito (Eds.), Stereochemistry of Optically Active Transition Metal Compounds. ACS Symposium Series, vol. 119, Americal Chemical Society, Washington, DC, 1980.
[386] S.F. Mason, B.J. Peart, J. Chem. Soc. Dalton Trans. (1977) 937.
[387] S. Alvarez, M. Pinsky, M. Llunell, D. Avnir, Cryst. Eng. 4 (2001) 179.
[388] K.B. Lipkowitz, S. Schefzick, J. Am. Chem. Soc. 123 (2001) 6710.
[389] S. Alvarez, M. Pinsky, D. Avnir, Eur. J. Inorg. Chem. (2001) 1499.
[390] S. Keinan, D. Avnir, Inorg. Chem. 40 (2001) 318.
[391] S. Grimme, Chem. Phys. Lett. 297 (1998) 15.
[392] S.F. Mason, R.H. Seal, Mol. Phys. 31 (1976) 755.
[393] P.E. Schipper, J. Am. Chem. Soc. 100 (1978) 1433.
[394] R.W. Strickland, Inorg. Chem. 12 (1973) 1025.
[395] R.S. Evans, A.F. Schreiner, P.J. Hauser, Inorg. Chem. 13 (1974) 2185.
[396] F.S. Richardson, T.R. Faulkner, J. Chem. Phys. 76 (1982) 1595.
[397] J.D. Saxe, T.R. Faulkner, F.S. Richardson, J. Chem. Phys. 76 (1982) 1607.
[398] A.J. McCaffery, S.F. Mason, B.J. Norman, J. Chem. Soc. A (1969) 1428.
[399] S.F. Mason, B.J. Norman, J. Chem. Soc. A (1969) 1442.
[400] M. Král, A. Moscowitz, C.J. Ballhausen, Theor. Chim. Acta 30 (1973) 339.
[401] M. Král, Theor. Chim. Acta 50 (1979) 355.
[402] J. Autschbach, F.E. Jorge, T. Ziegler, Inorg. Chem. (2003) in press.
[403] D. Yang, Implementation of ab initio vibronic coupling theory to interpret vibrational dichroism spectra, PhD thesis, University of Calgary, 1992.
[404] P.J. Stephens, J. Phys. Chem. 89 (1985) 748.
[405] L.A. Nafie, T.B. Freedman, J. Phys. Chem. 78 (1983) 7108.
[406] D.P. Craig, T. Thirunamachandran, Mol. Phys. 35 (1978) 825.
[407] L.A. Nafie, J. Chem. Phys. 96 (1992) 5687.
[408] D. Yang, A. Rauk, J. Chem. Phys. 100 (1994) 7995.
[409] P.J. Stephens, C.F. Chabalowski, F.J. Devlin, K.J. Jalkanen, Chem. Phys. Lett. 225 (1994) 247.
[410] Y. He, X. Cao, L.A. Nafie, T.A. Freedman, J. Am. Chem. Soc. 123 (2001) 11320.
[411] R. Dutler, A. Rauk, J. Am. Chem. Soc. 111 (1989) 6957.
[412] P.L. Polavarapu, P.K. Bose, J. Chem. Phys. 93 (1990).
[413] A. Rauk, D. Yang, J. Phys. Chem. 96 (1992) 437.
[414] D. Yang, A. Rauk, J. Chem. Phys. 97 (1992) 6517.
[415] K.L. Bak, P. Jørgensen, T. Helgaker, K. Ruud, H.J.A. Jensen, J. Chem. Phys. 98 (1993) 8873.
[416] J.R. Cheeseman, M.J. Frisch, F.J. Devlin, P.J. Stephens, Chem. Phys. Lett. 252 (1996) 211.
[417] F.J. Devlin, P.J. Stephens, J.R. Cheeseman, M.J. Frisch, J. Am. Chem. Soc. 118 (1996) 6327.
[418] P.J. Stephens, C.S. Ashvar, F.J. Devlin, J.R. Cheeseman, M.J. Frisch, Mol. Phys. 89 (1996) 579.
[419] H.G. Bohr, K.J. Jalkanen, M. Elstner, K. Frimand, S. Suhai, Chem. Phys. 246 (1999) 13.
[420] P.J. Stephens, F.J. Devlin, Chirality 12 (2000) 172.
[421] P. Bour, et al., Chirality 12 (2000) 191.
[422] T.B. Freedman, X. Cao, D.A. Young, L.A. Nafie, J. Phys. Chem. A 106 (2002) 3560.
[423] E.J. Corey, J.C. Bailar Jr., J. Am. Chem. Soc. 81 (1959).
[424] P.J. Stephens, J. Chem. Phys. 52 (1979) 3489.
[425] H.F. Hameka, J. Chem. Phys. 36 (1962) 2540.